Single Particle Tracking to Characterize the Mechanism of Pore Formation by Pore Forming Proteins

Dissertation

der Mathematisch-Naturwissenschaftlichen Fakultät

der Eberhard Karls Universität Tübingen

zur Erlangung des Grades eines

Doktors der Naturwissenschaften

(Dr. rer. nat.)

vorgelegt von

Yamunadevi Subburaj

aus Gopalapuram- India

Tübingen

2013

Tag der mündlichen Qualifikation:	22.01.2014
Dekan:	Prof. Dr. Wolfgang Rosenstiel
1. Berichterstatter:	Prof. Dr. Ana J. Garcia Saez
2. Berichterstatter:	Prof. Dr. Joachim Spatz

Acknowledgements

I would like to thank my supervisor, Prof. Dr. Ana Garcia Saez for her excellent guidance, encouragement, valuable and constructive suggestions during the research. She always had time to discuss about the results and the progress of the project.

My sincere thanks to Prof. Joachim Spatz and Prof. Jörg Langowski for their discussions and helpful suggestions. I wish to acknowledge the help provided my collaborator Dr. Markus Axmann for sharing his expertise in single particle tracking. I would like to thank Dr.Stephanie Bleicken, Carolin Stegmueller for providing me the proteins as well as helpful discussions.

A special mention to Dr. Uris Ros for her valuable help and discussions. I extend my thanks to Eduard Hermann, Rudi Tong for all their help in data analysis. I am grateful to Nikon imaging center in Heidelberg and director Dr. Ulrike Engel for letting me to use the microscope in facility. Many thanks to Raquel Salvador, Monika Zelman for helping with the cell culture. I extend my thanks to other lab members Corinna Wagner, Dr. Begona Ugarte, Dr. Katia Cosentino and Joseph Unsay for the scientific and nonscientific discussions.

I am so fortunate to have wonderful friends who have been there with me in all ups and downs. Thank you Dinesh, Bala, Babi, Reshmi, Anu, Swarna, Jasmin, Mile, Rajiv for the support and encouragement.

Nothing would have been possible without a very supportive and understanding family. Special thanks to my parents and husband who has always been a source of inspiration and motivation.

Table of Contents

Summary

Pore formation is a common natural mechanism occurring in large number of organisms where proteins are involved as toxins, effectors in immune response or apoptosis. These proteins have the capacity to increase membrane permeability by forming aqueous pores or channels in the phospholipid bilayer. The mechanism of pore formation involves several steps such as, i) secretion of unfolded polypeptide and folding into a water-soluble protein, ii) Binding of water soluble monomer to the target membrane and iii) subsequent oligomerization of several monomers on the surface of the membrane leading to the formation of a functional pore. Despite intense research, the structural and dynamic aspects of oligomerization and membrane permeabilization by pore forming proteins remains poorly understood. The aim of the project is to study the dynamics, oligomerization and pore forming process of two proteins; a) Equinatoxin II, b) Bax (Bcl2 family) via single molecule imaging.

Equinatoxin II (EqtII) is a pore forming protein of the actinoporin family. The activity of EqtII depends on the presence of sphingomyelin in the target membrane. Here, we examined the assembly mechanism of Equinatoxin II by exploiting state-of-the-art single molecule microscopy. Using total internal reflection fluorescence microscopy, we determined the spatiotemporal assembly of Equinatoxin II in plasma membrane of cells. Our results showed that, the toxin exists as a mixture of species ranging from monomers up to tetramers while forming pores in the plasma membrane of the target cell. This represents a change in paradigm with respect to current models of action of pore forming toxins.

We also observed that the distribution of species evolves with time towards an accumulation of tetramers mostly at the expense of monomers. Remarkably, the diffusion of the toxin particles is largely reduced upon oligomerization, suggesting confinement in membrane domains. Mathematical analysis of the temporal evolution of species led us to a new a model in which the toxic action of Equinatoxin II is exerted under a distribution of oligomeric species, whose assembly proceeds via sequential clustering of individual monomers. This has important consequences for the general understanding of pore forming toxins and supports a new concept in the field: only a small fraction of toxin molecules involved in pore formation is sufficient to potently kill the target cells.

BAX is a pro-apoptotic member of the BCL-2 protein family. During apoptosis BAX is activated by Bid and translocates from the cytoplasm to the outer mitochondrial membrane, where it inserts as a monomer, undergoes oligomerization and forms a pore through which cytochrome *c* and other apoptotic factors are released into the cytoplasm. These apoptotic factors induce the activation of the effector caspases that execute apoptosis However, the arrangement of Bax membrane-bound complexes, and how the complexes porate the membrane, is far from being understood. The antiapoptotic proteins of the family, such as Bcl2 or Bcl-xL, inhibit this process leading to cell survival. The interaction between these proteins affects the activity of Bax. In this work, we determined the stoichiometry of Bax oligomers in the lipid bilayer and interaction between Bcl2 proteins using single/dual color imaging with total internal reflection microscopy. We have shown that, Bax oligomerization occurs via dimer condensations and does not depend on the curvature of the membrane. Unlike Eqt II, the distribution of Bax oligomeric species does not evolve over time. The highest oligomeric species observed in our studies are hexamers.

We used dual color single molecule approach to examine the interactions between Bcl-2 proteins. Our results show that activation of Bax happens prior to the insertion into bilayer and that interaction with tBid is not necessary for oligomerization. In addition, we also found that cBid binds stably to the membrane in presence of Bcl-xL. Better understanding of interaction between these proteins and pore forming mechanism by Bax will help in designing the inhibitors for cancer therapy, ischemic heart disease etc.

Zusammenfassung

Die Formation von Poren ist ein verbreiteter natürlicher Mechanismus, der in einer großen Anzahl von Organismen auftritt, wenn Proteine als Toxine oder Effektoren in Immunreaktionen und Apoptose beteiligt sind. Diese Proteine haben die Fähigkeit, die Permeabilität von Membranen zu erhöhen, indem sie wässrige Poren oder Kanäle in Phospholipid-Doppelschichten ausbilden. Der Mechanismus, der der Ausbildung von Poren zu Grunde liegt, besteht aus einer Reihe von Schritten, wie etwa i) die Ausscheidung von entfalteten Polypeptiden und ihre Faltung in eine wasserlösliche Form, ii) die Bindung von wasserlöslichen Monomeren an die Zielmembran und iii) die darauffolgende Oligomerisierung mehrerer Monomere auf der Oberfläche der Membran, was schließlich zur Formation funktioneller Poren führt. Trotz intensiver Forschung sind die dynamischen Aspekte der Oligomerisierung und der Membran-Permeabilisierung durch Poren-formende Proteine nach wie vor nur wenig verstanden. Das Ziel dieses Projektes besteht darin, die Dynamik, Oligomerisierung und den Prozess der Poren-Bildung zweier Proteine – a) Equinatoxin II, b) Bax (Bcl2-Familie) – durch Einzelmolekülspektroskopie zu untersuchen.

Equinatoxin II (EqtII) ist ein Poren-bildendes Protein aus der Actinoporin-Familie. Die Aktivität von EqtII ist abhängig von der Präsenz von Sphingomyolin in der Zielmembran. In dieser Arbeit haben wir mit Hilfe modernster Einzelmolekülspektroskopie den Mechanismus des schrittweisen Aufbaus von EqtII untersucht. Dank interner Totalreflexions-Fluoreszenzmikroskopie (eng. Total Internal Fluorescence Microscopy, TIRF) haben wir die Assemblierung von EqtII in der Plasmamembran räumlich und zeitlich ermittelt. Unser Ergebnis zeigt, dass das Toxin als eine Mischung von Spezies von Monomeren bis Tetrameren in der Plasmamembran der untersuchten Zelle vorliegt. Dies legt einen Paradigmenwechsel bezüglich gegenwärtiger Modelle nahe, welche die Wirkung von Poren-formenden Toxinen beschreiben.

Wir haben außerdem beobachtet, dass die Verteilung der Spezies mit der Zeit in eine Akkumulation von Tetrameren mündet, die hauptsächlich auf Kosten von Monomeren zu Stande kommt. Bemerkenswerterweise führt die Oligomerisierung der Toxinpartikel zu einer weitgehenden Reduktion ihrer Diffusion, was eine räumliche Einschränkung in Membrandomänen nahelegt. Eine mathematische Analyse der zeitlichen Entwicklung des Oligomerisierungs prozesses führte uns zu einem neuen Modell, in dem die toxische Wirkung von EqtII unter der Koexistenz mehrerer oligomerisierter Spezies ausgeführt

wird, deren Aufbauprozess sich durch schrittweises Hinzufügen von Monomeren vollzieht. Das hat entscheidende Konsequenzen für das generelle Verständnis von Poren-formenden Toxinen und unterstützt ein neues Konzept in diesem Feld: Schon ein geringer Anteil von Toxinmolekülen, die an der Formation von Poren beteiligt ist, reicht aus, um die Zelle potentiell zu vernichten.

Bax ist ein proapoptotisches Mitglied der Bcl-2 Proteinfamilie. Während der Apoptose wird es von Bid aktiviert und wandert vom Cytosol zur mitochondrialen Außenmembran, in die es als Monomer eindringt, oligomerisiert und eine Pore ausbildet, durch welche Cytochrom c und andere apoptotische Faktoren ins Cytoplasma gelangen. Diese apoptotischen Faktoren aktivieren Effektor-Kaskaden, die schließlich die Apoptose ausführen. Es ist zu erwähnen, dass die Koordination von membrangebundenen Bax-Komplexen, sowie der Mechanismus, nach dem diese Komplexe die Membran permeabilisieren, nicht vollends verstanden ist. Die antiapoptotischen Proteine derselben Familie, wie etwa Bcl2 oder Bcl-xL, hindern diesen Prozess und führen zum Überleben der Zelle. Die Wechselwirkungen zwischen all diesen Proteinen beeinflusst maßgeblich die Wirkung von Bax. In dieser Arbeit haben wir die Stöchiometrie von Bax-Oligomeren in der Lipiddoppelschicht ermittelt, sowie die Wechselwirkung zwischen den Bcl2-Proteinen. Dazu haben wir interne Totalreflexions-Fluoreszenzmikroskopie mit einer und zwei Farben eingesetzt. Wir haben gezeigt, dass die Oligomerisierung von Bax durch Kondensation von Dimeren stattfindet und nicht von der Krümmung der Membran abhängt. Anders als EqtII verändert sich die Verteilung von oligomerisiereten Bax-Spezies nicht mit der Zeit. Die höchste beobachtete Spezies in unseren Untersuchungen sind Hexamere.

Wir benutzten einen Zweifarben-Einzelmolekülansatz, um die Wechselwirkungen zwischen den Bcl2-Proteinen zu untersuchen. Unser Ergebnis zeigt, dass die Aktivierung von Bax vor dem Eindringen in die Lipiddoppelschicht stattfindet und dass die Wechselwirkung mit tBid nicht notwendig ist für Oligomerisierung. Außerdem haben wir herausgefunden, dass cBid in Anwesenheit von Bcl-xL effektiv an die Membran bindet. Ein besseres Verständnis der Wechselwirkungen dieser Proteine sowie des Mechanismus, der der Porenbildung von Bax zu Grunde liegt, wird den Weg zur Entwicklung neuer Krebstherapien und ischämischen Herzbehandlungen ebnen.

Chapter 1

Pore forming proteins

1. Pore forming proteins

Pore forming proteins or peptides (PFPs) are produced by large number of organisms including pathogenic bacteria, sea anemones, earthworms etc. (Anderluh and Macek, 2002b; Iacovache et al., 2008; Shogomori and Kobayashi, 2008). Normally they are produced as a means of defense mechanism or to attack the host at the onset of infection. All these proteins have the capability to disrupt and alter the permeability of the cell membrane (Alouf, 2001; Bayley, 2009). The initial action of any pore forming protein is to bind to the target membrane and form a hydrophilic channel helping various compounds such as ions and saccharides to cross the hydrophobic area of the membrane (Andreeva-Kovalevskaya Zh et al., 2008). There are also other PFTs like Aerolysin (Diep et al., 1999), Anthrax toxin(Young and Collier, 2007), Diphtheria toxin (Kent et al., 2008) that pierce the membrane to allow the entrance of virulence factors.

Pore forming toxins (PFTs) produced by bacteria and higher organisms such as cnidarian (Sher et al., 2005a), sea anemones (actinoporins) (Anderluh and Macek, 2002b; Bernheimer and Avigad, 1976), earthworms (lysenin) (Shogomori and Kobayashi, 2008) and plants (enterolobin) (de Sousa and Morhy, 1989) are the well-studied systems used as models for PFTs. Although these different families of PFTs share no sequence homology, their mode of action is similar. The mechanism of pore formation involves several steps such as: i) secretion of unfolded polypeptide and folding into a water-soluble protein, ii) binding of the water soluble monomer to the target membrane and iii) subsequent oligomerization of several monomers on the surface of the membrane leading to the formation of a functional pore with size ranging from 10Å to several nanometers in diameter (Iacovache et al., 2008).

1.1. Classification of pore-forming proteins

PFPs can be classified in more than one way, for example, according to their membrane binding mode, pore size, or organism that produces them. One of the main classifications commonly used for PFPs is based on the structural features of the protein (Gouaux.E., 1997). According to this classification, the two major families are α–PFTs and β-PFTS (Parker and Feil, 2005). This is related to type of structure they use to insert into the lipid bilayer upon pore formation, i.e., α-PFPs cross the membrane as α-helices

and β–PFPs as β–sheets(Gonzalez et al., 2008; Iacovache et al., 2010; Parker and Feil, 2005). Some common PFPs and their classification is shown is Table 1.1.

PFP	Family	Producing organism	Role	PFP class
Aerolysin	Aerolysin family	*Aeromonas* sp.	Pore forming	ß (Diep et al., 1999; Fivaz et al., 1999)
α-Toxin	Aerolysin family	*Clostridium* sp.	Pore forming	ß (Kennedy et al., 2005)
Melittin		*Apis mellifera*	Pore forming	α (Ladokhin et al., 1997; Matsuzaki et al., 1997)
Pneumolysin	CDCs	*Streptococcus pneumoniae*	Pore forming	ß (Tilley et al., 2005)
Colicin A	Colicins	*E. coli*	Pore forming	α (Cascales et al., 2007; Lakey and Slatin, 2001)
Colicin N	Colicins	*E. coli*	Pore forming	α (Cascales et al., 2007; Lakey and Slatin, 2001)
α-Hemolysin	Staphylococcal PFTs	*S. aureus*	Pore forming	ß (Cortajarena et al., 2003; Menestrina et al., 1994)
LukF-PV	Staphylococcal PFTs	*S. aureus*	Pore forming	ß (Jayasinghe and Bayley, 2005; Miles et al., 2006)
Equinatoxin	Actinoporin family	*Actinia equina*	Pore forming	α (Anderluh and Macek, 2002b; Kristan et al., 2004)
Sticholysin	Actinoporin family	*Stichodactyla heliantus*	Pore forming	α (Gutierrez-Aguirre et al., 2004)
PFO	CDCs	*Clostridium perfringens*	Pore forming	ß (Rossjohn et al., 2007)
ILY	CDCs	*Streptococcus intermedius*	Pore forming	ß(Polekhina et al., 2005)
MAC/PF	MACPF	Eukaryotes	Pore forming	ß (Hadders et al., 2007; Lukoyanova and Saibil, 2008; Rosado et al., 2007)
Enterolobin	Aerolysin family	*Enterolobium contortiliquum*	Pore forming	ß (de Sousa and Morhy, 1989)
Diphtheria toxin	Colicin like	*Corynebacterium diphtheriae*	Translocation	α (D'Silva and Lala, 2000; Kent et al., 2008)

Table 1.1. Classification of commonly studied PFPs

1.1.1. α–PFPs

This family includes toxins like the colicins, which are the best characterized α-PFPs and are produced by *Escherichia coli*, (Cascales et al., 2007; Lakey and Slatin, 2001; Zakharov and Cramer, 2002), the actinoporins produced by sea anemones (Kristan et al., 2004), diphtheria toxin produced by *Corynebacterium diphtheriae*, exotoxin A from *Pseudomonas aeruginosa* (J.E. Alouf, 2005) and the insecticidal Cry toxins produced by *Bacillus thuringiensis* (Bravo et al., 2007a; Grochulski et al., 1995b). Much importance was given to Cry toxins due to their potential role in pest control in transgenic crops.

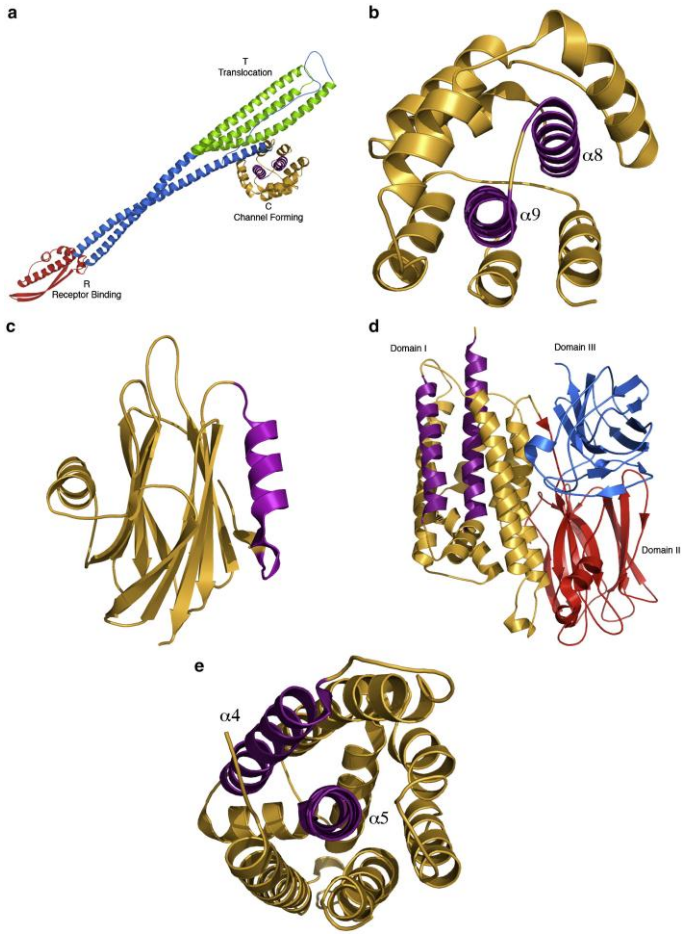

Figure.1.1. Ribbon representation of the crystal structures of some α-PFTs. The transmembrane region is colored in violet. (a) colicin Ia (PDB entry code 1CII): the T translocation, R receptor-binding domain and the C channel-forming domains are indicated, (b) close-up view of the C pore-forming domain of colicin Ia, (c) Equinatoxin II (PDB entry code 1IAZ), (d) Cry4Aa composed of domains I, II and III (PDB entry code 2C9K), (e) Domain I, the pore-forming domain of Cry4Aa. (Iacovache et al., 2008)

As shown in Fig.1.1, the atomic structures of several α-PFPs in their water-soluble state have been solved, however few structures of the oligomeric state are known to date. The first reported crystal structure of this family in soluble and pore form is colicin A secreted by *E.coli* (Mueller et al., 2009; Wallace et al., 2000). The polypeptide chain of 204 aminoacids was found to fold into ten alpha-helices arranged in a three-layer structure (Parker et al., 1989; Parker et al., 1992). Colicins kill cells by single hit inactivation kinetics, meaning that one molecule of colicin is sufficient to form a pore and kill the cell (Bullock and Kolen, 1995). A remarkable feature of colicin pore formation is their ability to translocate approximately 35% of 200 residues across the bilayer (Qiu et al., 1996; Slatin et al., 1994). A number of colicin structures have been solved subsequently and the pore-forming domains seemed to be similar with Colicin A. Interestingly, the structure of diphtheria toxin (DT) (Choe et al., 1992) and Cry δ–endotoxins (produced by *Bacillus thuringiensis)* (Grochulski et al., 1995a; Li et al., 1991) showed a close resemblance to colicins although their sequences were not identical.

Another example is *Pseudomonas aeruginosa* exotoxin A (PE), which is a 66kDa toxin consisting of three domains. Domain I (residues 1 to 252 and 365 to 404) has a core based on a 13-stranded *β*-roll and functions as the receptor-binding domain. Domain III (residues 405 to 613) adopts a complex *α/β* fold and is responsible for the toxin's catalytic activity. Domain II (residues 253 to 364), the domain responsible for membrane translocation, adopts an all alpha-helical structure of six helices of which two are 30 Å in length and hence long enough to span a membrane (Allured et al., 1986; Wedekind et al., 2001). The crystal and NMR structures of the soluble form of *Actina equina* equinatoxinII, and the related sticholysin II from *Stichodactyla helianthus,* have been determined a decade ago. These toxins adopt a 12-stranded ß-sandwich fold with an α-helix packing against the face of the sheet. The N-terminal α-helical region has shown to be responsible for membrane insertion and pore formation (Athanasiadis et al., 2001; Hinds et al., 2002; Mancheno et al., 2003). The assembly mechanism of Equinatoxin II has been characterized and described in detail in this thesis. (See chapters 2 and 6).

The Bcl-2 family of proteins is an important class of PFPs because they are the key regulators of apoptosis. They have been shown to form pores in the membrane via α-helices, hence classified under the class of α-PFPs. They have been investigated in this thesis and more about them is explained in chapters 3 and 7.

Currently, there are two models proposed for the type of pores formed by α-PFPs, which are mainly based on studies with pore forming peptides. In the "barrel–stave" model, the helices align closely in the bilayer forming a solvent exposed surface of the pore. This model is also called proteinaceous pore model as there are no lipids involved in the formation of the pore edge (Fig.1.2.A). Alamethicin, a 21 residue peptide produced by fungus *Trichoderma viride* (Qian et al., 2008a) and Cytolysin A (Mueller et al., 2009) are well known for forming barrel-stave pores. In the "toroidal" or "lipidic pore" model, the peptides lie on the membrane surface and when they aggregate, the surface tension of the membrane increases leading to membrane thinning and unstabilization. Because of this, the two leaflets merge and form a torus-shaped pore where the solvent exposed area is lined by lipid headgroups as well as protein molecules (Fig.1.2.B). Magainins (Matsuzaki et al., 1998) and melittins (Matsuzaki et al., 1997) were shown to form toroidal pore (Sengupta et al., 2008).

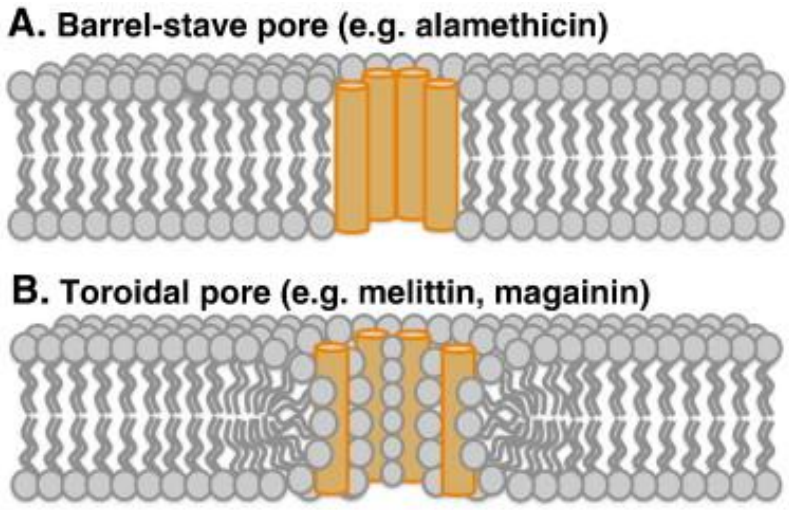

Figure.1.2. Two mechanisms by which PFPS might form pores. (A) In the barrel-stave model, α-helical peptide "staves" align to form a barrel-like pore that spans the membrane. Peptides are adjacent to the lipid acyl chains. (B) In the toroidal pore model, α-helical peptides induce membrane curvature such that the outer and inner leaflets are continuous. Peptides are adjacent to the lipid headgroups. (Westphal et al., 2011)

Some α-PFPs that do not have colicin-like domains do not form very stable oligomeric complexes. This is why it was very difficult to determine the structure of these proteins in the pore form (Anderluh and Lakey, 2008). The absence of stable oligomers and the ability to trigger lipid rearrangements are typical features of α-PFPs forming

toroidal pores (Anderluh et al., 2003; Qian et al., 2008b; Sobko et al., 2006). In fact, both Equinatoxin II and the proteins of the Bcl-2 family have been proposed to form toroidal pores.

1.1.2. ß-PFPs

Because they form stable structures and are easier to handle than their α–helical counterparts, ß-PFPs have so far been the largest and most studied group of pore forming proteins. Members include the large family of cholesterol dependent cytolysins (CDCs) (Tweten et al., 2001), Aerolysin (Diep et al., 1999), perforin (Hadders et al., 2007), *Staphylococcus aureus* α-hemolysin (Menestrina et al., 2003), *Bacillus thuringiensis* Cyt δ-endotoxins (Bravo et al., 2007b) and anthrax toxin (Young and Collier, 2007).

The first crystal structure from a member of this class was Aerolysin (produced by *Aeromonas hydrophila*), which revealed that they consist mainly of ß-sheets, unlike the α-PFPs (Parker et al., 1994).The monomer has a distinct bilobe shape with one large, elongated lobe (100Å) and a small lobe attached by a linker region**.** *A. hydrophila* (Fig.1.3.c) secretes a precursor toxin, proaerolysin, via a type II secretion system (Buckley, 1990). Proaerolysin is converted into aerolysin by gut proteases, *Aeromonas* proteases (Howard and Buckley, 1985) or members of the furin family of mammalian endoproteases (Abrami et al., 1998; van der Goot et al., 1992). Then, it binds to the target membrane in a monomeric or dimeric form (Barry et al., 2001; Fivaz et al., 1999), via the specific interaction with glycosyl phosphatidyl inositol (GPI)-anchored proteins (Cowell et al., 1997; Fivaz et al., 2002; MacKenzie et al., 1999). Aerolysin can form a heptameric ring (Moniatte et al., 1996; Wilmsen et al., 1992) when the concentration is high enough. The X-ray structure of proaerolysin in the dimeric form revealed an L-shaped elongated molecule divided into two domains, a small globular domain, and a large lobe linked together by a long stretch of residues (Parker et al., 1994) (Fig.1.4.b).

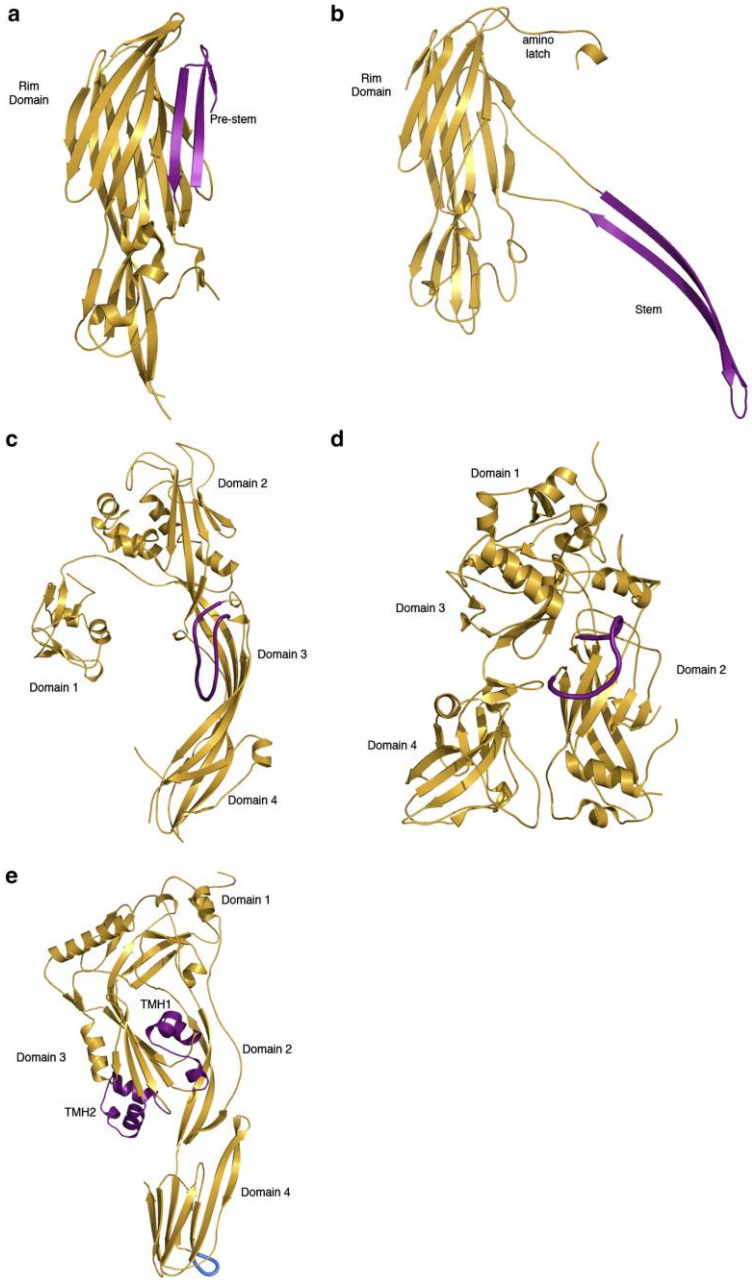

Figure.1.3. Ribbon representation of the crystal structures of ß-PFTs: the transmembrane region is colored in purple. (a) The water-soluble LukS-PV monomer with the prestem domain (PBD entry code 1T5R), (b) one α-toxin monomer in the oligomer (noted are the cap with the amino-latch, the rim and the stem domains) (PDB entry code 7AHL), (c) proaerolysin (PDB entry code 1PRE), (d) anthrax PA: one monomer from PA63 heptameric prepore is represented (PDB entry code 1TZO), (e) perfringolysin O, where the conserved undecapeptide is colored in blue (PDB entry code 1PFO) (Iacovache et al., 2008).

α-Hemolysin is released by *Staphylococcus aureus* as a 33-kDa water-soluble monomer and oligomerizes into hexamers or heptamers (pre-pore) (Fig.1.4.a) (Kawate and Gouaux, 2003; Olson et al., 1999; Walker et al., 1992) on the membrane surface, which then insert into the lipid bilayer to form the pore. The crystal structure of this toxin was the first to shed light on the pore configuration of ß-PFPs. α-Hemolysin pore

structure resembled a mushroom-shaped object consisting of cap, rim and stem domains (Song et al., 1996) (Fig.1.3b). The cap is about 100Å diameter and forms the core of the protein along with the rim. The stem is the transmembrane domain consisting of 14-stranded ß–barrel formed from 7 ß-hairpins with each hairpin contributed from a single monomer (Iacovache et al., 2008; Menestrina et al., 2003).

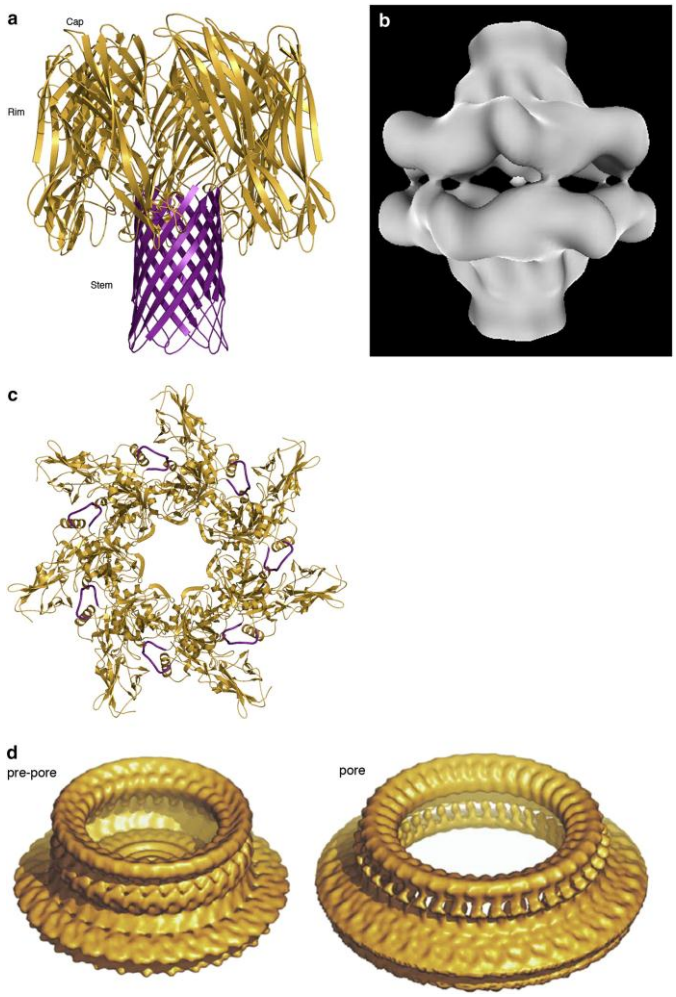

Figure.1.4. Ribbon representation of the crystal structures of β-PFTs in their transmembrane form. The transmembrane region is colored in violet. (a) α-toxin heptamer (PDB entry code 7AHL). (b) Molecular envelope of aerolysin Y221G heptamer. The image shows a dimer of heptamers joined together by their large base. (c) Prepore PA63 of the anthrax protective antigen (PDB entry code 1TZO). (d) Molecular envelope of the pneumolysin prepore and pore (Iacovache et al., 2008).

The largest family of β-PFPs is Cholesterol dependent cytolysins (CDCs), consisting of more than 20 members, which are secreted by Gram-positive bacteria such as *Clostridium* (Perfringolysin O) (Rossjohn et al., 2007), *Streptococcus* (Streptolysin O, Pneumolysin, Intermedilysin) (Tilley et al., 2005) and *Listeria* (Listeriolysin O) (Tweten

et al., 2001). They share a high degree of sequence similarity suggesting that they have similar structure and function (Tweten, 2005). CDCs require cholesterol for cell membrane binding, oligomerization and membrane insertion (Giddings et al., 2003). The most interesting aspect of CDCs is that they form very large pore of ~40 nm diameter with about 50 monomers. However, there is still debate concerning the size of the pore (Iacovache et al., 2010).

The crystal structure of soluble Perfringolysin O (PFO) (Nakamura et al., 1995) (Fig.1.3.e) and Intermedilysin (ILY) (Polekhina et al., 2005) reveal an elongated protein rich in β-sheet and composed of four domains. Domain 4 is involved in binding to cholesterol-rich membrane domains via three short hydrophobic loops (Heuck et al., 2000; Nakamura et al., 1995). This binding has been shown crucial for the conformational changes that occurs during the conversion of a prepore to pore (Heuck et al., 2007). Earlier, two mechanisms have been proposed for pore formation by the CDC family. On the one hand, the studies with Streptolysin O suggested that the monomers bind and insert into the membrane before oligomerization occurs to form a pore (Palmer et al., 1998). Whereas, on the other hand, studies with Perfringolysin O showed that monomers bind to the membrane and oligomerize to form a prepore ring followed by insertion to form a pore (Hotze et al., 2002; Shepard et al., 2000). But later, it has been demonstrated that even Streptolysin O forms a prepore ring indicating that the members of this family share a common mechanism of pore formation (Heuck et al., 2003).

1.2. Future perspectives

Pore formation is a complex process occurring in many steps. Although the number of studies on the mechanism of pore formation is increasing rapidly, there are still some key questions that remain unanswered or under debate. One of the major processes that haven't been understood well to date is the oligomerization of the proteins. The crystal structure of α-hemolysin, Fra C provides information about the stoichiometry of the pore. But, as PFPs form pores ranging from 1-2 nm to 25-30 nm, the structural information from one protein cannot be generalized for all PFPs. Moreover, the information about the dynamics of oligomerization is limited. Whether the oligomers are formed through sequential addition of monomers or through interaction of mutimeric intermediates has not been fully addressed for any PFP. With structural methods, it's difficult to trap the dynamic process and to get information about the intermediates. We

also do not know much about the interaction of PFPs with their receptors in the membrane. The receptors vary for different PFPs. For example, they can be lipids (Actinoporins, CDCs), proteins (Anthrax toxin) or sugars (Aerolysin, lysenin). These receptors help in binding to the membrane followed by conformational changes required for subsequent steps of pore formation. Further structural information is also required to understand about the type of pore (Toroidal or Barrel-stave) formed by PFPs and also about the existence of pre-pores.

In this work, we have made an attempt to characterize the pore forming mechanisms by Equinatoxin II (Actinoporins) and Bax (a member of the Bcl-2 family). For this purpose, we visualized individual, fluorescently labeled EqtII molecules and Bcl-2 proteins on the plasma membrane of living cells and on model membranes respectively, by total internal reflection fluorescence (TIRF) microscopy.

Chapter 2

Actinoporins

2. Actinoporins

Sea anemones secrete venomous substances in order to paralyze and prepare prey for digestion, and also as a defense mechanism against predators (Burks and Lodge, 2002; Sher et al., 2005b). They produce a large number of peptide and protein toxins including ion channel modifiers (Norton, 1991), enzymes (Lotan et al., 1996) and cytolysins (Anderluh and Macek, 2002b). As other pore forming proteins, cytolysins target and permeabilize the cell membrane of their targets by forming pores leading to cell lysis. The most common studied group is actinoporins, which are lethal to small crustaceans, molluscs and fishes (Anderluh and Macek, 2002b; Kem and Dunn, 1988; Macek, 1992) .

Actinoporins are 20 kDa cysteineless proteins and their activity depends on the presence of sphingomyelin in the target membrane and is enhanced by phase existence (Bakrac and Anderluh, 2010; Kristan et al., 2009). The two most studied representatives of this family are Equinatoxin II (EqtII) from the sea anemone *Actinia equina* (Macek et al., 1994) and Sticholysin II (StII) from *Stichodactyla helianthus* (Alvarez et al., 2009). These proteins an extremely conserved with high sequence similarity [60-80%] (Fig.2.1). Surprisingly, even small changes in their sequence lead to a major differences in their solubility and hemolytic activity (Garcia-Linares et al., 2013). Equinatoxin II (EqtII) has been shown to cause platelet aggregation (Teng et al., 1988), pulmonary edema (Lafranconi et al., 1984) and cardiac arrest (Bunc et al., 1999). All these effects are due to the ion imbalance, as the membranes become highly permeable for ions. Erythrocytes are lysed by Eqt II due to osmotic shock (Anderluh and Macek, 2002a).

The crystal structures of EqtII and StII in aqueous solution were resolved a decade ago and recently, the structure of another member of this family, Fragaceatoxin C (FraC), has been determined in the lipid membrane (Athanasiadis et al., 2001; Hinds et al., 2002; Mechaly et al., 2011a; Mechaly et al., 2009; Norton, 2009). All of them display a common fold consisting of a ß-sandwich core (10-12ß strands) flanked on both sides by α-helices. The N-terminal segment containing an amphipathic α-helix has been shown to displace from the core of the protein and insert into the bilayer forming the pore wall (Athanasiadis et al., 2001; Mechaly et al., 2011a). The final oligomeric pore structure of actinoporins has not been visualized yet. Based on crosslinking studies (Belmonte et al., 1993a) and kinetic data experiments (Tejuca et al., 1996), it has been suggested that three to four monomers are involved in the formation of a ~2nm diameter pore. However, the

crystal structure of FraC in the lipid bilayers instead suggests that a nonamer is responsible for pore formation (Mechaly et al., 2011a). Earlier, it was proposed that actinoporins form toroidal pores, where lipids are part of the pore wall, as four helices are insufficient to form a pore (Alvarez et al., 2009; Kristan et al., 2009; Mancheno et al., 2003). However, the recent structure of FraC shows that the pore formed is free of lipids, typical of a barrel stove pore (Mechaly et al., 2011a; Mechaly et al., 2009). Given these contradictions, there is still a debate on the number of monomers involved in the pore and the type of pore involved. Next we discuss in detail about an actinoporin, EqtII, which is the main object of our study.

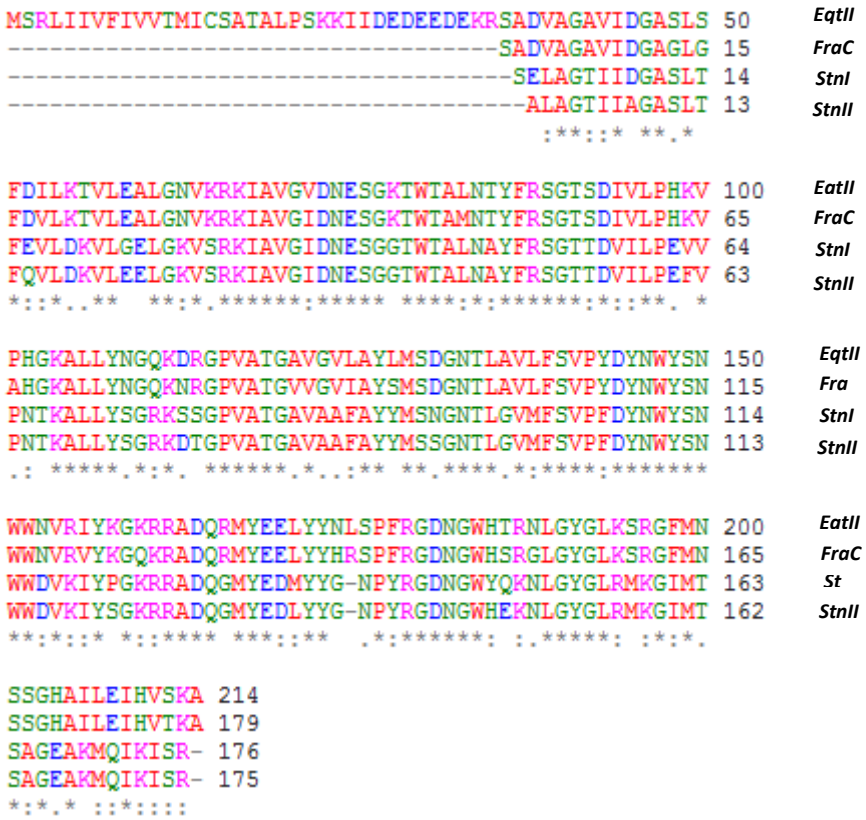

Figure.2.1. Sequence alignment of the four best-studied members of actinoporins showing the similarities between them. [Alignment done with Clustal W]. Colors are based on the physicochemical properties of the aminoacids; small hydrophobic (red), acidic (blue), basic (magenta), amine group (green). The symbols under the sequences, ":" indicates the similarity and "*" indicates the identity between the proteins.

2.1. Equinatoxin II

Equinatoxin II (EqtII) secreted by sea anemone *Actinia equina*, is a 179-residue, 19.8 kDa protein. Like other actinoporins, EqtII shows affinity for sphingomyelin and permeabilizes model lipid and cellular membranes. Athanasiadis *et al.* first reported the crystal structure of EqtII in aqueous solution (Athanasiadis et al., 2001). This toxin adopts a 12 stranded β-sandwich fold with an α-helix packed against the face of each sheet. The first 30 N-terminal residues including one of the helices were predicted to form the transmembrane region that is responsible for pore formation (Athanasiadis et al., 2001; Hinds et al., 2002) (Fig.2.2A). An interesting feature of the structure is the presence of a cluster of aromatic amino acids on the surface of the protein comprising Tyr-108, Trp-112, Tyr-113, Trp-116, Tyr-133, Tyr137 and Tyr-138 (Hong et al., 2002). Since aromatic residues have affinity for the lipid-water interface, these residues are predicted to play a role in membrane recognition and binding (Kennedy and Beauchamp, 2000). The structure of StII together with phosphocholine has revealed that the phosphocholine binding pocket is also involved in the initial membrane binding event. The residues in binding pocket are highly conserved, suggesting that the role played by this site is the same in all actinoporins (Mancheno et al., 2003). In addition, it has been shown that Trp112 and Tyr113 located in the vicinity of this binding site are important for sphingomyelin recognition and the initial contact with the membrane. Mutations in these residues to alanine inhibited the direct binding to sphingomyelin as well as insertion and binding to sphingomyelin-containing lipid monolayers and liposomes (Bakrac et al., 2008; Kristan et al., 2009).

Pore formation by EqtII is thought to be a multistep process (Fig.2.2.C): i) the soluble monomer of the toxin binds to the sphingomyelin-containing membrane as described above (Hong et al., 2002; Malovrh et al., 2000); ii) the N-terminal segment (residues 10-28) is transferred to the lipid water interface and lies flat on the membrane surface (Hong et al., 2002; Malovrh et al., 2003a); iii) the toxin oligomerizes on the membrane surface and the N-terminal α-helices of 3 to 4 monomers insert into the membrane and form so called toroidal pore (Alegre-Cebollada et al., 2007; Belmonte et al., 1993a; Malovrh et al., 2003a; Tejuca et al., 1996). In the alternative model based on the FraC structure, the toxin oligomerizes up to nonamers in order to from a barrel-stave pore. The N-terminus was shown to be involved in the final pore formation step, as toxins

lacking this region do not lyse red blood cells. Moreover, *Kristan et al*. showed that the N-terminal segment crosses the membrane and is also involved in the stabilization of the pore. Additionally, they showed that the first five aminoacids in the N-terminus help to stabilize the helix in the final pore (Kristan et al., 2007).

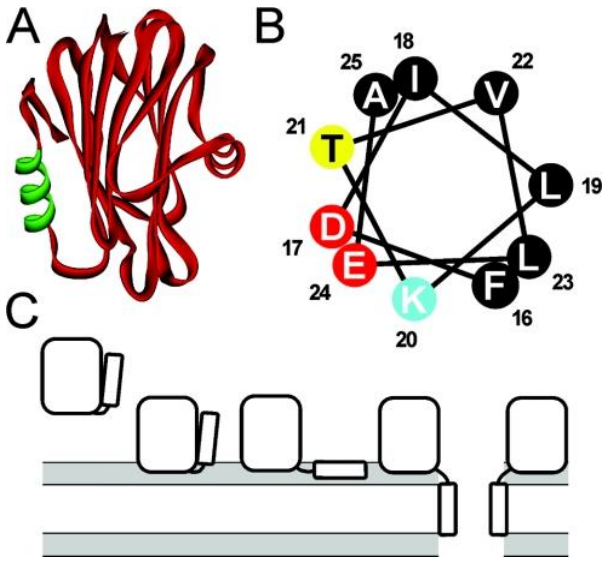

Figure.2.2. Three-dimensional models of EqtII. *A*) Three-dimensional model of EqtII in aqueous solution. The N-terminal amphipathic region 10–28 encompassing helix A is shown in *green*. *B*) Helical wheel view showing the amphipathicity of the 10–28 regions. The residues are colored according to physical properties (*black*, hydrophobic; *yellow*, polar; *red*, negatively charged; *blue*, positively charged). *C*) Current hypothesis of pore formation by EqtII. Pore formation involves at least four different conformational states of the toxin: a soluble form, a membrane-bound form attached to the membrane via the aromatic cluster (M1-state), a membrane-bound form with a dislocated N-terminal helix (M2-state), and the oligomeric form (P-state), when the N-terminal helix is part of the conductive pathway. The lipid-water interface is shaded *gray*. (Gutierrez-Aguirre et al., 2004)

Red blood cells (RBC) are lysed by EqtII due to osmotic shock. Aggregates of EqtII corresponding to dimers and trimers were observed on the RBS membranes. Other blood cells, leukocytes and platelets were also found to be affected by EqtII (Teng et al., 1988). Out of these, leukocytes were shown to be less sensitive to toxin than other blood cells (Macek et al., 1994). The activity of EqtII has shown to be enhanced by lipid coexistence (Barlic et al., 2004). Thinking of in a physiological level, this could correspond to the presence of lipid rafts in the cell membrane. The interface between the

two phases has been described to serve as concentration platforms where the proteins oligomerize and form pores. Moreover, the lipids at the interface are more disordered and redistribute while protein insertion leading to formation of toroidal pore, as suggested for EqtII. Although many PFPs use lipid rafts as receptors, their role in the pore formation has not yet been understood well (M.Fivaz, 2000). Recently, Garcia et al. has shown the reorganization of plasma membrane in cells induced by EqtII using a combination of advanced fluorescence microscopy techniques. According to their study, EqtII induces formation of microscopic domains and colocalizes with these domains. In addition, they have shown that EqtII also inhibits endocytosis (Garcia-Saez et al., 2011a).

Despite all these studies, the dynamic organization of the EqtII pore remains unknown. In addition, most of the studies regarding pore formation by EqtII were done *in vitro* using model membranes and, therefore, the behavior of the toxin in the cell membrane is poorly understood. In this work we have attempted to address these questions regarding the assembly mechanism of EqtII. For this, we have used total internal reflection microscopy to visualize individual EqtII molecules fluorescently labeled on the plasma membrane of living cells.

Chapter 3

The Bcl-2 Family

3.1. Apoptosis

In 1972, John Kerr, Andrew Wyllie and Alistair Currie first used the term "apoptosis" to name a distinct form of programmed cell death cell (or cell suicide) (Kerr et al., 1972). Since then, it has been shown that apoptosis plays a vital role in normal development, tissue homeostasis and the removal of damaged and infected cells. Its dysregulation leads to many human diseases such as cancer, autoimmunity and neurodegenerative disorders (Peng et al., 2009; Yip and Reed, 2008; Youle and Strasser, 2008). For example, auto-immune lymphoproliferative syndrome (ALPS) (Straus SE, 1999) is caused when autoreactive T cells are not removed by apoptosis after an immune response. Dysregulation of apoptosis during the maintenance of tissue homeostasis leads to cancer, as illustrated by B-cell lymphomas. Insufficient apoptosis can also lead to persistent infections due to a failure to eradicate bacteria or virus-infected cells. Inappropriate or excessive apoptosis can also be detrimental. Several neurodegenerative disorders such as Alzheimer's, Parkinson's and Huntington's diseases are characterized by the premature loss of specific neurons that can lead to irreversible memory loss, uncontrolled muscular movements, and depression (Fesik, 2000). Excessive apoptosis also contributes to the damage caused by inflammation, spinal muscular atrophy, myocardial infarction, and stroke (Hanahan and Weinberg, 2000; Rutledge et al., 2002; Thompson, 1995). Because of its fundamental importance, apoptosis is a highly regulated pathway. During this process, cells die by DNA fragmentation, cellular blebbing and formation of apoptotic bodies (Chipuk et al., 2010). The important feature of apoptosis is that it is a "clean" process and the intracellular components are not released to the extracellular medium, in contrast to other cell death types such as necrosis. The cells undergoing apoptosis are rapidly phagocytosed either by a neighboring cell or by a macrophage before the leakage of intracellular contents (Bruce Alberts, 2002). The main executioners of apoptosis are a family of cysteine proteases called caspases which leads to the morphological changes mentioned above (Taylor et al., 2008). Caspases involved in apoptosis have been classified by their mechanism either as initiator caspases (caspase-8 and -9) or executioner caspases (caspase-3, -6, and -7). Caspase-1, -2, -4, -5, and -9 contain a caspase recruitment domain (CARD), whereas caspase-8 and -10 have a death effector domain (DED) (McIlwain et al., 2013).

There are two main pathways of apoptosis, which differ with the role of mitochondria (Scaffidi et al., 1998; Scaffidi et al., 1999) (Fig.3.1). The extrinsic or death receptor pathway is shown to be important for the maintenance of tissue homeostasis and is triggered by the neighboring environment. In this pathway, the death receptors in the plasma membrane oligomerize and form death inducing signaling complexes (DISC) upon binding of ligands such as FasL or TNFα. This leads to the activation of caspase-8, which in turn activates the executioner caspases that cause cell death (Chinnaiyan et al., 1996; Medema et al., 1997; Peter et al., 1996).

The intrinsic or mitochondrial pathway is instead activated when the cell senses internal damage or stress induced by physico-chemical agents. The mitochondrial pathway of apoptosis is regulated by the proteins of the Bcl-2 family. The main regulatory step of this pathway is cytochrome c release after the permeabilization of the mitochondrial outer membrane (MOM) by Bax or Bak. Together with the proapoptotic cytosolic factors APAF1 and caspase 9, cytochrome c assembles into caspase activating complex termed the "apoptosome" (Zou et al., 1997). This complex contains and activates the initiator caspase 9, which cleaves the executioner caspases 3 and 7, leading to the activation of the downstream cascade as in the extrinsic pathway. Other intermembrane space proteins like SMAC/Diablo also contribute to cell death after being released into the cytosol (Bender and Martinou, 2013; Ghibelli and Diederich, 2010; Westphal et al., 2011).

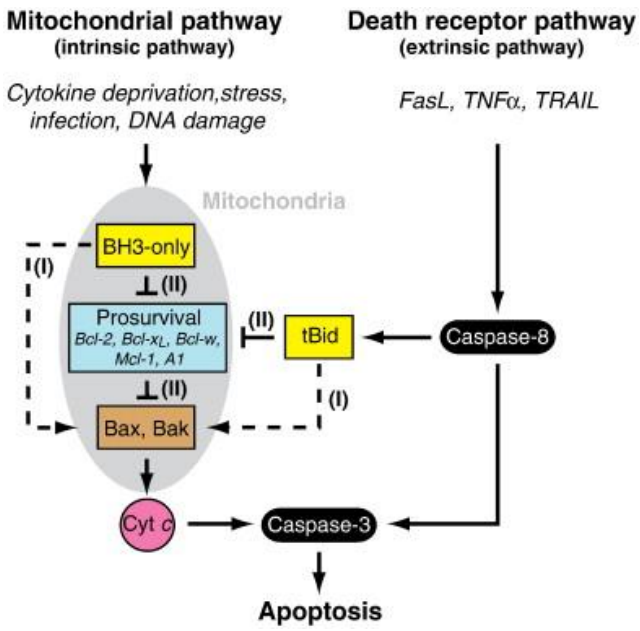

Figure. 3.1. Multiple pathways to apoptosis. The *mitochondrial* (or intrinsic) pathway is induced as a response to cellular stress and results in the activation of the pro-apoptotic BH3-only proteins. BH3-only proteins may *directly* bind and activate Bax and Bak (I, dashed lines), and may also bind to the prosurvival Bcl-2-like proteins to *indirectly* activate Bax and Bak (II). Once activated, Bax and Bak oligomerize to form pores in the mitochondrial outer membrane that release cytochrome *c*. Cytosolic cytochrome *c* leads to caspase activation and subsequent cell death. The *death receptor* (extrinsic) pathway is initiated by death ligands such as FasL, tumor-necrosis factor α (TNFα), or TNF-related apoptosis inducing ligand (TRAIL) binding to cell surface receptors, resulting in the activation of caspase-8. Active caspase-8 can either activate downstream caspases directly (in type I cells) or engage the intrinsic pathway via a cleaved form of the BH3-only protein Bid (tBid) (in type II cells). (Westphal et al., 2011)

However, the two pathways are not completely independent. In apoptosis initiated by the extrinsic pathway, mitochondrial damage is not required in most cells (type I cells) as caspase -8 directly activates the downstream caspases. But, other cells (type II) require the activation of the mitochondrial pathway for the activation of the caspase cascade. This leads to activation of Bid to its truncated form (tBid) (Scaffidi et al., 1998; Scaffidi et al., 1999). Type I and II cells differ in their content of intracellular X-linked inhibitor of apoptosis proteins (X-IAPs), which block executioner caspase function unless suppressed by proteins released from the mitochondria (McIlwain et al., 2013).

3.2. Bcl-2 family

The members of the Bcl-2 protein family fall into three sub-classes: the pro-apoptotic BH3-only proteins; the pro-apoptotic multi domain pore forming proteins; and the pro-survival or anti-apoptotic proteins (Willis and Adams, 2005) (Fig.3.2). Most cells express a variety of antiapoptotic and proapoptotic BCL-2 proteins, and the regulation of their interactions dictates survival or commitment to apoptosis. The BH3-only proteins (Bid, Bim, Puma, Noxa, Bad, Bmf, Hrk, and Bik) are pro-apoptotic and act as sensors for specific types of cellular stress (Giam et al., 2008; Lomonosova and Chinnadurai, 2008). The pro-apoptotic multidomain pore forming proteins, BCL-2 antagonist killer 1 (Bak) and BCL-2-associated x protein (Bax), were originally described to contain only BH1-3 domains; however, structure-based alignment of globular BCL-2 family proteins revealed a conserved BH4 motif (Kvansakul et al., 2008). These are the critical effectors of apoptosis by altering the permeability of the MOM (Lindsten et al., 2000; Wei et al.,

2001). Antiapoptotic Bcl-2 proteins contain four Bcl-2 homology domains (BH1–4) and are generally located at the MOM, but may also be in the cytosol or ER membrane. This subclass includes Bcl-2, Bcl-xL, Bcl-w, Bcl-2 -related gene A1 (A1) and myeloid cell leukemia 1 (MCL-1) (Kvansakul et al., 2008). The function of these proteins is to preserve the MOM integrity by directly inhibiting the proapoptotic Bcl-2 proteins. Apart from these proteins there are additional, less- known Bcl-2 family members described to function as pro-apoptotic (Bcl-G, BOK, Bcl-Rambo) or prosurvival (Bcl-B) protein (O'Neill et al., 2006).

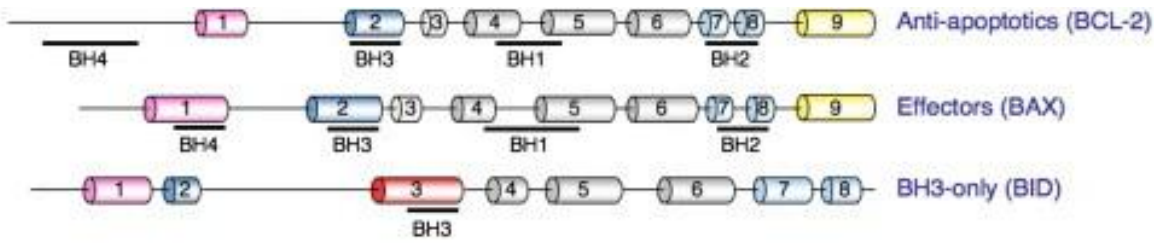

Figure.3.2. The classification of Bcl2 proteins. (Chipuk et al., 2010)

The BH3-only proteins serve as sensors of intrinsic stimuli arising from various cellular stresses and regulate Bax/Bak activation via complex interactions with the pro- and/or anti-apoptotic members. They are further subdivided into two categories: sensitizers or activators. BH3-only proteins that only bind to the antiapoptotic repertoire and displace Bax and Bak are referred to as “sensitizer”, or “derepressor”. Examples of this type of BH3-only proteins are BAD (BCL-2 antagonist of cell death) and Noxa (Antignani and Youle, 2006). Activators are those that bind directly to Bax and Bak and induce their homo/hetero oligomerization leading to MOM permeabilization. Some examples are Bid (Bcl-2-interacting domain death agonist) (Desagher et al., 1999), Bim (Bcl-2-interacting mediator of cell death) (Czabotar et al., 2009) and Puma (Gallenne et al., 2009). Despite their function as sensitizers or activators, the end result is the activation of Bax/Bak generating the ‘apoptotic pore’ in the mitochondrial outer membrane. In the following sections, we discuss in detail the activation and pore formation by Bax.

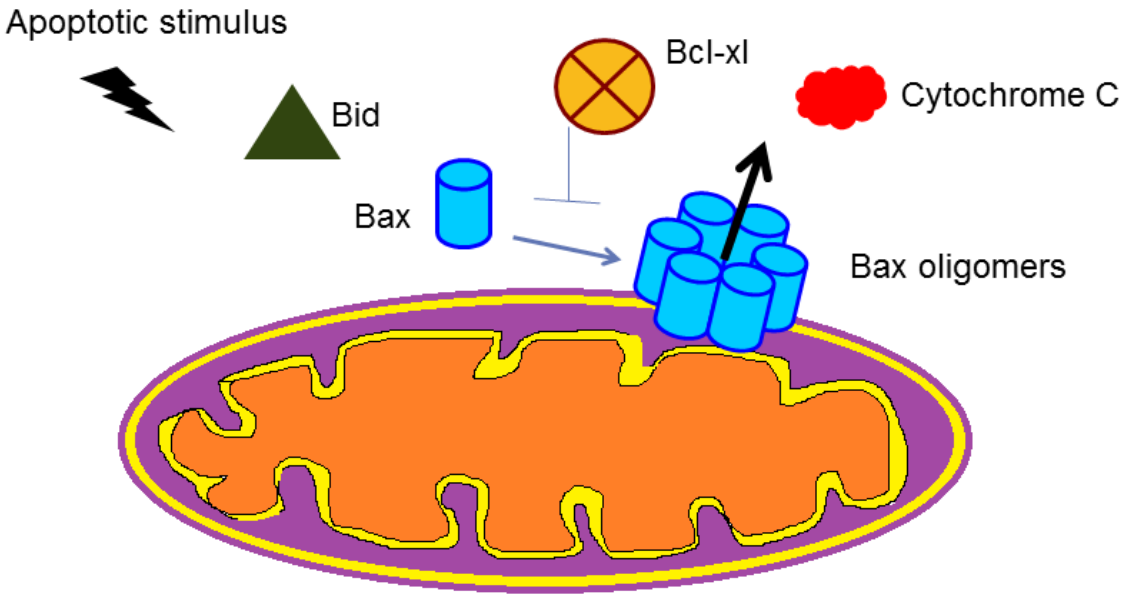

Figure.3.3. Schematic representation of Bax oligomerization during apoptosis

3.2.1. Bax

Bax is a 21kDa protein of 192 amino acids. *Suzuki et al*. determined the three dimensional crystal structure of the soluble form of Bax (Suzuki et al., 2000). The protein is formed by nine α-helices connected by short loops. Three of these helices namely, α5, α6 and α9 are shown to be involved in the interaction of Bax with MOM (Fig.3.4.B) (Bleicken et al., 2010a; Garcia-Saez et al., 2004). α5 and α6 are amphipathic helices organized as a hairpin similar to the bacterial toxins known to form pores in lipid bilayers (Garcia-Saez et al., 2005; Garcia-Saez et al., 2006; Schendel et al., 1998; Schlesinger et al., 1997). α9 is a hydrophobic helix that masks the hydrophobic groove formed by the BH3 domains. This is in the conformation adopted by Bax in its inactive cytosolic form. And this is why Bax was the first protein from the Bcl-2 multidomain protein for which the structure of the full-length protein has been resolved. Bcl-x_L was crystallized without helix α9, and Bid does not display a transmembrane domain. Apart from these 3 helices, there is another domain of the protein shown to play a vital role in the translocation. This domain termed as "Apoptotic Regulation of Targeting" (ART) consists of the first 19 residues of Bax that precede the α1-helix (Goping et al., 1998). The structural reorganization of this domain is required for the mitochondrial translocation of Bax. The

BH3 domain of Bax resides in the α2 helix and is involved in the hetero dimerization with other Bcl-2 members (Kelekar and Thompson, 1998) and in homooligomerization (Bleicken et al., 2010b).

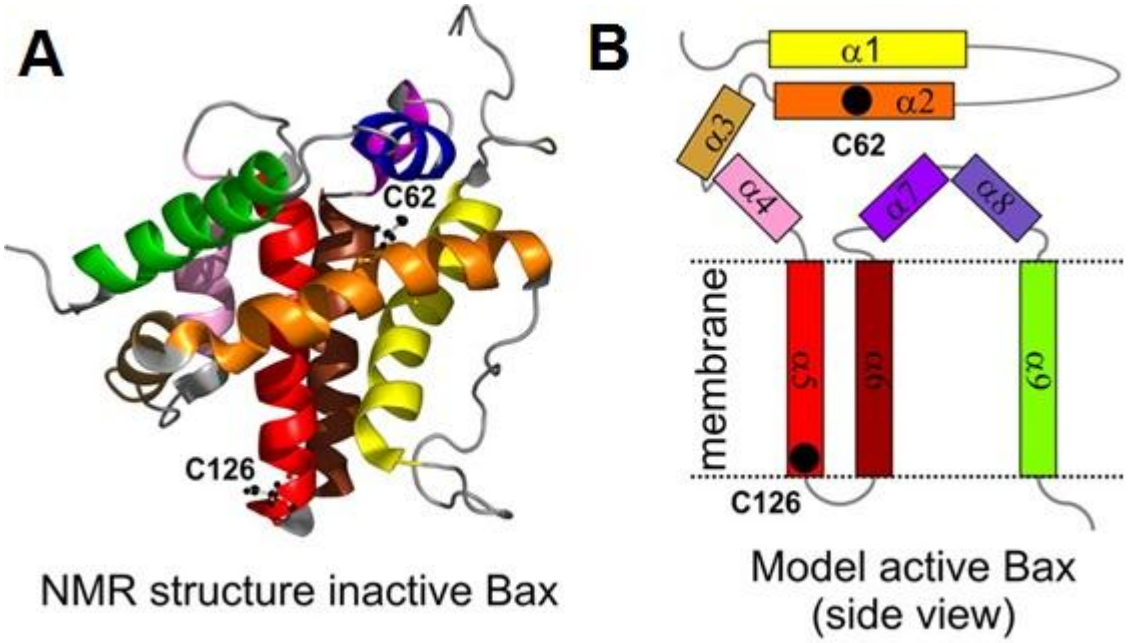

Figure.3.4. Monomeric Bax and putative models for the activated state. A), ribbon diagram of the NMR structure of Bax in the inactive monomeric form (Protein Data Bank code 1F16 (14)). The *color code* is shown in *B*. The two native cysteines (Cys-62 and Cys-126) are represented as *ball-and-stick* models (Cβ–Cβ average distance, 2.6 nm). B), putative model of Bax inserted in the membrane obtained from cysteine scanning analysis (Bleicken et al., 2010a).

After engagement of the TNF/Fas receptors, the pro-apoptotic BH3-only protein Bid is cleaved by caspase-8, resulting in the truncated form of the protein, tBid and its translocation to the MOM. *In vitro*, tBid induces a conformational change in Bax leading to the exposure of the N-terminal residues, followed by insertion of the Bax protein into the MOM (Roucou et al., 2002). In order to insert into the mitochondrial membrane, helix α9 has to be displaced from the hydrophobic pocket (Gavathiotis et al., 2010; Zhang et al., 2010). And indeed, as a consequence of the conformational change at the N-terminus, the dislocation of helix α9 from the hydrophobic core of the protein occurs leaving the BH3 domain of Bax exposed (Gavathiotis et al., 2010). Because of this, another Bax molecule can bind to this rear pocket and get activated leading to formation of higher

order Bax oligomers in asymmetric fashion. In contrast to this, some biochemical studies have suggested that Bax forms oligomers via symmetric dimers (Bleicken et al., 2010a; Kim et al., 2009). Here, the oligomerization of Bax starts when the BH3 domain of one monomer is exposed and engages the binding groove of another activated monomer, forming "BH3-groove" dimers. The BH3-groove dimers further oligomerize by helix 6/ helix 6 interactions (Dewson et al., 2009; Dewson et al., 2008; Dewson et al., 2012). Recently, a domain-swapped dimer of Bax has been proposed, where helixes from α6- α8 ("latch domain") are swapped between two Bax molecules. In addition, the authors have shown that α1- α5, termed as the "core domain", can form dimers in a symmetric fashion (Czabotar et al., 2013). However, the oligomerization of Bax leading to MOM permeabilization is still a mystery. Currently there is no structural information available for the activated form of Bax.

3.2.2. Bax and mitochondrial lipids

As mentioned earlier, Bax targets the MOM during apoptosis. This preference raises questions like why Bax selectively targets and permeabilizes the MOM and not any other cellular membranes or if it has any specific receptor in the mitochondria. The lipid composition of the MOM is very much similar to that of Endoplasmic reticulum (ER) except the presence of cardiolipin (diphosphatidylgylcerol). This phospholipid is specific to mitochondria and the signature lipid of the inner membrane of mitochondria. In eukaryotic cells, the inner mitochondrial membrane (IMM) contains 5-10% of cardiolipin and outer mitochondrial membrane (MOM) contains 20% of cardiolipin (Hoch, 1992; Schlame and Greenberg, 1997; Schlame and Hostetler, 1997). Because of their ability to assemble in to inverted micelles (Hexagonal structure H II), it has been proposed that cardiolipin could stabilize the contact sites between the membranes. Although phosphatidylglycerol can provide the same surface charge density as cardiolipin, it cannot assemble into H II structure and therefore it cannot help the formation of contact sites (Hoch, 1992). Several studies have shown that cardiolipin does not play a crucial role in the mitochondrial localization of Bax (S.L. Iverson, 2004), but that it is needed for the mitochondrial localization of tBid (Lutter et al., 2000), the activator of Bax (Renault and Manon, 2011; Roucou et al., 2002). Kuwana *et.al* proposed that Bax forms larger pores only in the presence of cardiolipin. In their studies, they observed that the binding of Bax

was similar to liposomes with or without cardiolipin but the increased release of vesicular contents happened only in the cardiolipin containing liposomes (Kuwana et al., 2002). Furthermore, in a recent study, it has been shown that cardiolipin might play a role in the activation of Caspase- 8 (Gonzalvez et al., 2008) in the extrinsic pathway of apoptosis by acting as a receptor for the pro-caspase-8. Moreover, cardiolipin is required for Drp1-dependent membrane hemifusion that would help Bax-oligomerization (Montessuit et al., 2010).

The concentrations of cardiolipin at the MOM determined from the mitochondria of rat liver and yeast ranges from 0.3 and 1.4% of the total phospholipids respectively. But the liposomes used for in vitro studies usually contain 4-40% of cardiolipin, which exceeds the fractions measured in MOM. However, since cardiolipin in enriched in the contact sites between the outer and inner membrane, the local concentration may be high enough to promote Bax activation (Lutter et al., 2001). Several other studies have proposed that outer mitochondrial proteins such as VDAC, the TOM receptor complex or the fusion and fission machinery could act as receptors for Bax targeting to mitochondria. Another family of lipids has recently emerged as a possible regulator of the function of Bcl-2 family. A neutral sphingomyelinase was identified from the purification of microsomal fractions that promote MOMP by Bax. Chipmuk et al recently showed that Bax interacts with hexadecenal, a sphingolipid metabolite that leads to the structural rearrangements of Bax that take place during apoptosis (Chipuk et al., 2012).

3.2.3. Pore formation by Bax

Several biochemical and biophysical methods have been employed to understand whether oligomerized bax has direct effects on the membrane and if it is capable of forming pores that allow the passage of large proteins across the MOM. There was a hypothesis in earlier times that Bcl-2 proteins target the pre-formed pore (permeability transition pore) in mitochondria (Vander Heiden et al., 1997). But later studies support that Bcl-2 family doesn't use this mechanism to permeabilize MOM (Nakagawa et al., 2005; Tsujimoto and Shimizu, 2007). A patch clamp analysis with isolated mitochondria from cells undergoing apoptosis showed that Bax oligomers form a protein channel termed as mitochondrial apoptosis-induced channel (MAC) (Dejean et al., 2005). In the

presence of anti-apoptotic proteins, MAC could not be formed. An identical channel was also observed with MOM of yeast cells expressing human Bax providing further evidence that Bax is responsible for the formation of large channels with sizes that allow the passage of 12.5 kDa cytochrome c.

Model systems like planar lipid bilayers or liposomes were used to determine the size of the apoptotic pore. The estimated pore diameter is 4 nm comprising minimum of four Bax molecules (Saito et al., 2000), however the pore diameter and number of Bax molecules differs. For example, the MAC pore formed by Bax is proposed to comprise 9 molecules with a diameter of 6 nm (Martinez-Caballero et al., 2009). Supramolecular pores with more than 100 Bax molecules were also observed (Nechushtan et al., 2001; Zhou and Chang, 2008). In GUVs, the size of the Bax pore has been measured as 7 ± 3 nm and the size of the bax pores are tunable depending on protein concentration (Bleicken et al., 2013a; Bleicken et al., 2013b). Since pores of varying size are observed, it is not easy to speculate that Bax forms toroidal pores or proteinaceous pore. The structure of activated Bax is required for a better understanding of the pore formation by Bax. In this dissertation, we have employed single molecule microscopy to elucidate the oligomeric state of Bax using model systems.

Chapter 4

The experimental approach

4. Single particle tracking

Over the last decade, single-particle and single-molecule techniques have become essential tools in the fields of biophysics and cell biology (Weiss, 1999). The reason for their emergence as a remarkable tool for studying the dynamics of biological processes is because they provide crucial information that is averaged out in other traditional ensemble methods. In many cellular processes, several individual molecules come together and interact in order to transmit information or to respond the environmental cues. Hence, it is very important to understand the mechanism by which the motion of related molecules is regulated in the cell. However, molecular behavior is very inhomogeneous, and even molecules of a single species interact stochastically with distinct molecules or cellular structures in a variety of local environments. Approaches such as FRAP (Axelrod et al., 1976) or even fluorescence correlation spectroscopy (Kusumi et al., 2004) can only report on the tendency of molecular behavior averaged over all molecules under observation and may not be able to distinguish various stochastic processes occurring in very inhomogeneous environments. Single particle tracking (SPT) has the advantage of being able to view individual characteristics of a molecule that may be washed out in the ensemble averaging inherent in bulk studies.

The first SPT experiment was performed in 1982 by Barak and Webb to follow the lipoprotein receptor (Barak and Webb, 1982). The technique was further improved in later years (Schnapp BJ, 1988; Sheetz and Kuo, 1993). A large body of work on imaging and tracking of single lipid molecules on artificial and cell membranes was catalyzed by Schutz and coworkers (Schutz et al., 1997). Later on, the technique was further developed to track particles in 3D with different strategies (Digman and Gratton, 2009; Katayama et al., 2009; Ragan et al., 2006).

SPT relies on the specific attachment of a probe, usually fluorescent, to the proteins or lipids of interest, followed by the detection of its position as a function of time with 30–100 Hz acquisition frequency and spatial resolution of 10–40 nm. It provides an improved resolution compared to the usual resolution of a light-focusing microscope, which is limited to $k / 2NA \approx 200–500$ nm, where k is the light wavelength and NA the numerical aperture of the lens (Kusumi et al., 2004). In this section, we aim to provide the

theoretical principles of SPT and briefly discuss about their applications in membrane dynamics.

4.1. Fluorescent labels for single particle tracking

Several strategies have been developed for single particle detection, which differ in the nature of the probe, the linker used to attach it to the molecule of interest and the detection mode. They are more or less adapted depending on the location of the protein or lipid of interest (e.g. cytoplasmic or external membrane layer) and the temporal and spatial resolution needed. One of the main constraints in single-molecule detection is the ability to obtain a high signal-to-noise ratio (SNR), which depends on the photo physical properties of the probe itself and the optical system used to monitor the signal. To date, the most popular probes used are quantum dots (QDs) and organic dyes (Fernandez-Suarez and Ting, 2008).

4.1.1. Quantum dots

Quantum dots (QDs) are nanometer-sized semiconductor crystals surrounded by a ZnS shell (Michalet et al., 2005). The diameter of the optically active inorganic core varies between 2 and 10 nm. The photophysical properties of QDs have made them a major probe for single-molecule tracking (Jaiswal and Simon, 2004). Once solubilized and functionalized, QDs can be used as biological fluorescent probes although, due to their crystalline nature, they have distinct optical properties compared to conventional organic fluorophores or fluorescent proteins (Carter et al., 2005). In particular, their extinction coefficient often exceeds 10^6 in the visible spectrum, which means that they are bright emitters that can be detected individually, with a high SNR (up to 25), even under standard wide-field illumination. Their narrow emission wavelength, which is dependent on the QD core size, gives access to the whole visible spectrum with high spectral resolution, allowing multicolor imaging. In addition, they have excellent photostability, which allows recording over a period of time from milliseconds to several minutes. However, QDs present some properties that can be problematic. The main issue limiting their use is their large size, several times larger than that of the molecule to which they are attached. It is therefore crucial to check that the function and behavior of the molecule of interest are not essentially modified by linking the QDs. Moreover, they can change between ‘on’ and ‘off’ states, a phenomenon called blinking, which complicates the

particle tracking. On the positive side, this ensures the identification of single QDs because signals alternate between 0 and 1, and would be fractional in the case of multiple QDs. QDs functionalized with biotin, streptavidin or IgG are commonly used and are commercially available (Cheezum et al., 2001) .

4.1.2. Organic fluorophores

Organic dyes are much smaller fluorescent probes (< 1 nm) and can be easily coupled to any ligand. These dyes can be attached, using well-established conjugation protocols, to a large variety of biomolecules, including proteins, lipids, nucleic acids, and sugars (Saxton, 1993). Organic fluorophores exhibit a conjugated π-electron system for absorption in the visible or near-visible spectrum. Single-molecule studies have used fluorophores that absorb above 450 nm. These fluorophores can be classified into groups such as rhodamine, cyanine, oxazine, bodipy, and perylene. Further development was made with the introduction of functional groups for labeling (NHS, maleimide, hydrazide), sulfonic or carboxylic acid to increase water solubility and blocking reactive positions to increase the photostability. The use of high numerical aperture objectives, appropriate filter sets with high light transmission, and electron-multiplying charge coupled devices (EMCCD cameras) enhances the fluorescence detection efficiency of organic dyes. Moreover, the background noise can be improved by using total internal reflection microscopy (TIRF). A TIRF microscope uses an evanescent wave to selectively illuminate and excite fluorophores in a restricted region of the sample immediately adjacent to the glass-water interface. The evanescent wave is generated only when the incident light is totally internally reflected at the glass-water interface. The evanescent electromagnetic field decays exponentially from the interface, and thus penetrates to a depth of only approximately 100 nm into the sample medium (see section 4.2 for details). This greatly improves the signal-to-noise ratio (SNR) (Sako and Uyemura, 2002) .

4.1.3. Fluorescent proteins

Fluorescent proteins (FPs) are small 25–30-kDa proteins that can be attached to any protein of interest as genetically encoded fluorescence markers. The first member of this family was green fluorescent protein (GFP), which is composed of 238 amino acid residues (26.9kDa) and isolated from the jellyfish *Aequorea victoria*. A number of

fluorescent reporters and sensors such as GFP and its many variants can be prepared and inserted into the genome. The availability of a broad selection of colors for fluorescent proteins (Shaner et al., 2005) has provided researchers with the means to image the localization of proteins-of-interest (Rizzuto et al., 1995). Due to this, there was a rapid increase in the applications of these labels in single-molecule biophysics.

4.2. TIRF Microscopy

TIRF was first introduced by Hirschfeld in 1965 for selective surface illumination at a solid/liquid interface. Further developments was made by Axelrod (Axelrod, 1984, 1983), Reichert (Reichert, 1989), Truskey (Reichert, 1990) and Burmeister (Burmeister et al., 1994) (see Burmeister et al., 1998). TIRF microscopy is based on the total internal reflection phenomenon that occurs when a light beam passes from a medium with a high refractive index n_1 into a medium with a low refractive index n_2. At the interface, the light will bend and travel along the interface if the incident angle is equal to the critical angle. If the incident angle is higher than the critical angle, the light will turn back into the high refractive medium and only a short-range electromagnetic disturbance called the evanescent field will pass into the low refractive medium. The evanescent field intensity (*I*) decreases exponentially with distance from the interface *(Z).* As a result, high-contrast images of the near-glass area are obtained with maximum penetration depth of 100 to 200 nm. Normally TIRF images have very low background, which makes it a very suitable technique for single particle tracking (Fig.4.1).

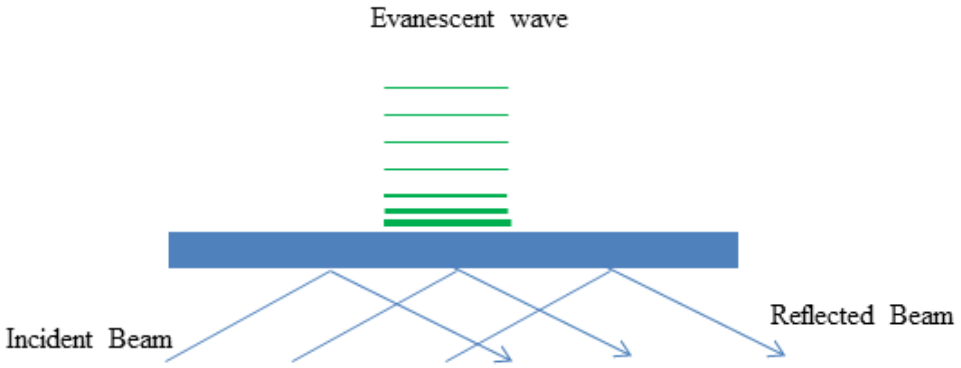

Figure.4.1. Principle of TIRF: the excitation beam enters from the left at an incidence angle θ, which is greater than critical angle θ_c. The excitation beam is then reflected off the coverslip-sample

interface and an evanescent field is generated on the glass surface that illuminates the sample with 100-200 nm depth.

The critical angle, depth of evanescent waves and intensity at depth can be calculated with the equations below. The critical angle $\theta_{c,\,is}$ given by Snell's law:

$$\theta_c = sin^{-1}\left({}^{n_1}/_{n_2}\right) \qquad (1)$$

The depth of the evanescent field, *d*, refers to the distance from the cover slip at which the excitation intensity decays to 1/e, or 37%, of I_0. Depth *d* is defined by:

$$d = {}^{\lambda_0}/_{4\pi}\left(n_2{}^2 sin^2\theta - n_1{}^2\right)^{-1}/_2 \qquad (2)$$

where λ_0 is the wavelength of the excitation light in a vacuum. Typical values for *d* are in the range 60–100 nm. The intensity of the evanescent field at any position *z* is described by:

$$I_z = I_0{}^{-z}/_d \qquad (3)$$

where I_0 (initial intensity) is the intensity of the evanescent field at *z*= 0 (Axelrod, 1989) and I_Z is the intensity at depth z (Trache and Meininger, 2008).

4.3. Single-Molecule and Single-Particle Detection

A wide-field fluorescence or a TIRF microscope are usually used for tracking moving molecules and objects. Under these conditions, an isotropic emitter that is smaller than the diffraction limit will appear as a diffraction-limited spot in the image plane. The image of the emitter is characterized by a symmetrical signal distribution around the center, with the maximum intensity at the center of the spot. The intensity distribution *I* (x, *y)* of such an object on a highly sensitive charge-coupled device (CCD) or a EM-CCD camera, as used in SPT experiments, is determined by the point spread function (PSF). An approximation of the PSF is given by a 2D Gaussian with a full-width-at-half-maximum (FWHM) equal to *w*=1.03 λ /NA (Anderson et al., 1992; Schmidt et al., 1995; Zhang et al., 2007):

$$I(x,y) = N\frac{4ln2}{\pi w^2}\exp\left[-4ln2\left(\frac{(x-\mu_x)^2}{w^2}+\frac{(y-\mu_y)^2}{w^2}\right)\right] \qquad (4)$$

where μ_x *and* μ_y are the *x* and *y* coordinates of the object, and *N* is the total number of detected photon - counts. Even though the size of the generated image, *w*, is larger than the object, the position of the object is determined with nanometer precision (Thompson et al., 2002).

Image pre-processing and reliable background subtraction is necessary for an accurate identification of individual molecules. Especially in living cells, it is complicated to identify the molecule because of out-of-focus problems and auto-fluorescence. After background subtraction, particle detection and localization analysis is performed. The main algorithms used for this purpose involve cross-correlation (Bachir et al., 2006; Gelles et al., 1988; Kusumi et al., 1993b), centroid (Ghosh and Webb, 1994) or Gaussian fits (Fernandez-Suarez and Ting, 2008). A simple and rapid way of determining the position of the object is calculating the center of mass, or centroid, of its image for each axis:

$$\mu_x = \sum_{i=1}^{M_y}\sum_{j=1}^{M_x}(x_i.I_{ij}) \Big/ \sum_{i=1}^{M_y}\sum_{j=1}^{M_x} I_{ij} \qquad (5)$$

where $\mathbf{I}_{ij}$ is the signal at a pixel (*i* , *j*) (Carter et al., 2005; Cheezum et al., 2001). Since this method does not require any prior knowledge about the shape of the intensity profile, it can be used to analyze objects with imaging errors or objects that are larger than the diffraction limit (Falcon-Perez et al., 2005). However, when considering a single molecule labeled with a fluorescent probe with sub-wavelength size, then a two-dimensional Gaussian fit on thresholded images provides the best results in terms of localization, even at relatively low SNR (< 4). This is done by fitting the image to the 2D Gaussian intensity profile of the PSF, as explained in Equation 9. A fit of the intensity distribution to Equation 9 determines the position of the object with nanometer precision (Schmidt et al., 1996a; Thompson et al., 2002). The accuracy is thereby inversely proportional to SNR and is approximated by $w/\sqrt{8N\ln 2}$ (Holtzer et al., 2007). This

approximation assumes that additional noise due to background signals is negligible. In typical applications using fluorescent proteins, a positional accuracy of < 30 nm can be achieved (Bobroff, 1986; Lommerse et al., 2002).

A very low concentration of fluorescent molecules is normally used in single molecule fluorescence experiments, so that only a few molecules are visible in an image of typical size (10×10 μm^2). When they are at low densities, the distance between each molecule is sufficiently large (> 3 *w)* and their intensity profiles are independent. However, if such low densities are not achievable, then a recursive fitting approach must be applied. Several of these recursive runs are required to obtain the correct position and intensity of all individual molecules. In this way, densities of up to one molecule per μm^2 can be reliably handled (Serge et al., 2008)(Fig.4.2).

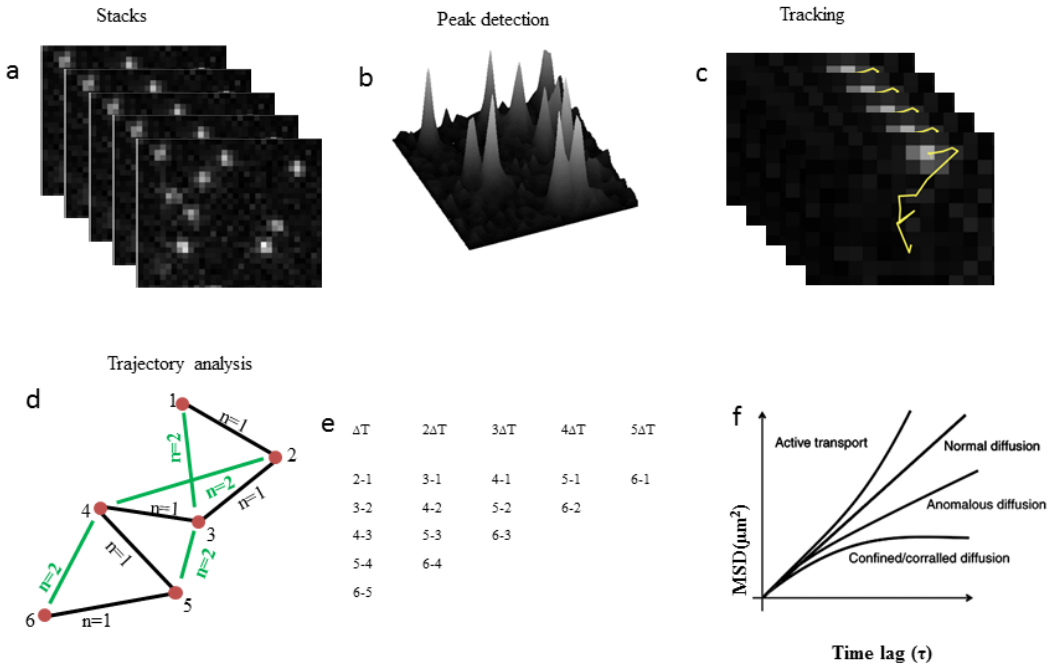

Figure.4.2.: Single particle tracking: a) Stack of images obtained with the microscope, b) Particles detected are analyzed with a 2-D Gaussian fit, c) Detected particles are tracked through successive frames, d), e) Trajectory analysis for the traces obtained in c), and f) different modes of diffusion.

4.4. *Tracking*

The process of reconstructing trajectories consists of linking the position of a particle at a given time frame to its position in the next frame. The linking procedure can be carried out using efficient automatic algorithms. However, the final trajectories have to be checked manually. Tracking is much easier for the particles that are sparsely distributed and slowly diffusing (Geerts et al., 1987; Ghosh and Webb, 1994), whereas for large particle densities per frame and with higher mobility, the process gets complex (Cheezum et al., 2001). Therefore a high computational effort is required. The current tracking algorithm is based on a numerical approximation developed by Vogel (Reinfeld 1958). According to this, a translational matrix $p_i(j,k)$ is built up that describes the probabilities that a particle j in an image i (containing L objects) at position $\vec{r}_{j,i}$, moves to particle k in image $i + 1$ (containing M objects) at position $\vec{r}_{k,i+1}$ by diffusion in a d-dimensional system characterized by a diffusion constant D :

$$P_i(j,k) = exp\left\{-\frac{\left(\vec{r}_{j,i} - \vec{r}_{k,i+1}\right)^2}{2dDt}\right\} \qquad (6)$$

The process of automating trajectory reconnection requires robust criteria of assignment such as spot sizes, explored distances, intensities etc. and must be able to reject uncertain trajectories efficiently. Algorithms to circumvent these issues have recently been published, and dealt particularly with blinking (Bachir et al., 2006; Reinfeld 1958), signal-to-noise ratio and threshold in spot detection, as well as with automation of detection and tracking (Jaqaman et al., 2008; Serge et al., 2008). As mentioned earlier, when the density of tagged molecules is high, a recursive detection algorithm can be used to discriminate particles whose fluorescent spots would merge transiently during their trajectories. It becomes difficult to link the particles when they can cross over, merge, split, interact, blink (in the case of QDs) or bleach. In order to solve these problems, a multiple-hypothesis tracking algorithm has been developed, which tends to determine the largest non-conflicting ensemble of trajectories via a temporally global optimization incorporating the history of every single trajectory (Jaqaman et al., 2008). Being able to carry out SPT at a high density of labelled single molecules is an important challenge in order to obtain statistically relevant samples including minor populations of biologically

relevant behaviors. In addition, studying transient interactions at the level of single molecules requires high density of labeling to improve the probability of detecting such events (Fig.4.2).

4.5. Trajectory analysis

A straightforward method to obtain information regarding the mobility of an object is by calculating its mean square displacement (MSD) versus lag time. For each trajectory of a particle, the two-dimensional MSD, for every time interval was calculated according to the formula (Gross, 1988; Lee et al., 1991b),

$$MSD = \langle (\Delta r_t)^2 \rangle = \frac{\sum_{i=1}^{T-t} (r_i - r_{i+1})^2}{T - t} \qquad (7)$$

where T is the total length of the trajectory in time. The type of diffusion of the object can be extracted from the MSD versus lag time plot. In case of simple two-dimensional Brownian motion, the MSD is related to the diffusion coefficient D by:

$$MSD(\Delta t) = 4D\Delta t \qquad (8)$$

Therefore, a linear relationship between MSD and lag time indicates free Brownian motion. For the other models of diffusion see table 4.1. Here V is the velocity, α is the anomalous factor and <1, r_c^2 is the confinement size, A_1 and A_2 are constants determined by the confined geometry (Saxton and Jacobson, 1997).

The probability density $p(r^2,t_{lag})$ is the probability that a particle at the origin at time zero will be found in a circle of radius r after a time t_{lag}. For the 2D case, the cumulative distribution function (*cdf*) for the squared displacements r^2 is

$$P(r^2, t_{lag}) = 1 - \exp\left(-\frac{r^2}{MSD(t_{lag})}\right) \qquad (9)$$

The *cdf* is very useful for a system where there are two fractions of a certain particle, which experimentally are only distinguishable by their different *D* values (Deverall et al.,

2005; Lommerse et al., 2002; Schutz et al., 1997). For two fractions, Equation 14 becomes

$$P(r^2, t_{lag}) = 1 - \left[\alpha . \exp\left(-\frac{r^2}{MSD_1(t_{lag})}\right) + (1-\alpha) . \exp\left(-\frac{r^2}{MSD_2(t_{lag})}\right)\right] \quad (10)$$

where α indicates the fraction size, and $MSD_1(t_{lag})$ and $MSD_2(t_{lag})$ are the two MSD values at t_{lag} , respectively.

Type of diffusion	Model
Normal diffusion	$MSD(\Delta t) = 4D\Delta t$
Directed motion with diffusion	$MSD(\Delta t) = 4D\Delta t + v^2(\Delta t)^2$
Anomalous diffusion	$MSD(\Delta t) = 4D\Delta t^{\alpha}$
Confined diffusion	$MSD(\Delta t) = \langle r_c^2 \rangle [1 - A_1 exp(-4A_2 Dt/\langle r_c^2 \rangle)]$

Table 4.1: Diffusion models

4.6. Single molecule stoichiometry analysis

An application of single molecule imaging apart from learning about dynamics of molecules is to determine the stoichiometry based on the fluorescence intensity of the molecule. This method provides an opportunity to study local stoichiometries and aggregation in complex systems such as biomembranes (Meckel et al., 2011b; Schmidt et al., 1996b). In this method, individual particles are detected and the fluorescence intensity of each particle is estimated by fitting a 2-D Gaussian and averaging from the beginning of the movie till they are photobleached in a control experiment. The number of bleaching

steps indicates the number of fluorophores. By fitting a Gaussian curve to the distribution of fluorescence intensities, the mean intensity μ and standard deviation σ of a single fluorophore can be calculated. With μ and σ, the fluorescence intensity of N colocalized fluorophores can be given by $\mu_N = N\mu_1 \pm N^{1/2}\sigma_1$. The number of Gaussians that can be fitted to the distribution of fluorescence intensity is estimated according to (Schmidt et al., 1996b),

$$N_{max} = (\mu_1/\sigma_1)^2 \quad (11)$$

The distribution of the fluorescence intensity of all the particles is globally fitted with a sum of Gaussians (estimated according to equation (11)) using obtained μ and σ values. The Gaussian model used for the fit is given by:

$$\varphi(i) = \sum_{n=1}^{N_{max}} A_n \cdot \frac{1}{\sigma\sqrt{2\pi}} e^{-\frac{(i-\mu.n)^2}{2(\sigma.n)^2}} \quad (12)$$

where $\varphi(i)$ is the frequency of particles having intensity i, n is the component number and A_n is the area under the curve of component n. The area A under the curve of each component is used to estimate the percentage of occurrence of each species as described in (Calebiro et al., 2013).

In case of immobile particles, the fluorescence intensity measured for each particle over time can be used for photobleaching analysis. The number of bleaching steps provides the information about the stoichiometry of the particle (Thompson et al., 2011). Recently, a method called TOCCSL (Thinning out clusters while conserving stoichiometry of labeling) for the stoichiometric analysis of molecular aggregates in the cellular plasma membrane has been developed (Moertelmaier et al., 2005). The fluorophores within a small region of plasma membrane are selectively photobleached, whereas the fluorophores in the remaining part of the membrane are undisturbed. Due to diffusion, the photobleached area is repopulated which can be an individual molecule or aggregates. These molecules are then quantified for their stoichiometry (Brameshuber and Schutz, 2012).

4.7. Applications

SPT has been widely used to study protein diffusion, the effect of post-translational lipid modifications and raft affinity (Douglass and Vale, 2005), protein–protein interactions (Suzuki et al., 2007a; Suzuki et al., 2007b), and the actin cytoskeleton (Andrews et al., 2008). SPT was used to assess the contribution of lipid modifications on protein dynamics on the surface of T cells. Palmitoylation of LAT or dual acylation of the Src-family kinase Lck did not alter their diffusion significantly, but when these signaling proteins are trapped in cholesterol-independent clusters of the co-receptor CD 2, their diffusion slowed down up to two-fold (Douglass and Vale, 2005). Two-color SPT helps greatly with detecting differential modes of movement. In the case of the T cell plasma membrane, protein–protein interactions have to be taken into account for the interpretation of modes of motion, as it is likely to be the case also for other cell types where stimulation of surface receptors results in multi-molecular protein complexes. Dual-color tracking of the GPI-anchored receptor CD59 in the outer leaflet and signaling proteins anchored to the inner leaflet also revealed how ligand clustering of the receptor induces temporary immobilization domains, termed STALLs (stimulation-induced temporary arrest of lateral diffusion) that serve as short-lived platforms for signaling activities (Suzuki et al., 2007a; Suzuki et al., 2007b). Pinaud et al used dual-color TIRF imaging and single-quantum dot tracking, to quantify the lateral diffusion and interactions of GPI-avidin with glycosphingolipid GM1-rich microdomains and with caveolae on the plasma membrane. Their study revealed that GPI-anchored avidin can dynamically partition in and out of GM1-rich microdomains, which are in close proximity to, but distinct, from caveolae. The partitioning was characterized by changes in diffusion coefficients and was cholesterol-dependent. Their observations provided direct evidence that membrane microdomains which have the proposed composition of lipid rafts induce molecular compartmentalization in the plasma membrane (Pinaud et al., 2009).

Membrane receptors or membrane associated proteins have been widely studied using SPT. SPT revealed the dynamics of Fcε RI receptors with non-bleachable quantum dots (Andrews et al., 2008). Different modes of motion – immobile, free, directed, and confined – were all observed for the same receptor. Confined motion was attributed to the presence of the actin cytoskeleton, which was indeed found to dynamically confine the receptor into micron-sized domains. Transient confinement zones (TCZs), detected by

SPT, define areas where an observed molecule stays much longer than expected from the average diffusion coefficient and is thought to bear some resemblance to lipid rafts. TCZs are typically 200–300 nm in diameter (Simson et al., 1998), preferentially trap GPI-anchored proteins and glycosphingolipids (Sheets et al., 1997), and are cholesterol dependent (Dietrich et al., 2002). Yet, whether viscosity differences inside and outside the raft are sufficient diffusion barriers is questionable (Dietrich et al., 2001), particularly since TCZs appear to be temperature independent (Dietrich et al., 2002).

Lommerse et al. tracked fluorescent fusion constructs of only the membrane anchor regions of H-Ras (raft), K-Ras (non-raft), and Lck (raft). The three constructs had similar diffusion coefficients, but two populations of diffusing molecules were observed (Lommerse et al., 2006). The major population displayed similar diffusion times to small molecule membrane dyes (0.6–1.6 μm^2/ s); however, a second population (16% for Lck and 27% for K-Ras) was confined to domains roughly 200 nm in size. In addition, the authors found out that cholesterol depletion did not affect the confinement. For H-Ras, the mobile fraction was 73% with a diffusion coefficient of 0.53 μm^2/ s (Lommerse et al., 2002). Interestingly, the 200 nm confinement of the slow-diffusing fraction was only observed for active (GTP-bound, 'raft-associated') K-Ras, not the inactive (GDP-bound) form, suggesting that confinement is not solely controlled by lipid–lipid interactions. Similar confinement has been reported for a G-protein coupled odorant receptor with ~50% of the receptor being confined to larger domains (300–550 nm), ~30% in small domains (180–200 nm), and the remaining 20% being either immobile or diffusing freely (Jacquier et al., 2006). For a different G-protein-coupled receptor, the μ-opioid receptor, Daumas et al. found that 90% of the receptors diffuse within a domain that diffuses itself, a motion they termed as walking confined diffusion. Taken together, these studies suggest that confinement areas are unique to each of the observed receptors, thus implying that specific receptor interactions define these zones rather than generic 'raft domains'(Daumas et al., 2003). Another study showed that unstimulated β_1- and β_2AR are immobilized in the plasma membrane of H9c2 cardiomyocyte-like cells. Their complex formation is mediated by carboxy-terminal PDZ domain and AKAP interactions and not by association with caveolae (Sieben et al., 2011).

By developing SPT with ultra-high temporal resolution (25 μs instead of the typical video rate of 30 ms), Aki Kusumi was able to detect a different types of diffusion, termed

'hop diffusion', in which the entire membrane is compartmentalized into 30–250 nm-sized compartments. Proteins and lipids are slowed down as they hop from one compartment to the next, but within each compartment diffusion is not significantly lower than that observed for free diffusion. Hence, these membrane compartments are distinctly different to TCZs formed by lipid microdomains and are thought to be the result of an underlying membrane skeleton to which transmembrane proteins are anchored creating a 'picket-fence' within the membrane (Morone et al., 2006). It should be remembered that distinguishing between Brownian motion and hop diffusion requires a time resolution of tens of microseconds, without which hop diffusion is simply interpreted as free diffusion with a slower average diffusion coefficient. Renner et al. applied SPT on curved geometries (GUVs) inorder to analyze the diffusion of lipid on model tubular membranes (Renner et al., 2011). The authors observed that 2D-SPT over the tubular surface provided a diffusion coefficient that is 25 to 50% lower than the real *D* and the diffusion strongly depends on the diameter of the tube.

Chapter 5

Aims of this work

5. Aims of this work

In general, pore-forming proteins oligomerize to form a pore after binding to the target membrane. Till date, the structural information on the oligomeric state of the pore is available only for a very few of them. In this work, we focus on the biophysical characterization of the mechanism followed by two proteins forming toroidal pores: Equinatoxin II and Bax, for which the final oligomeric state of pore remains unknown. As the oligomeric complexes formed by these proteins are very unstable, it is extremely difficult to obtain the structural information on the stoichiometry of the pore. To get a better understanding on the dynamics and oligomerization process of these proteins, the following objectives were proposed:

a) Characterization of the assembly mechanism of Equinatoxin II in living cells. For this we have used total internal reflection microscopy (TIRF) and followed the dynamics and oligomerization process of the protein on the cell surface.

b) Stoichiometry analysis of Bax oligomers in the lipid bilayer at the single molecule level. To address this, we have reconstituted a fluorescently labeled form of Bax in model membranes (planar supported lipid bilayers) and characterized the oligomeric state using TIRF microscopy.

c) Direct visualization of the interactions between Bcl-2 proteins. The activity and oligomerization of Bax highly depends on the interaction between other Bcl-2 proteins, like for example its activator Bid and inhibitor Bcl-xL. With this aim, we have used the proteins of interest labeled with fluorophores of two different wavelengths and analyzed their co-localization at the single molecule level with dual color total internal reflection microscopy.

Our results from this investigation can provide more information on the pore forming mechanism by Equinatoxin II and Bax that could generalized for other α-pore forming proteins.

Chapter 6

Materials and Methods

6.1. *Protein Purification and Labeling*

6.1.1. Equinatoxin II

We worked with a single cysteine mutant of EqtII at L26C purified as described in (Kristan et al., 2004; Malovrh et al., 2003b) and labeled with Alexa Fluor 555 C5 maleimide (Invitrogen) (EqtII-Al555) with a babeling efficiency of 86%, as determined by fluorescence spectroscopy with a Specord S 100 (Analytik Jena, Jena, Germany) (see (Garcia-Saez et al., 2011a) where the toxin was used). When we compared the activity of EqtII-L26C in hemolysis assays, we found that this mutant is less active than the wild type form, but labeling with Alexa555 partially recovered activity (Fig.6.1.) [Hemolysis assay done by Uris Lianne Ros]. The activity of EqtII-Al555 has been extensively characterized *in vitro* and *in vivo* systems (Garcia-Saez et al., 2011a; Schon et al., 2008) and reproduces all the important events described for wild type EqtII. Regarding the oligomerization studies here, the use of EqtII-Al555 was instrumental, as it induces cell death with slower kinetics, allowing us to follow the process of EqtII assembly with sufficient temporal resolution. EqtII L26C was a kind gift from Gregor Anderluh.

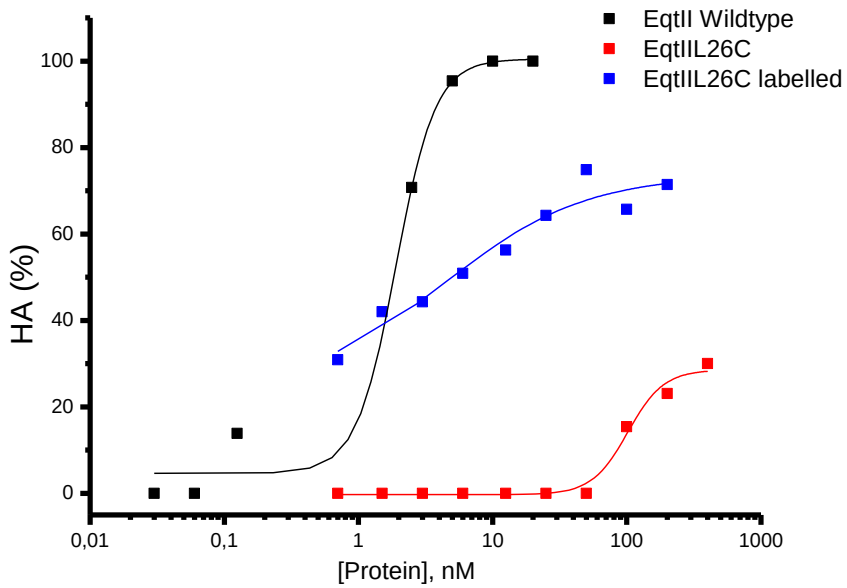

Figure.6.1. Comparison between the hemolytic activity of EqtII wild type, EqtII L26C and EqtII L26C labelled with Alexa 555.

6.1.2. Bcl-2 proteins

Full-length mouse Bid and human Bax, and single-cysteine mutants Bid C30S and Bax S4C, C62S, and C126S, as well as full-length human Bcl-xL C151A and S4C, were expressed in *Escherichia coli* and purified and, in the case of cBid, cleaved as described in (Bleicken et al., 2010b; Desagher et al., 1999). For tBid, Bid was cleaved *in vitro* with caspase 8 in 50 mM Hepes pH 7.5, 100 mM NaCL, 10 mM DTT, 1 mM EDTA and 10% (w/v) sucrose. Then tBid was separated from the N-terminal fragment with a NTA-agarose column and a combination of imidazole and octylglucoside gradients (Garcia-Saez et al., 2009b). Protein quality was checked by sodium dodecyl sulfate polyacrylamide gel electrophoresis and liquid chromatography-mass spectroscopy (micrOTOF LC, Bruker Daltonics, Bremen, Germany). Alexa (Invitrogen, Darmstadt, Germany) dyes were covalently attached to the cysteines of the mutants as described by the manufacturer. Proteins labelled with Alexa 488 are named Bax-Al488, Bcl-xL-Al488 and proteins labelled with Alexa dyes are named cBid-Al633 and tBid-Al647. Excess of label was removed with desalting columns (BioRAD, Munich, Germany). The activity of the labeled proteins was controlled with calcein release assays. Purification and labeling has been carried out by Stephanie Bleicken, Ana J. Garcia Saez and Carolin Stegmeueller.

6.2. Cell Culture

COS-1 cell is a cell-line derived from African monkey kidney tissue. COS-1 cells are obtained from CV-1 simian cells transformed by origin-defective mutant of SV40 which codes for wild type T Antigen. COS1cells were cultured in DMEM (high glucose; Sigma) with 10% fetal calf serum 1% antibiotics (penicillin and streptomycin) at 37 °C and in presence of 5% CO_2. All cells were regularly passaged at subconfluency and plated at 2–5 × 10^4 cells/ml density. For imaging experiments, the cells were seeded in LabTek chambers (Nunc). Experiments were carried out 24 or 48 h after seeding.

6.3. Glass Slide Preparation

The glass slides (24 mm x 60 mm, thickness=1, Menzel) used to prepare supported lipid bilayers were cleaned using a freshly prepared 3:1 mixture of

concentrated sulphuric acid (95−97 %, Baker) with hydrogen peroxide (30 %, Merck) via immersion for at least 1 h. The cleaning is specifically done in order to remove organic residues and to enhance hydrophilicity. Slides were thoroughly rinsed with deionized water and sonicated with deionized water for five minutes. Before further usage, they were dried using a clean nitrogen stream. Individual slides were glued on the upper part of the measurement chamber (Lab-tek 155411, Nunc, original borosilicate coverglass was manually removed) using glue**.** Chambers were used immediately for the preparation of supported lipid bilayers.

6.4. Lipid mixtures

All lipids were purchased from Avanti Polar Lipids. We used three different types of lipid mixtures for our experiments. In case of Equinatoxin II, we used DOPC (1, 2-dioleoyl-*sn*-glycero-3-phosphocholine), sphingomyelin and cholesterol in 4:4:2 ratios. For Bcl-2 proteins, EggPC (phosphatidylcholine) and cardiolipin in 8:2 ratio and mitochondrial like lipid composition (0.46 mg egg phosphatidylcholine, 0.25 mg egg phosphatidylethanolamine, 0.11 mg bovine liver phophatidylinositol, 0.10 mg 18:1 phosphatidylserine, and 0.08 mg cardiolipin) were used.

6.5. Planar supported lipid bilayers

The desired lipid mixtures were dissolved in chloroform. The solvent was evaporated under nitrogen flux and then subjected to vacuum for 1 h. Lipid mixtures were rehydrated to a final concentration of 10 mg/mL in 3 mM KCl, 1.5 mM KH2PO4, 8 mM Na2HPO4, and 150 mM NaCl, pH 7.2. A small aliquot of the multilamellar vesicle suspension (10 µl) was diluted in 140µl of 3 mM CaCl2, 150 mM NaCl, 10 mM Hepes, pH 7.4, The suspension was then vortexed and bath-sonicated until small unilamellar vesicles (SUVs) were obtained. The mixture was incubated at 37˚C for 2min and was rinsed several times with 150 mM NaCl, 10 mM Hepes (pH7.4) to remove the non-fused vesicles (Chiantia et al., 2005). Glass slides used for preparation of bilayers were treated with piranha solution (see section 5.3).

6.6. Large Unilamellar Vesicles (LUV)

Large unilamellar vesicles (LUV) were prepared as described in (Dalla Serra and Menestrina, 2003). Lipids were dissolved in chloroform, and mixed in an appropriate ratio. The organic solvent was evaporated using a dry nitrogen steam and vacuum dried for atleast 1h. The dried lipid film was resuspended with 150 mM NaCl, 10 mM Hepes (pH7.4) to a final concentration of 1mg/mL. To prepare LUVs, the lipid solution was passed through 5 cycles of freezing and thawing after which they were manually extruded (Fig.6.2) through a polycarbonate membrane of defined pore size (50, 100, 200, 400 nm) using glass syringes. The sample is passed through the membrane by pushing the sample back and forth between two syringes for about 31times. The LUVs were stored at 4^{o}C up to 2 days for later usage.

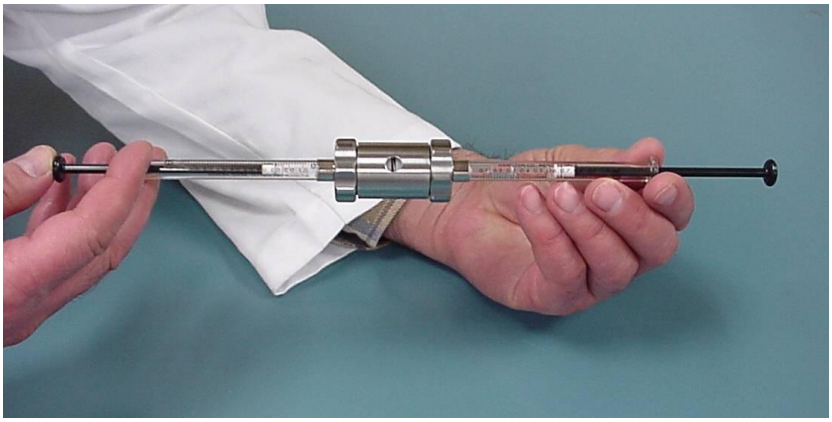

Figure.6.2. The fully assembled manual extruder used for preparing the large unilamellar vesicles. Image taken form the Avestin product webpage.

6.7. Giant Unilamellar vesicles (GUVs)

GUVs were prepared by the electroformation method (Dimitrov, 1986). To begin with, the electroformation chambers were cleaned with water, ethanol, and chloroform and air-dried. The lipids dissolved in chloroform were mixed at the desired ratios to reach a final concentration of 1mg/mL. About 2.5 µL of the lipid mixture was spread on each of the platinum wires attached to the cap of electroformation chamber (Fig.6.3. a). Once the lipid solution was dried, the cap is screwed to the electroformation chamber, which was filled with 300 µL of 300 mM sucrose solution. Then the cables from the power

generator were connected to the platinum wires (Fig.6.3. c). Electroformation proceeded at 1.2 V and 10 Hz for 2 h. Then it was kept at a frequency of 2 Hz for 30 min to detach the GUVs from the wires. GUVs were stored at 4^{o}C upto 2 days for later usage.

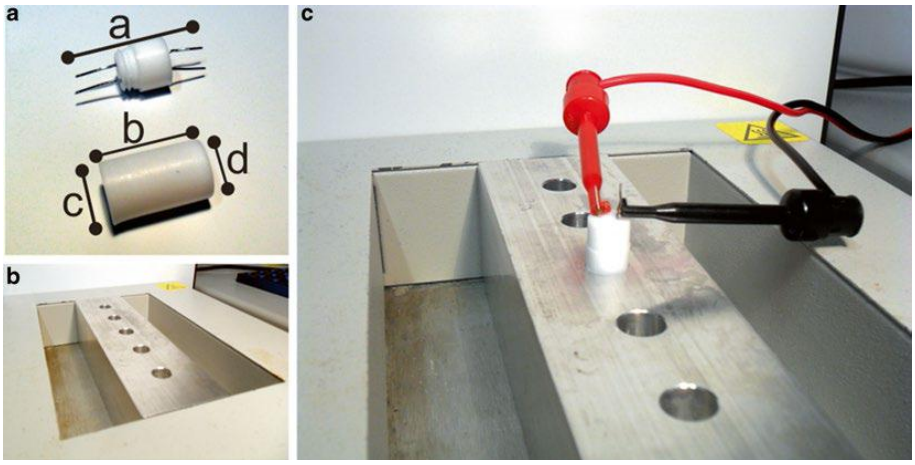

Figure.6.3. Electroformation chamber and setup. (a) A homemade Pt-and-teflon chamber with the following dimensions is shown: *a* 30 mm, *b* 15 mm, *c* 8 mm, *d* 4 mm. The distance between the two electrodes is about 4 mm. (b) Homemade aluminum block is shown. (c) The connection of the chamber to the function generator and the whole setup is shown (Unsay and Garcia-Saez, 2013).

6.8. Measurement of Vesicle Size

Large unilamellar vesicles extruded with membranes of pore size 50, 100, 200 and 400 nm were prepared as described in the section 5.5. About 500 µL of the liposome suspension was diluted up to 2 mL with sterile distilled water. After transferring the suspension to a clean disposable cuvette, vesicle size was measured using Dynamic Light Scattering (DLS) (Malvern Z-sizer). The Brownian motion of particles or molecules in suspension causes laser light to be scattered at different intensities. Analysis of these intensity fluctuations yields the velocity of the Brownian motion and hence the particle size using the Stokes-Einstein relationship.

6.9. Proteoliposomes

The liposomes of different sizes (SUVs, LUVs, and GUVs) were incubated with Bcl-2 proteins for 1h as follows: a) 2.5 nM of Bax-Al488 and 5 nM cBid unlabeled, b) 2.5 nM of Bax-Al488 and 5 nM cBid Al-633, c) 2.5 nM of Bax-Al488 and 5 nM tBid At-655, d) 2.5 nM of Bcl-xL-Al488 and 5 nM cBid Al-633, e) 2.5 nM of Bcl-xL-Al488 and 5 nM

tBid Al-647. After 1h incubation, these liposomes were used to prepare planar bilayers as described in section 5.4 (Fig.6.4.). Unbound protein and non-fused vesicles were removed by careful washing with buffer [150 mM NaCl, 10 mM Hepes (pH7.4)].

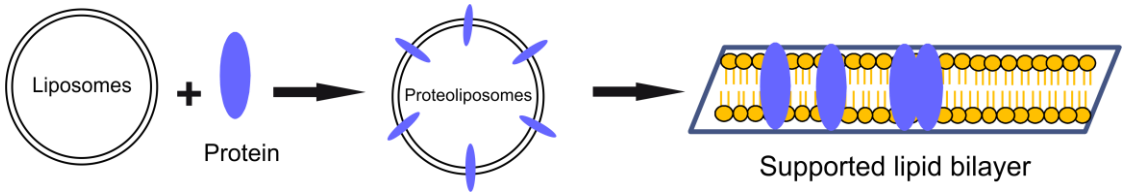

Figure.6.4. Schematic representation for the preparation of proteoliposomes and supported lipid bilayers.

6.10. Total internal reflection microscopy

For EqtII experiments, single molecule images were acquired using a total internal reflection microscope equipped with an EMCCD camera (Andor iXon3 DU-897), a Nikon Apo TIRF 60x oil immersion objective (NA 1.49) and a 561nm diode laser. The cells were maintained at 37^{o}C during the whole experiment and imaged in a buffer containing 150 mM NaCl, 20 mM Hepes, pH 7.4, 20 mM trehalose, 15 mM glucose, 5.4 mM KCl, 0.9 mM $MgSO_4$, and 0.5 mM $CaCl_2$. After single cells were selected and focused using bright field, 140nM (2.8µg/mL) of EqtII labelled with Alexa-555 was added. Movies were acquired with an exposure time of 200 ms at 1, 5, 10 and 15 min after toxin addition. In order to obtain the fluorescence signal corresponding to monomeric EqtII-Al555, free Alexa 555 dye was dried on a clean glass coverslide and imaged under the same conditions used for cells until all the particles were photobleached. In order to make sure that the fluorescence intensity of the dye does not significantly change when it is in membranes, we also tested with SLBs. SLBs were prepared from lipid mixtures containing DOPC: SM: Chol (2:2:1) and EqtII-Al555 was added to the SLBs. Movies were acquired under the same conditions used for cells until all the particles were photobleached. Since EqtII-Al555 does not diffuse in the SLBs, we observed mostly monomers. The fluorescence intensity obtained from calibration with dye on cover slide was comparable to the signal from SLBs. This calibration procedure with the glass slide was repeated prior to every experiment to avoid artifacts due to changes in the microscope setup.

For the experiments with Bcl-2 proteins, single molecule experiments were performed on a Zeiss Axiovert 200 microscope equipped with a 100× NA = 1.46 α Plan - illuminated using 488 nm light from an Ar^{+}-Laser and 647 nm light from a Kr^{+}-Laser with intensities of 5 kW cm^{-2}. The microscope is also equipped with an Image splitter (Optosplit) to record images simultaneously at two different wavelengths. Images and movies were acquired simultaneously in both channels with an exposure time of 2 ms and a delay of 90 ms between each frame. We observed fast bleaching of proteins labelled with Al-633/Al-647 when illuminated with both lasers simultaneously. To avoid this, we acquired the images with alternating illumination, where the samples are illuminated with 647 nm first and then 488 nm with a delay of 5 ms between the acquisitions.

For stoichiometry analysis of Bax, we prepared SLBs (EggPC: CL) followed by addition of 2.5 nM of Bax. Movies were acquired under the same conditions until all the particles were photobleached. For the colocalization studies, the position of the red and green detection channels has to be aligned properly. In order to align the red and green detection channels on a pixel-per-pixel basis, the position of different, immobilized and diffraction-limited beads (T-7279, 0.01 μm Tetraspeck microspheres, Invitrogen) was determined in both channels. Variances in their individual position in the two detection channels were used to correct the alignment of the two-color images by shifting and stretching the green detection channel, while red detection channel remained unaltered. This calibration procedure was repeated prior to every experiment to avoid artifacts due to changes in the microscope setup. All experiments were performed at 37˚ C.

6.11. Single particle tracking

Particles were detected and tracked using the u-track software (Jaqaman et al., 2008). The detection parameters used were as follows: psfsigma-2.5, integration window-3 and alphaLocMax-0.2. Tracking was constrained to the particles that were present in at least 10 consecutive frames. The particles detected and tracked were subjected to further analysis using Matlab (Mathworks) and Origin8.5. For each particle trajectory, the two-dimensional mean square displacement (*MSD*) for every time interval was calculated according to (Kusumi et al., 1993a; Lee et al., 1991a; Qian et al., 1991):

$$MSD(t) = \frac{1}{N}\sum_{i=1}^{N}\left[(X_{i+t} - X_i)^2 + (Y_{i+t} - Y_i)^2\right] \quad (1)$$

where N is the number of frames, and X and Y describe the particle position at each frame. The diffusion coefficient was calculated by fitting the data of *MSD* versus time lag (Δt) to diffusion models. In case of simple two-dimensional Brownian motion, the *MSD* is related to the diffusion coefficient D by:

$$MSD(\Delta t) = 4D\Delta t \qquad (2)$$

and for sub-diffusion the relation is given by:

$$MSD(\Delta t) = \langle r_c^2 \rangle \left[1 - A_1 exp\left(-4A_2 Dt/\langle r_c^2 \rangle\right)\right] \qquad (3)$$

where r_c^2 is the confinement size, and A_1 and A_2 are constants determined by the confined geometry (Saxton and Jacobson, 1997). See also section 4.5.

6.12. Stoichiometry analysis

To calibrate the fluorescence signal in the microscope, TIRF images of Alexa 555 dye dried on a cover slide and Bax Al-488 inserted in SLBs were used and based on it, the fluorescence intensity distribution of a monomer was calculated. Briefly, the individual particles were detected and the fluorescence intensity of each particle was estimated by fitting a 2-D Gaussian and averaging from the beginning of the movie till they were photobleached. The number of bleaching steps indicated the number of fluorophores. In our experiments, the bleaching step was always 1 or 2. By fitting a Gaussian curve to the distribution of fluorescence intensities, the mean intensity μ and standard deviation σ of a single fluorophore was calculated. With μ and σ, the fluorescence intensity of N colocalized fluorophores can be given by $\mu_N = N\mu_1 \pm N^{1/2}\ \sigma_1$. This calculation can be done only with photon counts, as they are a discrete variable following Poisson distribution. The grey values (Arbitrary units) cannot be used for this kind analysis because they are a continuous variable and do not follow Poisson distribution. We calculated the μ and σ values for 1 to 4 fluorophores in case of EqtII and 1 to 6 fluorophores for Bax and used them for fitting with a sum of Gaussians to the intensity distribution of the particles in the cell experiments. The number of Gaussians that can be fitted to the distribution of fluorescence intensity was estimated according to (Schmidt et al., 1996b),

$$N_{max} = (\mu_1/\sigma_1)^2 \qquad (4)$$

For determining the stoichiometry of the EqtII-Al555, images acquired with cells at different time points (1, 5, 10 and 15 min) after adding the protein were used. Approximately 500 individual particles were detected and analyzed for each time point. The distribution of the fluorescence intensity of all the particles at all-time points was globally fitted with a sum of four Gaussians using obtained μ and σ values. The Gaussian model used for the fit is given by:

$$\varphi(i) = \sum_{n=1}^{Nmax} A_n \cdot \frac{1}{\sigma\sqrt{2\pi}} e^{-\frac{(i-\mu.n)^2}{2(\sigma.n)^2}} \quad (5)$$

where $\varphi(i)$ is the frequency of particles having intensity *i*, *n* is the component number and A_n is the area under the curve of component *n*. The area *A* under the curve of each component was used to estimate the percentage of occurrence of each species and at each time point as described in (Calebiro et al., 2013).

For determining the stoichiometry of Bax-Al488, images acquired with SLBs prepared from SUVs and proteoliposomes (Section.6.9) were used. Approximately 500 individual particles were detected and analyzed for each data set. The distribution of the fluorescence intensity of all the particles was fitted individually or globally depending on the type of data with a sum of six Gaussians using the obtained μ and σ values. For the experiments with different membrane curvature and time points, global fitting was used. The Gaussian model used for the fit is shown in the equation (5). The percentage of occurrence of each species was estimated from the area *A* under the curve of each component as described for EqtII.

6.13. Mathematical simulations

We modeled the kinetics of EqtII oligomerization with a simple model based on mass action kinetics. The system is represented by a set of 4 coupled ordinary differential equations (ODEs) with 8 reaction rate constants which are used as fitting parameters. Numerical integration was performed in Matlab 7.0 (The MathWorks Inc., Natick, MA) using the ODE45 routine. We fitted the model to the experimental data of concentration of species over time with the LSQCURVEFIT routine of Matlab 7.0. The Matlab application for integration and subsequent fitting was written by Sandro M. Goñi (UNLP,

Buenos Aires, Argentina). The model is represented by 4 coupled ODEs originating from mass action kinetics:

$$\frac{dx_1}{dt} = -2k_1x_1^2 + 2k_{-1}x_2 - k_2x_1x_2 + k_{-2}x_3 - k_3x_1x_3 + k_{-3}x_4$$

$$\frac{dx_2}{dt} = k_1x_1^2 - k_{-1}x_2 - k_2x_1x_2 + k_{-2}x_3 - 2k_4x_2^2 + 2k_{-4}x_4$$

$$\frac{dx_3}{dt} = k_2x_1x_2 - k_{-2}x_3 - k_3x_1x_3 + k_{-3}x_4$$

$$\frac{dx_4}{dt} = k_3x_1x_3 - k_{-3}x_4 + k_4x_2^2 - k_{-4}x_4$$

x_i stands for the concentration of species i (monomers, dimers, trimers, tetramers). In this model, the total number of molecules is conserved. Mathematical simulations were carried out by Eduard Hermann.

Chapter 7

Equinatoxin II assembly mechanism in living cells revealed by single-molecule imaging

7. Equinatoxin II assembly mechanism in living cells revealed by single-molecule imaging

Equinatoxin II (Eqt II) is a α-pore forming toxin secreted by sea anemone *Actinia equina* whose activity depends on the presence of sphingomyelin in the membrane. Eqt II induces permeabilization in the target membrane via several steps. Initially, it binds to the membrane as a water-soluble monomer and subsequently oligomerizes to form a pore. The α-helix at N-terminus is involved in both membrane insertion and pore formation. Although, cross-linking studies and kinetic experiments suggested an approximate number of 3-4 monomers involved in the formation of a 2 nm pore, there is still a debate regarding the stoichiometry of the pore. For example, a recent study has shown that Fragaceatoxin C, which belongs to the same toxin family as Eqt II, forms pores via higher oligomeric species, which is in contrast to the tetramers proposed for EqtII. In this work, we have aimed to provide a better understanding of the molecular events involved in pore formation by Eqt II under physiological conditions. For this purpose, we have characterized the spatiotemporal organization of Eqt II at the single molecule level in living cells.

To analyze the oligomeric state of EqtII molecules in the plasma membrane of the target cells with single molecule resolution, we first calibrated the fluorescence signal in the TIRF microscope (Fig.7.1.A) (see section 6.12.). To this aim, we acquired movies of single Alexa555 molecules dried on a coverslip under the same conditions as in the cell experiments. The decrease in fluorescence intensity of single photobleaching steps (n=25) (Fig.7.1.B) followed a normal distribution and was fitted with a Gaussian curve that provided the average fluorescence signal of one Alexa555 molecule and the error of the estimation. This value was comparable to that obtained in similar experiments using EqtII labeled with Alexa555 (EqtII-Al555, see section 6.1.1, page no: 48) dried on a coverslip or inserted in lipid bilayers, and was used to calculate the fluorescence signal corresponding to dimers, trimers, tetramers, etc. (Fig.7.1.C).

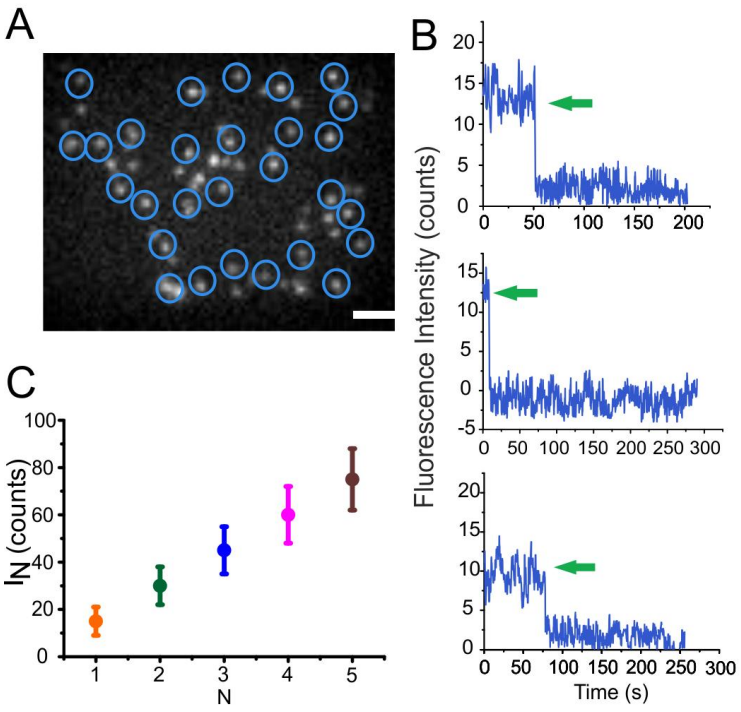

Figure.7.1. Detection of single Alexa555 fluorophores by TIRF microscopy. A) TIRF image of single Alexa555 molecules immobilized on a clean glass coverslip. Scale bar, 5 µm. Each particle was detected and the fluorescence intensity measured over time. B) The intensity of the particles that showed a single bleaching event were averaged over time and considered as the intensity of one single fluorophore. Some representative fluorescence intensity traces of individual Alexa555 particles with a single bleaching event are shown in blue. The green arrows indicate the bleaching step. C) μ (mean fluorescence intensity) and σ (standard deviation) values calculated for one (orange), two (green), three (blue), four (magenta) and five (brown) fluorophores. The μ and σ for a single fluorophore was determined from (B) and for 2-5 fluorophores was estimated according to the equation $\mu N = N\mu 1 \pm N1/2\ \sigma 1$ *(Schmidt et al., 1996b)* .N corresponds to the number of fluorophores. The Y-axis shows the fluorescence intensity (counts).

To visualize EqtII-Al555 in the plasma membrane of living cells, we used observation chambers containing seeded COS-1 cells at low confluence and equilibrated at 37°C. Prior to toxin addition, an area containing individual cells was selected and focused using bright field microscopy. Then, we added EqtII-Al555 at a final concentration of 140 nM and quickly proceeded with image acquisition in the TIRF mode. The evanescent wave generated under TIRF illumination ensured that only the EqtII-Al555 molecules bound to the part of the plasma membrane in contact with the coverslip glass were excited, thus providing a signal-to-noise ratio that allowed the

detection of individual particles (Fig.7.2.A). Single molecules of EqtII-Al555 appeared as bright spots diffusing in a dark background (Fig.7.2.B).

The individual EqtII spots detected in the microscopy images at 5 min after toxin addition were fitted with a 2D Gaussian to determine the maximum fluorescence intensity of each particle (Fig.7.2.C). The intensity distribution of single EqtII particles in the membrane of living COS-1 cells was then plotted as a histogram (n=489) (Fig.7.2.D). Visual inspection of the broad distribution of fluorescence intensities already indicates the presence of multiple species brighter than monomers. For a quantitative estimation of the distribution of EqtII oligomers, we fitted the histogram of fluorescence intensities with a linear combination of Gaussian curves (Cocucci et al., 2012; Meckel et al., 2011a; Schmidt et al., 1996b; Xia et al., 2013). The maximum number of Gaussians and therefore oligomeric species that can be used in the fitting was determined using equation (4) (see section 6.12.). With the quality of our data, N_{max} is 4, so we restricted our fittings to four species, corresponding to monomers, dimers, trimers and tetramers. The center and width of the Gaussian curves were set according to the calculated fluorescence signal and its error, respectively, for each species in the calibration experiments (Fig.7.2.D). The area under each curve was used to calculate the percentage of occurrence of each species. All the percentage values mentioned here were corrected considering that 86% of the protein is fluorescent. We found that the signal from EqtII-Al555 in the cell membrane corresponds to 26±6% monomer, 42±9% dimer, 25±9% trimer and 7±9% tetramer. Strikingly, these results indicate that EqtII exists in the plasma membrane of living cells as a mixture of oligomeric species.

7.1. Temporal analysis of Equinatoxin II oligomerization

In order to investigate the temporal dynamics of EqtII oligomerization, we took images at 1, 5, 10 and 15 min after adding the fluorescently labeled toxin to COS-1 cells. This is the time frame under which EqtII-Al555 induces plasma membrane reorganization and blebbing, associated to pore formation and followed by cell death (Garcia-Saez et al., 2011b). The histograms of fluorescence intensity distribution measured for ~500 particles at each time point were fitted with a sum of four Gaussians corresponding to monomers, dimers, trimers and tetramers (Fig.7.3.A-D), as explained above. As the fluorescence signal of the different species is expected to be the same at all measured times, we

minimized the error of the fitting by performing a global fit of all the intensity distributions in parallel.

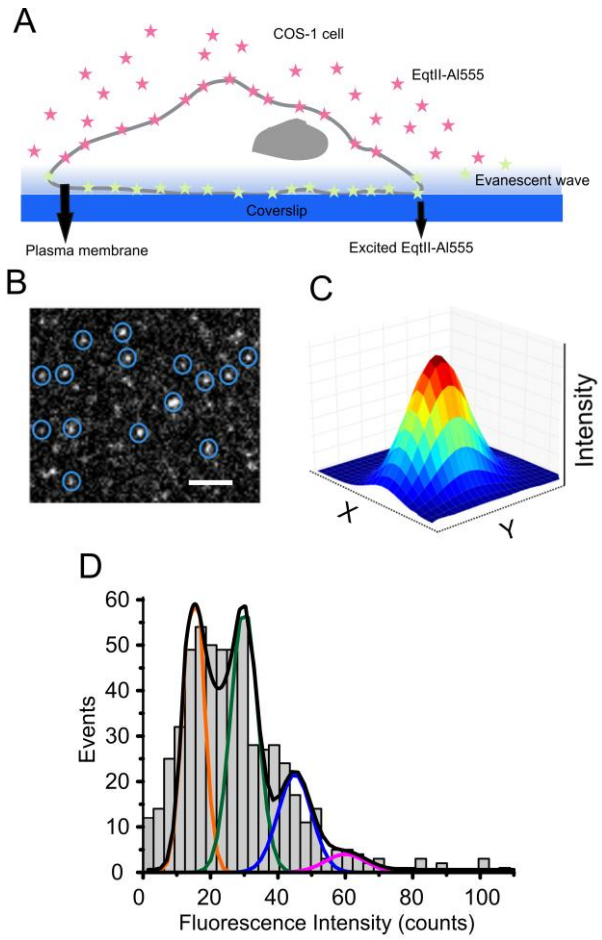

Figure.7.2. Schematic representation of the experimental design and data analysis. A) Scheme of the TIRF imaging strategy used in the experiments. Upon addition to the extracellular medium, EqtII-Al555 binds quickly to the plasma membrane of COS-1 cells. Only the fraction of them bound to the part of the plasma membrane closer than ~100 nm to the glass coverslip is illuminated and emits fluorescence. B) Single molecules of EqtII-Al555 in the plasma membrane appear in the images as bright spots and can be detected by image processing (blue circles). C) The intensity distribution of an individual molecule in the detected area is then fitted with a two-dimensional Gaussian curve from which the fluorescence intensity of the molecule is calculated. D) By analyzing several hundreds of individual particles, the intensity distribution of EqtII-Al555 on the cell surface is obtained. To calculate the fraction of the different oligomeric species present on the membrane, we fitted the fluorescence intensity distribution with a sum of Gaussians whose centers and widths correspond to the values calculated for monomers, dimers, trimers and tetramers, as estimated from the single molecule calibration of fluorescence intensity (Fig.7.1). The area of each Gaussian is proportional to the fraction of that species in the EatII-Al555 ensemble.

Our analysis revealed that even 1 min after adding the toxin to the cells (Fig.7.3.A), we could observe a high percentage of dimers (55±8%), 7±9% trimers and 14±8% tetramers along with 23±6% of monomers. This shows that the oligomerization of EqtII is very fast.

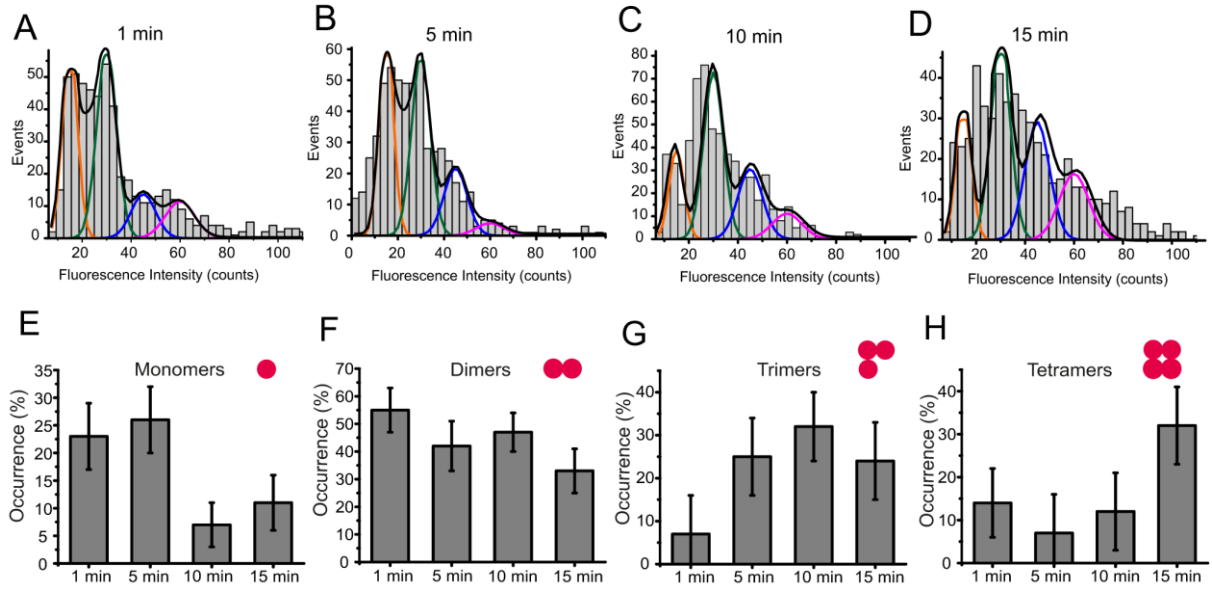

Figure.7.3. Stoichiometry analysis on the surface of COS-1 cells: EqtII-Al555 is present as a mixture of species that evolves with time. (A-D) Intensity distribution of EqtII-Al555 on the cell surface at the indicated incubation times. For each condition, ~500 particles were analyzed. The resulting histograms were fitted with a sum of Gaussians in order to estimate the occurrence of monomers (orange), dimers (green), trimers (blue) and tetramers (magenta). The area of the fitted Gaussians is proportional to the fraction of each species. (E-H) Temporal evolution of the distribution of EqtII-Al555 species on the cell surface. The percentage of monomers E), dimers F), trimers G) and tetramers H) observed at the time points in (A-D) are shown.

After 5 min of toxin addition to the cells (Fig.7.3.B), we observed a shift in the distribution of species, with 26±6% of monomers, 42±9% of dimers, 25±9% of trimers and 7±9% of tetramers. The fraction of EqtII-Al555 oligomeric forms on the cell surface continued to evolve resulting in 7±4% of monomers, 47±7% of dimers, 32±8% of trimers and 12±9% of tetramers 10 min after adding the protein (Fig.7.3.C). The analysis at the final time point of 15 min yielded 11±5% monomers, 33±8% dimers, 24±9% trimers and 32±9 % tetramers (Fig.7.3.D). At long incubation times, there were a small number of brighter particles that could be due to higher oligomeric species or to the presence of more than one particle within the same pixel (Hastie et al., 2013; Reiner et al., 2012).

However, when we tried to include larger oligomers, the fits did not converge or adjusted worse to the experimental data, indicating that oligomers larger than a tetramer did not contribute significantly to the toxin population.

Overall, we found that the monomers (Fig.7.3.E) and dimers (Fig.7.3.F) decreased over time, whereas the fraction of trimers (Fig.7.3.G) showed an increase up to 10 min and then decreased. Tetramers (Fig.7.3.H), the form commonly associated with pore formation, was present from the initial moments and significantly increased with time. These findings show that the spatiotemporal organization of EqtII on the host membrane is dynamic and evolves in a time frame comparable to the time for cell death induction.

7.2. Mobility of Equinatoxin II at the plasma membrane is drastically reduced for higher oligomers

Upon binding to the target cell, EqtII induces the reorganization of the plasma membrane and the formation of immobile raft-like domains where the toxin is localized (Garcia-Saez et al., 2011b). However, the mobility of the individual EqtII particles in the plasma membrane of the target cell and how it relates with stoichiometry remains unknown. To address this question, we tracked the particles of EqtII in time-lapse experiments (see scheme in Fig.7.4). The mobility of the constituents of the plasma membrane of mammalian cells has been shown to be compatible with a model of hop diffusion (Kusumi et al., 2011). However, the time resolution of our experiments is not fast enough to accurately distinguish between diffusion models (Ritchie et al., 2005; Wieser and Schutz, 2008). For this reason, the results of our analysis correspond to the *apparent* diffusion of individual EqtII particles under observation conditions of 200 ms integration time and continuous acquisition.

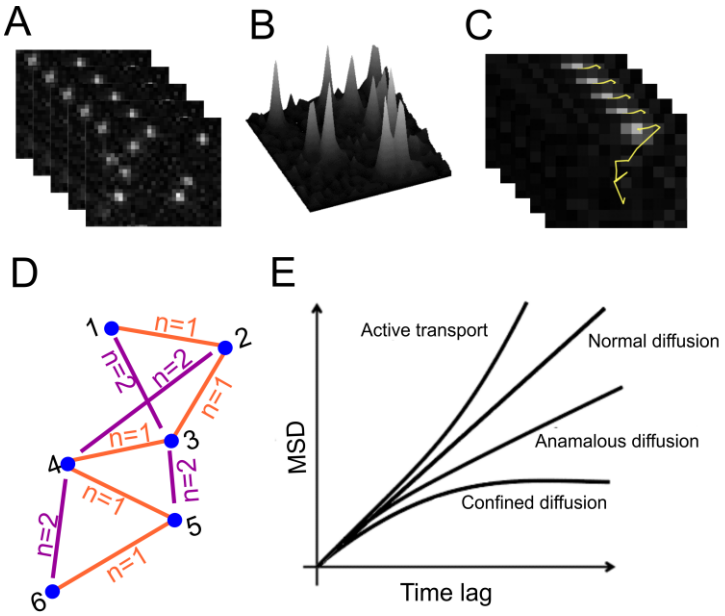

Figure.7.4. Schematic representation of single particle detection and tracking. A) Stacks of TIRF images recorded at 1min after addition of toxin to the cells. B) The subpixel localization (x, y position) of the particles is determined by the center of a 2-D Gaussian fitting. C) The particles detected in (B) are tracked over time. D) The trajectories are analyzed by calculation of the mean square displacement (MSD) at different time lags. E) Expected plot of MSD *vs.* time lag for different diffusion models.

Fig.7.5.A shows representative trajectories of EqtII particles from movies acquired 1 min after toxin addition. The mean square displacement (*MSD*) analysis showed two different populations: ~10% particles exhibited *apparent* Brownian diffusion, while the rest moved with *apparent* sub-diffusion, which was best compatible with a model of confined diffusion (Fig.7.6) (Wieser and Schutz, 2008). The average *MSD* curves of both populations are shown in Fig.7.5.B. The histogram for the diffusion coefficients of the individual particles also identifies these two populations (Fig.7.5.C). The *apparent* diffusion coefficients averaged for the free- and sub-diffusing populations were $0.60\pm0.01\mu m^2/s$ and $0.36\pm0.03\mu m^2/s$ respectively. To further confirm that the particles do not undergo anomalous diffusion, we plotted the *log (MSD)* as a function of *log (time)* (Fig.7.6.A) and *log (MSD/time)* as a function of *log (time)* (Fig.7.6.B) (Murase et al., 2004). Our results showed that there is no change in the diffusion characteristics as indicated by the horizontal flat line in Fig.7.6. A, B, ruling out the possibility of anomalous diffusion in the time resolution we used.

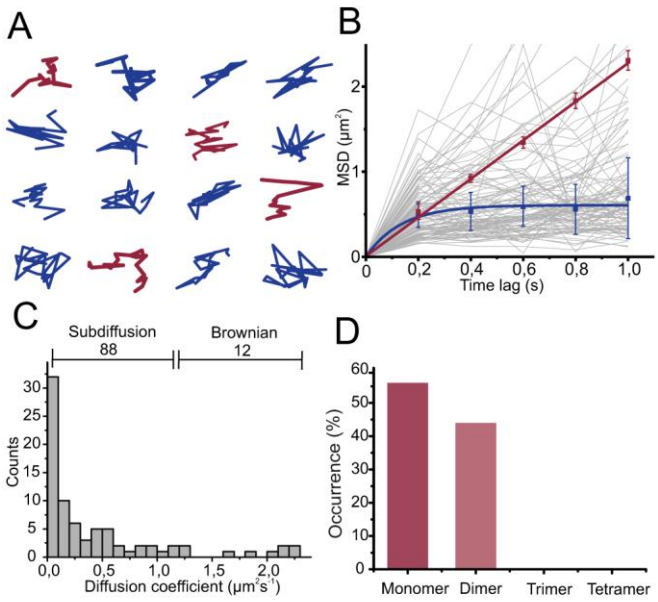

Figure.7.5. Mobility analysis of EqtII-Al555. A) Representative trajectories of individual EqtII-Al555 molecules on the surface of COS-1 cells. Trajectories typical for Brownian motion (red) and sub-diffusion (blue) are shown. B) Plot of MSD versus time lag for 100 EqtII-Al555 particles (grey lines). The average MSD curve (including SD) for trajectories classified as Brownian or as confined are shown in red and blue, respectively. C) Distribution of diffusion coefficients *D* of EqtII-Al555 particles. The corresponding classification of diffusion mode is indicated. D) The particles following Brownian diffusion are monomers and dimers, as calculated by stoichiometry analysis.

Interestingly, we found that the particles with *apparent* Brownian motion were low oligomeric forms of EqtII, formed by a mixture of monomers and dimers (Fig.7.5.D). As a consequence, the fraction of sub-diffusing particles is enriched in higher EqtII oligomers. This indicates that the mobility of EqtII depends on the stoichiometry of the particles and is reduced by oligomerization.

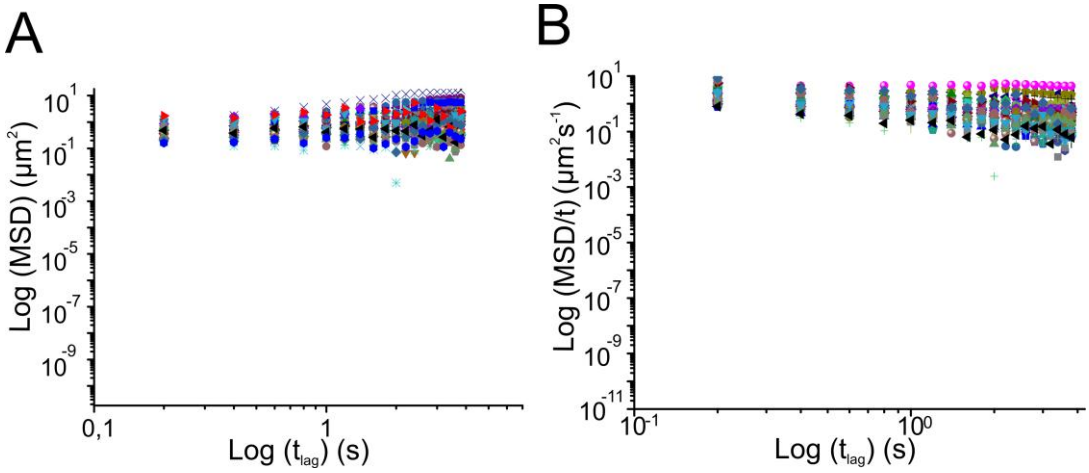

Figure.7.6. Subdiffusion analysis of individual EqtII-Al555 trajectories. (A) Plot of Log (MSD) as a function of Log (time lag) for the same 100 particles used in Fig 4. (B) Plot of Log [(MSD)/t] as a function of Log (time lag) for the same 100 particles used in Fig 4. The almost horizontal distribution of the points discards anomalous diffusion.

Fig.7.7.A shows an example of two diffusing EqtII-Al555 particles forming a complex that remains associated during the rest of the observation time. For clarity, the trajectories of both particles and of the complex they form are depicted in Fig.7.7.B. In agreement with the mobility analysis, the two individual particles exhibit *apparent* free diffusion that becomes confined upon association. Fig.7.7.C shows the fluorescence signal of the particles over time. The brightness of the newly formed oligomer corresponds to the sum of the fluorescence intensity of the initial particles.

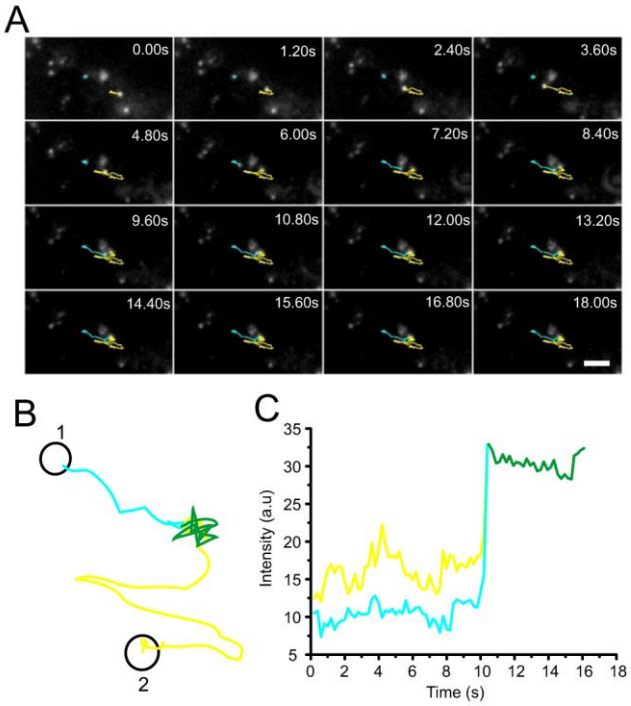

Figure.7.7. Direct visualization of the association of individual EqtII-Al555 molecules. A) TIRF images from a movie showing two EqtII-Al555 molecules diffusing on the surface of HEK cells and forming a stable complex. The trajectories of the two particles are shown in cyan and yellow. Scale Bar, 1µm. B) Representation of the same traces as in (A), the trajectory after association is shown in green. C) The fluorescence intensity signal of the complex equals the sum of the two individual EqtII-Al555 particles.

7.3. Oligomerization of Equinatoxin II proceeds via sequential addition of monomers

The temporal analysis of the distribution of EqtII-Al555 species on the cell surface indicates that all oligomeric states up to tetramers are populated during the observation time. Based on these data, we modeled the process of EqtII assembly from the initial moment of association with the cell surface. For this purpose, we built a simple kinetic model of EqtII oligomerization based on differential equations of all possible reactions of complex formation up to tetramers: two monomers forming a dimer, dimer and monomer forming a trimer, trimer and monomer forming a tetramer and two dimers forming a tetramer (see Fig.7.8.A and section 6.13.). By assuming that EqtII first binds to the membrane as a monomer and considering all reactions reversible, we fitted the system of differential equations to the experimental data of evolution of oligomeric species over time shown in Fig.7.2. We estimated the total area concentration of EqtII molecules in the plasma membrane by counting all the individual particles in a cell, taking into account the stoichiometry of each particle and dividing by the observed membrane area.

From the fitting, we obtained the kinetic constants for the forward and backward reactions of oligomerization (Fig.7.8.B). In all cases, the forward reactions presented kinetic constants in the order of 100 fold higher than the backward reactions, indicating that complex dissociation is an unlikely event. In addition, the reactions of dimerization and trimerization proceeded with comparable rates, 9.4±0.4 and 7.4±0.4 μm^2 $molecule^{-1}$ s^{-1}, respectively. In contrast, the addition of a monomer to a trimer was one order of magnitude higher, 140±15 μm^2 $molecule^{-1}$ s^{-1}, indicating cooperativity in the formation of higher oligomers. Interestingly, the tetramerization via condensation of two dimers was negligible in our model. Finally, Fig.7.8.C shows that the modeled evolution of oligomeric species over time (solid lines) fits very well to the experimental data (circles). For the best fit, we obtained a sum of squared residues of 1.1×10^{-3} [molecules/μm^2]. This corresponds to an averaged uncertainty of 8.3×10^{-3} molecules/μm^2 for each concentration curve. Simulation of the distribution of species with time suggested that at 15 min incubation the different oligomeric forms were already close to equilibrium (Fig.7.9). [Modeling was done in collaboration with Eduard Hermann in the group].

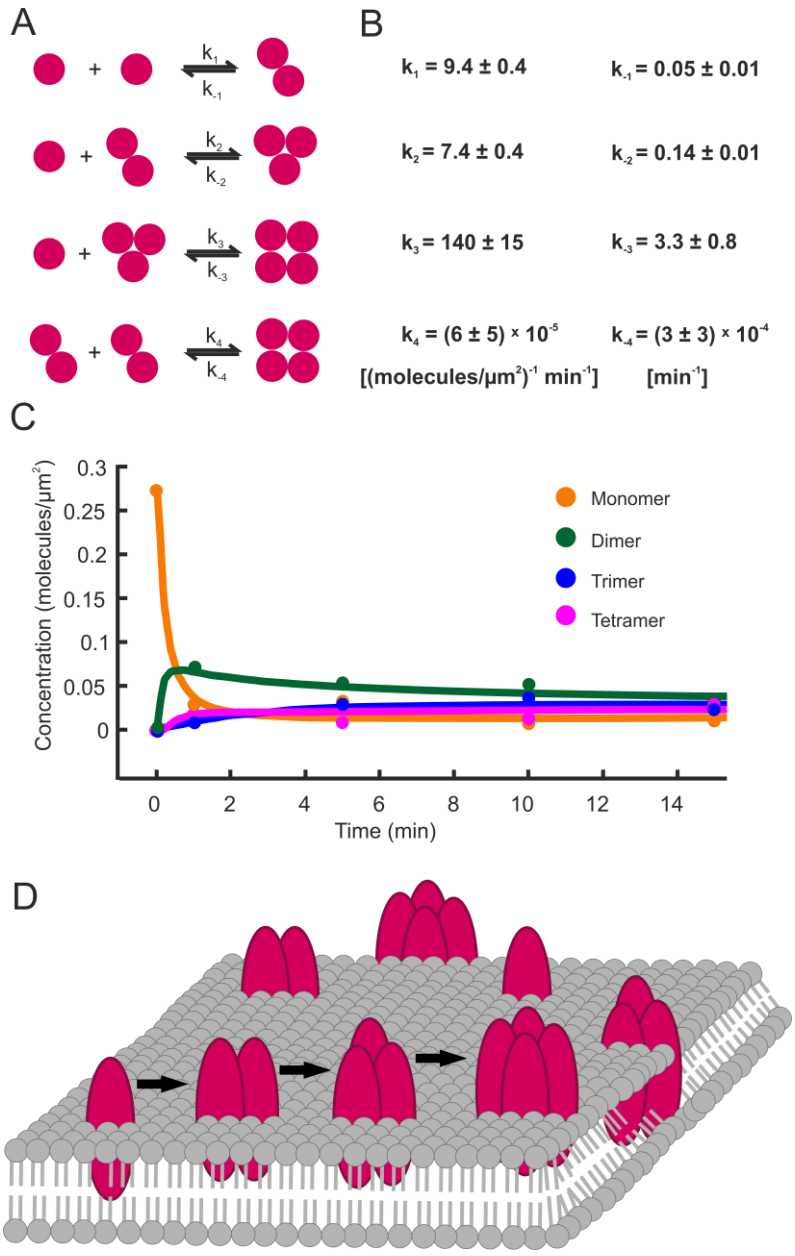

Figure.7.8. EqtII assembly mechanism. A) The kinetics of EqtII oligomerization was analyzed by a simple mass action model with 4 reactions. Tetramers are produced either by oligomerization of one monomer with one trimer or of two dimers. B) We calculated the rate constants for the forward and backward reactions by fitting the theoretical model to the experimental data. The errors represent the standard deviations of the three best fits. C) The temporal evolution of the concentrations of EqtII monomers (blue), dimers (green), trimers (orange) and tetramers (cyan) calculated from the model is shown. The circles at t = 1, 5, 10 and 15 min represent the experimental data points. We considered that EqtII binds to the membrane as a monomer. Therefore, only monomers are present at t = 0. D) Proposed model for the mechanism of EqtII assembly on the surface of the target cells. Upon binding, EqtII oligomerizes on the plasma membrane via sequential addition of monomers. Despite cooperativity in the formation of tetramers, EqtII is present on the membrane always as a

mixture of species, whose distribution is close to equilibrium after 15 min of incubation. The presence of lipids in the pore structure is not shown for the sake of clarity. [Panels A, B and C kindly provided by Eduard Hermann].

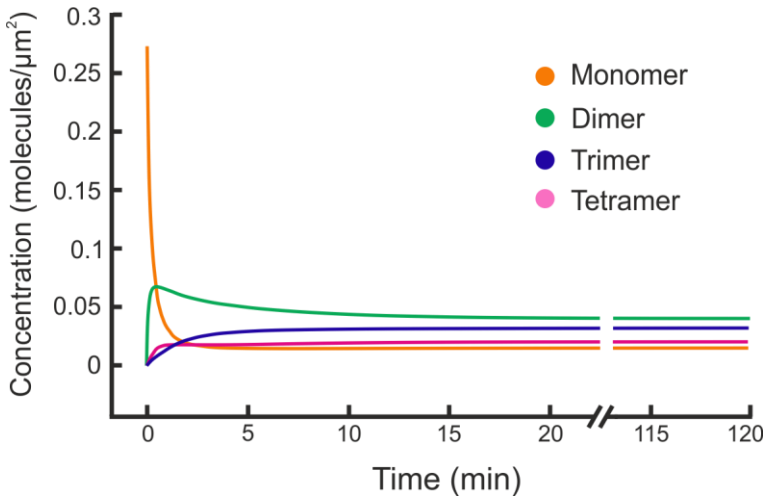

Figure.7.9. Simulated temporal evolution of the concentrations of individual EqtII species. The ODEs for EqtII oligomerization (Supplementary Methods) were used to plot the concentrations of species as a function of time. The parameters were obtained by fitting the model to experimental data (Fig. 5). Our model predicts that the species achieve equilibrium after around 20 minutes. [Figure kindly provided by Eduard Hermann].

7.4. Discussion

Using single molecule fluorescence microscopy methods, we have determined the spatiotemporal assembly of EqtII-L26C during its toxic action on the surface of living target cells. Upon binding, we observed that EqtII rapidly initiates its oligomerization on the cell membrane. In contrast to previous assumptions that actinoporins are present exclusively as monomers and tetramers on the membrane (Garcia-Ortega et al., 2011), we found that EqtII-L26C clearly exists in the plasma membrane as a mixture of oligomeric species that evolves over time. As early as one minute after incubation, all oligomeric forms ranging from monomers up to tetramers can be found on the cell surface. The relative amounts of each species are dynamic and reorganize yielding a larger fraction of tetramers at the expense of all other forms. However, even 15 min after binding, when the membrane has been pierced and undergone dramatic reorganization (Garcia-Saez et al., 2011b), smaller particles of EqtII-L26C can be found on the plasma membrane at

significant ratios: monomers and dimers account for more than 40% particles and trimers for 25% particles. This indicates that full conversion of all EqtII-L26C molecules into tetramers, which have been proposed to be responsible for pore formation, is not necessary to efficiently kill cells. Based on this, it is tempting to speculate, that the potent killing activity of α-PFTs is achieved with a relatively small number of pores compared to the total amount of toxin molecules bound to the target cell.

Our study has been performed close to physiological conditions of EqtII-L26C attack to its target cell. This is important because our data include conditions out of equilibrium, unlike most work so far with artificial model membranes. Here we offer, for the first time, direct visualization of how PFTs assemble on the cell surface. Indeed, kinetic modeling of EqtII-L26C oligomerization based on the changes in the fraction of the different species over time suggests that the association process is significantly faster than complex dissociation. The results of the analysis also indicate that the condensation of trimers and monomers is the fastest, suggesting cooperativity in the latter step of EqtII-L26C oligomerization. Based on this, we hypothesize that tetramers may be the preferred EqtII-L26C arrangement in the lipid bilayer. This leads to the observed accumulation of tetramers over time. The relative amount of EqtII-L26C complexes is close to equilibrium 15 min after toxin addition, indicating that the coexistence of species is intrinsic to EqtII-L26C action and that the same distribution should be expected until the final moment of cell death. Remarkably, such a simple model also reveals that the formation of tetramers via dimer condensation is highly unlikely. This has important consequences for the mechanism of EqtII-L26C assembly, because it indicates that EqtII-L26C oligomerization proceeds via the sequential addition of toxin monomers.

The analysis of EqtII-L26C mobility on the plasma membrane yields a small percentage of EqtII-L26C particles that freely diffuse, which interestingly corresponds to monomeric and dimeric forms of EqtII-L26C. This could likely be the case for EqtII molecules loosely associated to the cell surface and that have not yet inserted their N-terminal helix involved in membrane permeabilization. However, the majority of EqtII-L26C particles, including all trimeric and tetrameric complexes, show apparent confined diffusion. This is probably due to a stronger association with the membrane via N-terminus insertion and to the formation of larger oligomers, both of which increase the likelihood that particle diffusion is affected by membrane crowding, interactions with the cytoskeleton and/or presence of raft-like domains (Kusumi et al., 2011; Lingwood and

Simons, 2011). This is also in agreement with a recent report suggesting that the insertion of the N-terminal anchor of EqtII-L26C proceeds prior to toxin oligomerization (Jaqaman et al., 2008).

Based on the present results, we propose a model for the mechanism of EqtII-L26C toxic action on the target cells (Fig.7.9.D). Upon binding to the cell surface, EqtII-L26C rapidly starts oligomerizing and the first pore-forming tetramers appear in less than one minute. Importantly, EqtII-L26C assembles via sequential addition of individual monomers. This yields a mixture of species on the cell surface that includes all oligomeric forms from monomers to tetramers. The distribution of species evolves over time and reaches equilibrium in a time range comparable to attain cell death. The low percentage of EqtII-L26C molecules engaged in pore-forming tetramers is enough to potently kill the cell.

Our findings have general implications for PFTs. It is tempting to speculate that the coexistence of species is a general attribute of α-PFTs. This would be a change of paradigm in the current view, more focused on the predominance of the pore-forming form of the toxin on the target membrane. This feature could also be related to the tendency of many α-PFTs to form pores lined by both lipids and proteins, also known as toroidal pores, as proposed for actinoporins, the apoptosis regulators Bax and Bak, and a large number of antimicrobial peptides (Basanez et al., 2002; Huang et al., 2004; Landeta et al., 2011; Qian et al., 2008b; Terrones et al., 2004; Valcarcel et al., 2001). In addition, the large number of coexisting species present in the membrane, with the pore-forming oligomers not being the most common, could be a reason for the difficulties to study structurally these proteins with high resolution.

New questions in the field of PFTs arise from the research here. It will be interesting to see if β-PFTs, which form better-defined structures, are also present as a mixture of species on the cell surface. A recent study in artificial membrane systems identified only heptamers in the case of α-hemolysin (Thompson et al., 2011). In the case of actinoporins, our work supports a model of pores formed by tetramers, as previously suggested for EqtII and the sticholysins (Belmonte et al., 1993b; Garcia et al., 2012; Mancheño et al., 2006; Martín-Benito et al., 2000). Additional work will be necessary to see if the related protein Fragaceatoxin C, which has been proposed to form larger species (Mechaly et al., 2011b), is an exception to the family. Given the high proportion of monomers, dimers and trimers on the plasma membrane, the question remains whether

these lower oligomeric species are also able to permeabilize the membrane. In addition, the identification of the structural determinants that impede higher oligomerization while allowing the existence of low oligomers will help optimizing the killing activity of α-PFTs and improve their biotechnological applications.

In summary, here we found that EqtII-L26C exists in the surface of the target cell as a mixture of species where the pore-forming tetramers are not the dominating form. The distribution of species is dynamic and evolves with time in a way consistent with rapid oligomerization that reaches equilibrium in a time range comparable to cell death. We propose a model for EqtII-L26C assembly that proceeds via the sequential condensation of monomers and where a low ratio of pore-forming particles with respect to the total EqtII-L26C on the membrane is enough to efficiently kill the target cell. A similar mechanism may be general for α-PFTs.

Chapter 8

Stoichiometry analysis of Bax oligomers in the lipid bilayer at the single molecule level

8. Stoichiometry analysis of Bax oligomers in the lipid bilayer at the single molecule level

The proteins of the Bcl-2 family are key regulators of the mitochondrial pathway of apoptosis. The members of this family are classified into three subgroups: a) Proapoptotic proteins, such as Bax, b) BH3 only proteins such as Bid, PUMA, Bim, c) antiapoptotic proteins such as Bcl-xL, Bcl2. During apoptosis Bax is activated by Bid and translocates from the cytoplasm to the outer mitochondrial membrane, where it inserts as a monomer, undergoes oligomerization and forms a pore through which cytochrome *c* and other apoptotic factors are released into the cytoplasm. These apoptotic factors induce the activation of the effector caspases that execute apoptosis. However, the activation and oligomerization of Bax to form a pore in the membrane is far from being understood. There is no structural information available for activated form of Bax. There are several contradicting observations on the oligomeric state of Bax while forming a pore. The antiapoptotic proteins of the family, such as Bcl2 or Bcl-xL have shown to inhibit the oligomerization process leading to cell survival. The interaction between these proteins affects the activity of Bax. In this work, we have aimed to determine the stoichiometry of Bax oligomers using model membranes. We have also investigated the effect of membrane curvature on Bax oligomerization and kinetics of Bax oligomerization. In addition, we examined the interactions between Bax and cBid/tBid, Bcl-xL and cBid/tBid.

8.1. Binding of Bax to supported lipid bilayers

Supported lipid bilayers (SLBs) were prepared from lipid mixtures containing EggPC, EggPC: CL (8:2) and Mitomix as described in chapter 6. SLBs were labeled with the lipophilic dye DiD (1,1'- dioctadecyl- 3,3,3',3'- tetramethylindodicarbocyanine, 4 chlorobenzensulfate) and appeared as flat and homogenous while imaging with fluorescence microscopy. Prior to every experiment, the formation and fluidity of the SLBs were tested. Fig.8.1.A shows the trajectories of DiD tracked over time in SLBs. Our results showed that the it follows Brownian motion with a diffusion coefficient D= 1.86±0.08 $\mu m^2 s^{-1}$ and that the bilayer is therefore in a fluid state (Fig.8.1.B).

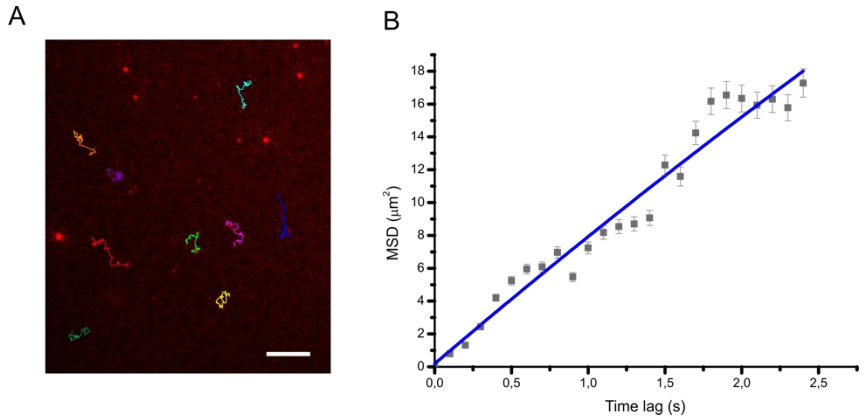

Figure.8.1. Mobility analysis of DiD in the lipid bilayer. A) TIRF image of the SLB containing PC: CL (8:2) and 0.005% DiD showing the trajectories of the lipophilic probe. B) Plot of MSD versus time lag showing the mean and standard deviation from 25 particles. The linear fit typical of Brownian motion is shown in Blue.

In our experiments for the stoichiometry analysis of Bax, we activated Bax-Al488 with unlabeled cBid in order to induce its binding to the membrane. Bax-Al488 and unlabeled cBid were added to the SLBs composed of EggPC: CL (8:2). Fig.8.2 shows the image of a representative bilayer acquired with TIRF microscopy. The right panel shows the fluorescence of the bilayer and left panel shows the binding of protein to the bilayer. We could observe the immediate binding of the protein to the bilayer, but then the Bax particles did not diffuse. As a control, we added only Bax-Al488 to the membrane and we observed very few Bax particles associated with the membrane compared to those activated by cBid. In addition, we also observed that many Bax particles could not insert into the membrane, but diffused close to it leading to high SNR. Because of this, imaging the few particles that were bound to the membrane also became technically difficult (Fig.8.3.A).

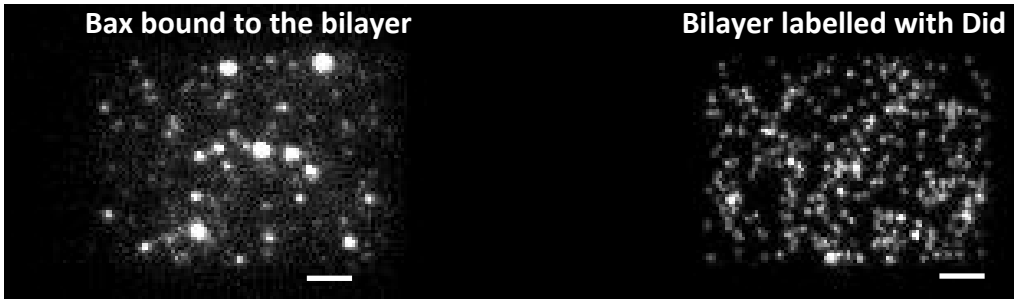

Figure.8.2. Dual color TIRF image showing the bilayer containing PC: CL (8:2) labelled with DiD and Bax-Al488 bound to the membrane. Scale bar 5 µm

In addition, we also had another control where SLBs were prepared from PC alone and no cardiolipin. As expected from previous reports in the literature, activated Bax did not bind to the membrane (Gonzalvez et al., 2008; Kuwana et al., 2002). Fig.8.3.B, C shows the difference in binding of Bax in the absence and presence of cardiolipin respectively. Our results are in agreement with the previous studies demonstrating that Bax activation and oligomerization requires CL in the membrane (Kuwana et al., 2002).

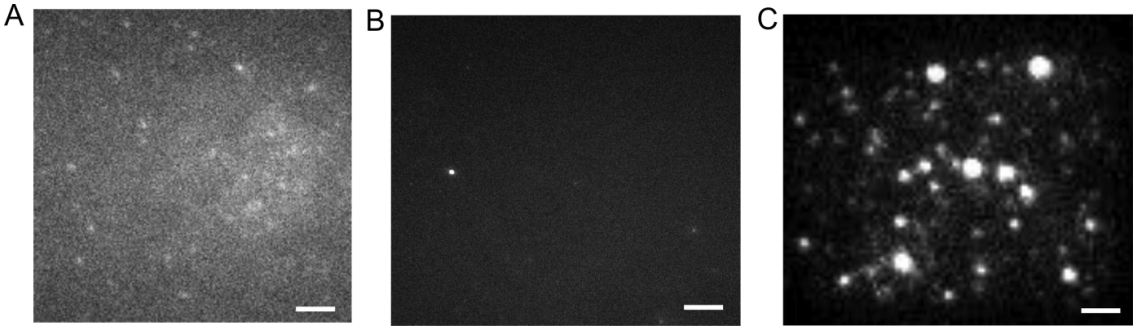

Figure.8.3. TIRF images of Bax-Al488 particles on SLBs. A) Binding of Bax-Al488 particles to the bilayer prepared from PC: CL (8:2) without being activated by cBid. B) Binding of cBid activated Bax-Al488 to the bilayer prepared from PC alone. C) Binding of cBid activated Bax-Al488 particles to the bilayer prepared from PC: CL (8:2). Scale bar 5 µm

Furthermore, we also tested the binding efficiency of Bax-Al488 with a lipid composition mimicking the outer mitochondrial membrane (Mitomix). There was no significant difference in the binding between PC: CL (8:2) and Mitomix (Fig.8.4.A,B). However, the difference in the stoichiometry of Bax-Al488 between these two different lipid mixtures has not been analyzed yet. This might give an insight to the role played by CL and other lipids (in the case of Mitomix) influencing the oligomerization of Bax.

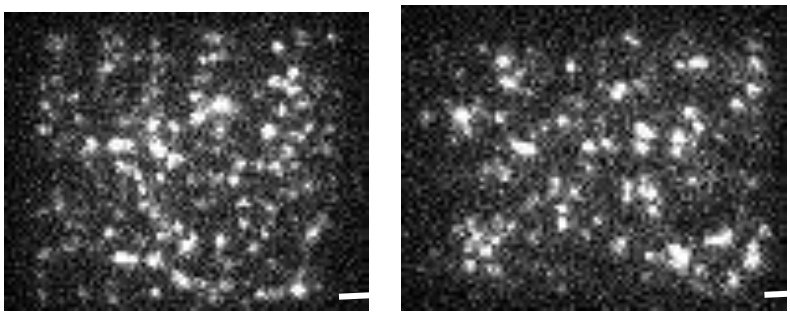

Figure.8.4. TIRF images of Bax-Al488 particles on the supported lipid bilayer. A) Binding of Bax-Al488 particles to the bilayer prepared from PC:CL (8:2). B) Binding of Bax-Al488 particles to the bilayer prepared from Mitomix. Scale bar 5 µm

8.2. Fluorescence of monomeric Bax

As explained previously in chapter 6, we first calibrated the fluorescence signal in the TIRF microscope. Once the protein is bound to the SLB, we acquired movies of Bax labelled with Alexa 488 under the same conditions [exposure time 2 ms with a delay of 90 ms] as in the experiments later on (Fig 8.5 A,B). Generally, movies were acquired until the particles disappeared due to photobleaching. Since Bax was not diffusing in the lipid bilayers, it was easy to detect a particle in the first frame and follow it during the entire movie. The fluorescence intensity of each particle was measured. The number of bleaching steps indicates the oligomeric state of each particle. Fig.8.5.C,D shows examples of the bleaching steps of a Bax monomer and a dimer. The decrease in fluorescence intensity of single photo bleaching steps (n=25) followed a normal distribution and was fitted with a Gaussian curve that provided the average fluorescence signal of one Bax-Alexa488 molecule and the error of the estimation. This value was used to calculate the fluorescence signal corresponding to dimers, trimers, tetramers, pentamers and hexamers (Fig.8.5.E). The calculated values are then used to fit the sum of Gaussians to the fluorescence intensity distribution (Fig.8.5.F).

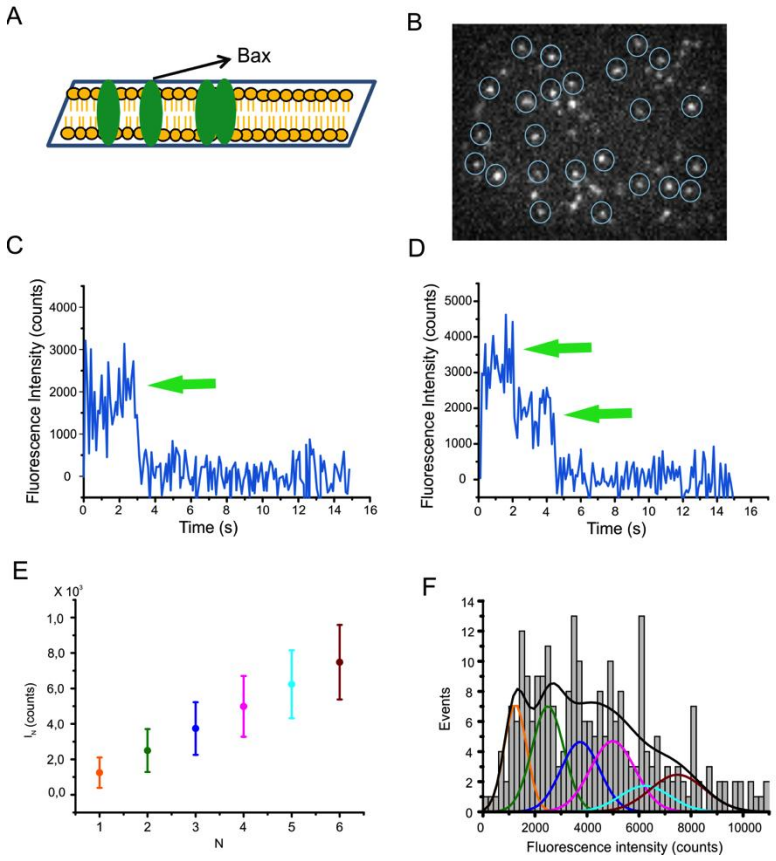

Figure.8.5. Detection of single Bax-Alexa488 fluorophores by TIRF microscopy. A) Schematic representation of a supported lipid bilayer with Bax bound to it as the one used for calibrating the fluorophore signal. B) TIRF image of Bax-Alexa488 molecules immobilized on a supported lipid bilayer. Scale bar, 1 µm. Each particle was detected and the fluorescence intensity measured over time. C) The intensity of the particles which showed a single bleaching event were averaged over time and considered as the intensity of one single fluorophore. A representative fluorescence intensity trace of one individual Bax-Alexa488 particle with a single bleaching event is shown in blue. D) A representative fluorescence intensity trace of a Bax-Alexa488 particle with two bleaching events is shown in blue. The green arrows indicate the bleaching steps. E) μ (mean fluorescence intensity) and σ (standard deviation) values calculated for one (orange), two (green), three (blue), four (magenta), five (cyan) and six (red). F) The calculated values from E) used to fit the fluorescence intensity distribution with sum of Gaussians.

8.3. Bax oligomerization

In order to visualize the oligomerization process, Bax-Al488 along with unlabeled cBid (needed to activate Bax) were added to SLBs (PC:CL, 8:2) prepared on a glass slide and quickly imaged. Each particle was detected and analyzed for the fluorescence intensity as described in chapter 7. Fig 8.6.A,B shows the intensity distribution of ~500 particles and the corresponding sum of Gaussian fittings. The high occurrence of monomers (Fig 8.6 C), even after increasing the concentration of protein four-fold, indicates that activated Bax binds to the bilayer as a monomer. Since the protein does not diffuse in the membrane, oligomerization is hindered and it is not possible to study the stoichiometry of Bax pores under these experimental conditions.

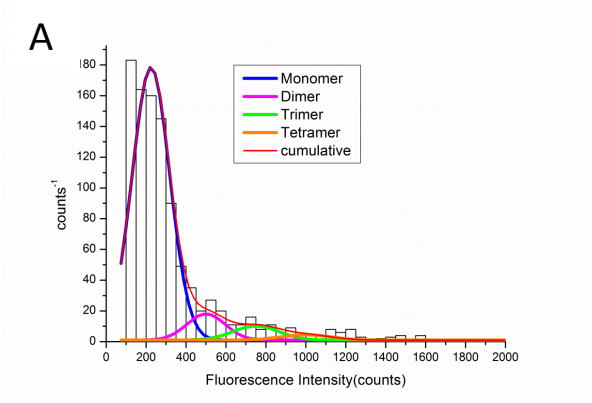

Bax (140 nM) -1 min

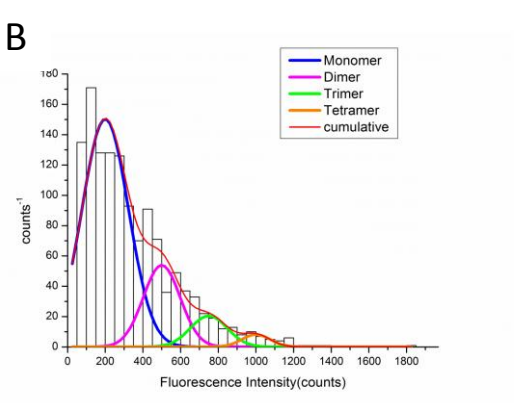

Bax (560 nM) -1 min

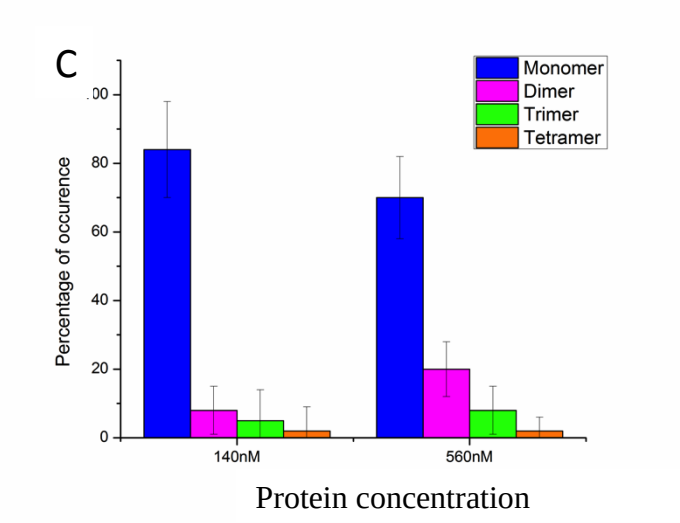

Figure.8.6. Stoichiometry analysis of Bax-Al488 added to SLBs. Intensity distribution of Bax-Al488 bound to the supported lipid bilayer when added at different concentrations, A) 140 nM Bax, B) 560 nM Bax. For each condition, ~500 particles were analyzed after 1 min incubation. The resulting histograms were fitted with a sum of four Gaussians in order to estimate the occurrence of monomers (blue), dimers (magenta), trimers (green) and tetramers (orange). The area of the fitted gaussians is proportional to the fraction of each species. (C) The percentage of monomers, dimers, trimers and tetramers at different concentrations of Bax. Color code is the same as in the fittings in (A) and (B).

In order to capture the process of Bax oligomerization in the membrane, we incubated 2.5 nM Bax-Al488 and 5 nM unlabeled cBid with small unilamellar vesicles (SUVs) and large unilamellar vesicles (LUVs) (extruded through a 200 nm filter) for 1 h. Then we prepared bilayers in the same way as described earlier. Unbound proteins and unfused vesicles were removed by careful washing with SLB buffer. Movies were acquired with TIRF microscopy and data analysis was carried out to determine the stoichiometry of Bax particles. Under these conditions, we could detect higher order oligomers up to hexamers (Fig. 8.7). When compared with the previous results in Fig.8.3 there are only 10-20% monomers with SUVs and LUVs respectively. We see a clear difference in the oligomerization of Bax, when added to SLB directly or when we incubated it with liposomes for 1 h and then prepared the SLB. This is because Bax can diffuse freely in the liposomes (free standing bilayer) and oligomerize effectively.

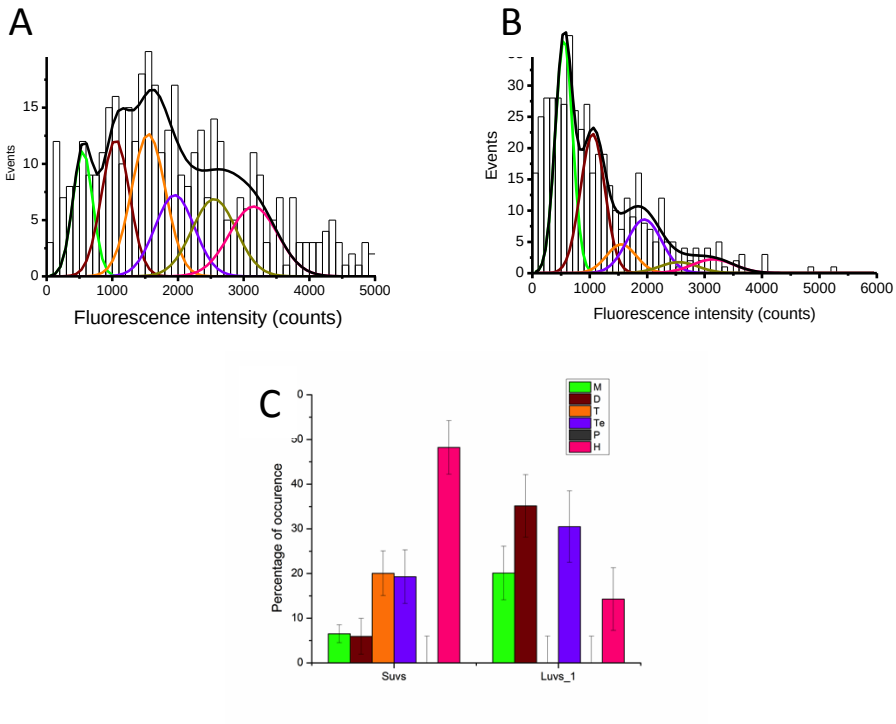

Figure.8.7. Stoichiometry analysis of Bax-Al488 particles on SLBs prepared from proteoliposomes. Intensity distribution of Bax-Al488 bound to the SLB when incubated for 1 h with A) SUVs, B) LUVs. For each condition, ~500 particles were analyzed 1 min after SLB preparation. The resulting histograms were fitted with a sum of four Gaussians inorder to estimate the occurrence of monomers (blue), dimers (magenta), trimers (green) and tetramers (orange). The area of the fitted gaussians is proportional to the fraction of each species. C) The percentage of monomers (green), dimers (brown), trimers (orange), tetramers (violet), pentamer (dark green) and hexamers (pink).

8.4. Effect of membrane curvature on Bax oligomerization

It has been proposed that membrane curvature affects Bax oligomerization (Basanez et al., 2002; Terrones et al., 2004). In order to test the efficiency of Bax oligomerization with differently curved bilayers, we prepared liposomes of different sizes and the lipid composition PC: CL (8:2). Liposomes were extruded through polycarbonate filters with pore diameters ranging from 50-400 nm. The mean diameter of the vesicles was determined with dynamic light scattering. The vesicles extruded through 50 and 100 nm filters resulted in a mean diameter of ~100 nm, 200 nm filters yielded similar size as the 400 nm filter and gave a diameter of ~220 nm (Table 8.1). For this reason, we chose vesicles extruded with 50 nm and 200 nm filters for our experiments. In addition, we prepared small unilamellar vesicles (SUVs) (30-50 nm) by sonication and giant

unilamellar vesicles (GUVs) with heterogeneous diameter in the order of micrometers by electroformation.

LUV size extruded	*Radius in nm*	*Diameter in nm*
50	62,71±22.86	125,42
50	60,72±19.80	121,44
100	66,4±25	132,94
100	66,36±22	132,72
200	88,22±28	176,44
200	89,77±34	179,54
400	109,3±48	218,6
400	114,6±50	229,2

Table.8.1. LUVs size measured by Dynamic light scattering.

` Bax-Al488 was incubated for an hour with these different preparations of liposomes and analyzed to determine its oligomeric state. We observed a distribution of species upto hexamers with all sizes of liposomes. With SUVs, we observed the occurrence of a lower amount of monomers (7±2%) and dimers (6±4%) compared to 20±5% trimers, 19±6% tetramers and 48±6% hexamers (Fig.8.8). The analysis with 100 nm-sized liposomes resulted in very few monomers (2±4%) and 18±5% dimers, 42±7% tetramers and 38±7% hexamers (Fig.8.8.A &E). Liposomes of 200 nm diameter showed a similar distribution, with 21±5% dimers, 44±10% tetramers, and 35±10% hexamers (Fig.8.8.B &F). Interestingly, even with larger sized (GUVs) liposomes, we observed 1±4% monomers, 8±6% dimers, 44±9% tetramers, and 49±11% hexamers (Fig.8.8.C &G). These results are very interesting because the low percentage of monomers, trimers and pentamers suggests that Bax oligomerizes via dimer condensation. They also indicate that change membrane curvature (at least in this range) does not affect Bax oligomerization.

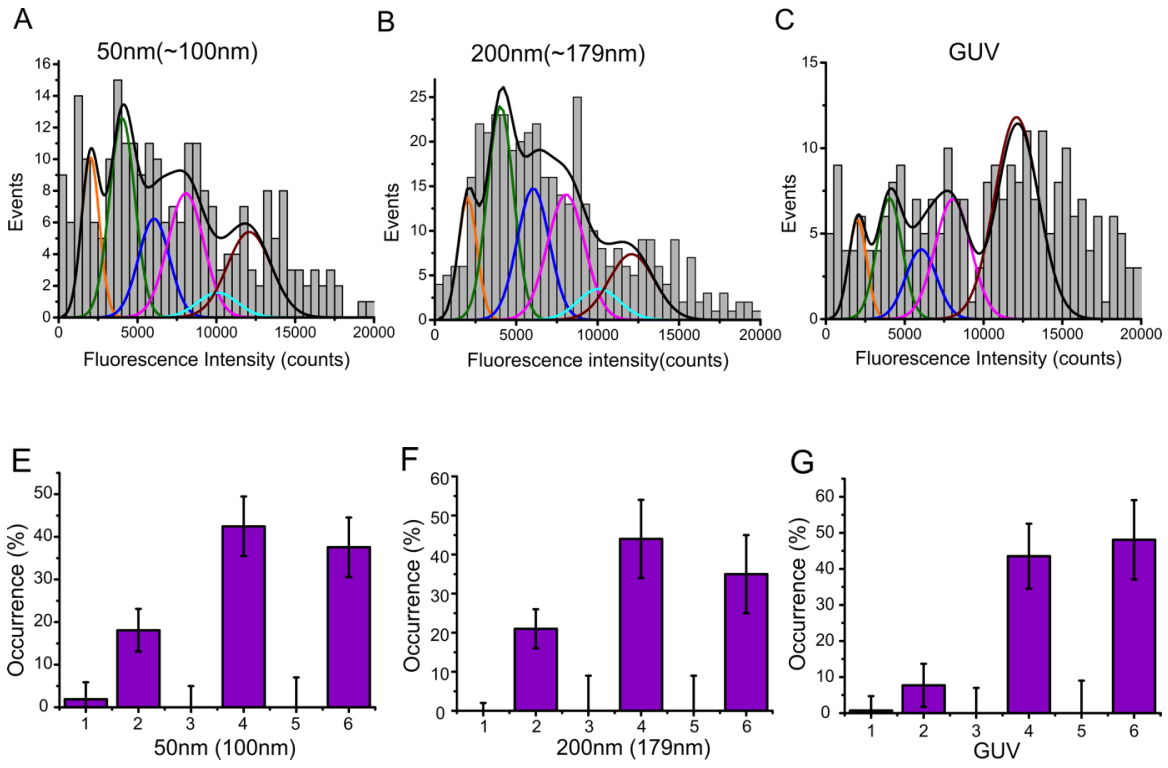

Figure.8.8. Stoichiometry analysis of Bax-Al488 in supported lipid bilayers prepared from liposomes of different sizes. Intensity distribution of Bax-Al488 particles bound to the supported lipid bilayer prepared from proteoliposomes, A) 50 nm LUVs, B) 200 nm LUVs and C) GUVs. For each condition ~500 particles were analyzed. The resulting histograms were fitted with a sum of six Gaussians in order to estimate the occurrence of monomers (orange), dimers (green), trimers (blue), tetramers (magenta), pentamers (cyan) and hexamers (red). The cumulative fit is shown in black. (E-G). The area of the fitted gaussians is proportional to the fraction of each species. The percentage of the different oligomeric species when Bax-Al488 is incubated with different size liposomes, 50nm LUVs (E), 200nmLUVs (F) and GUVs (G). The numbers in the X-axis indicate the oligomeric species.

8.5. Temporal evolution of Bax oligomerization

In order to investigate the dynamics of Bax oligomerization in membranes, we analyzed the stoichiometry of Bax particles at different incubation times. We took to our advantage the effective stop of Bax diffusion once the SLBs were formed, which allowed the accurate control of the time time allowed for oligomerization. LUVs extruded with a 200 nm filter, final size of 180 nm, were incubated with Bax-Al488 and unlabeled cBid during 1 min, 2.5 min, 5 min, 10 min, 1 h and 2 h. SLBs were prepared from these LUVs and imaged under the same conditions as earlier. Analysis of these data showed that Bax oligomerization is a very fast process, as we detect higher oligomers already at 1min

incubation. Concretely, we found 30±7% dimers, 54±15% tetramers and 16±8% hexamers (Fig.8.10.A). After 2.5 min of incubation, the fractions of species are 30±12% dimers, 39±13% tetramers and 31±9% hexamers (Fig.8.10.B). The percentage of oligomers detected after 5 and 10 min are 14±5% dimers, 50±14%tetramers, 36±9% hexamers (Fig.8.10.C) and 34±10% dimers, 55±16% tetramers, 11±8% hexamers respectively (Fig.8.10.D). The LUVs incubated with protein for 1h and 2h yielded 21±5% dimers, 55±12%tetramers, 24±7% hexamers (Fig.8.10.E) and 7±4% monomers, 21±7% dimers, 30±6% tetramers, 42±12% hexamers respectively (Fig.8.10.F). As a control, Bax was also activated by heat and incubated with LUVs for 1h. Bax activated by heat could also oligomerize effectively after 1h resulting in 42±10% dimers, 38±9% tetramers, and 20±6% hexamers (Fig.8.10.G). This indicates that Bid is able to activate Bax, but it is not necessary for its oligomerization.

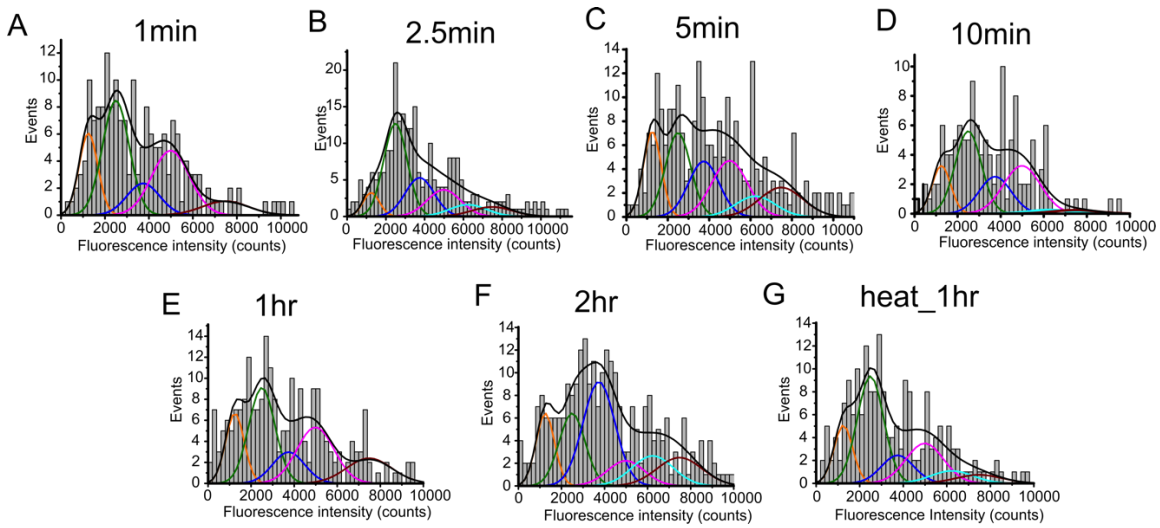

Figure.8.9. Stoichiometry analysis of Bax-Al488 in supported lipid bilayers prepared from proteoliposomes of 200 nm at different incubation times. (A-G) Intensity distribution of Bax-Al488 bound to the supported lipid bilayer prepared from proteoliposomes at incubation times: 1min (A), 2.5 min (B), 5 min (C), 10 min (D), 1 h (E), 2 h (F) and Bax activated by heat for 1 h (G). The resulting histograms were fitted with a sum of six Gaussians in order to estimate the occurrence of monomers (orange), dimers (green), trimers (blue), tetramers (magenta), pentamers (cyan) and hexamers (red). The cumulative fit is shown in black.

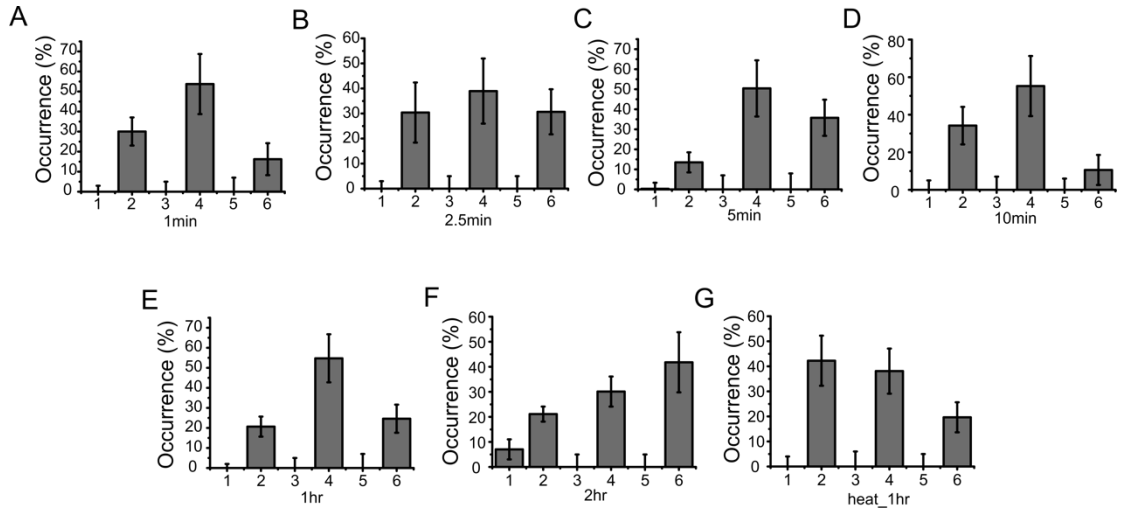

Figure.8.10. The percentage of occurrence of different oligomeric species at different incubation times. The area of the fitted Gaussians in Fig 7.6 is proportional to the fraction of each species. (A-G) The distribution of Bax-Al488 species in the supported lipid bilayers. The percentage of different oligomeric species when Bax is incubated at different times with 200 nm sized liposomes, 1 min (A), 2. 5 min (B), 5 min (C), 10 min (D), 1 h (E), 2 h (F) and Bax activated by heat for 1 h (G). The numbers in the X-axis indicate the oligomeric species.

On the whole, there is no significant difference in the occurrence of oligomers between the initial time points (1-10 min) and 1 h/2 h. Tetramers are the highest occurring species, except at 2 h where the fraction of hexamers is larger. Strikingly, we don't observe any trimers or pentamers in any of these samples proving again that Bax forms oligomers via dimer condensation. The experiments with Bax activated by heat indicate that cBid is not essential for Bax oligomerization and that it does not significantly affect the process at least under the conditions tested.

8.6. Preliminary studies of interactions between Bcl2 proteins

8.6.1 Bax is activated by tBid before insertion

In our studies of interactions between Bcl2 proteins, we used two variants of Bid; cBid and tBid. *In vivo,* Bid has to be cleaved and therefore activated by caspase-8 in order to trigger the activation of Bax in apoptosis. For this purpose, we also used recombinantly expressed Bid cleaved with caspase-8 in our *in vitro* studies. The resulting protein after the cleavage is called cBid and contains the two protein fragments P7 and P15, which

remain associated. In contrast, truncated Bid (tBid) comprises only the P15 fragment and lacks P7 (separated by chromatography). Binding of Bax and cBid/tBid to the membrane and their interactions were examined by two-color TIRF microscopy. For these experiments, we used 2.5 nM Bax-Al488, 2.5 nM cBid-Al 633 or 2 nM tBid-Al647 (see Chapter 6 for protein purification and labeling). SUVs and LUVs were prepared from lipid mixtures containing EggPC:CL (8:2). SLBs were prepared from SUVs and proteins (Bax +cBid/tBid) were added directly to the bilayers. Images were acquired immediately. Additionally, we also incubated LUVs with proteins (Bax + cBid/tBid) for 1 h and 1.5 h in order to allow them to reach equilibrium, and prepared bilayers from those proteoliposomes (Fig.8.8.A).

To investigate the interactions between cBid/tBid and Bax in our system, we analyzed the colocalization of both labeled proteins in the images/movies acquired with dual color TIRF microscopy. As shown in Fig.8.11.B, D, we didn't observe any interactions between Bax and cBid when they were added directly to bilayer or previously incubated with LUVs. Under these conditions, cBid was sparsely bound to the membrane, probably due to the ability of this protein to constantly associate and dissociate from the lipid bilayer (Wang et al., 1998). In order to work under conditions of stable binding to the membrane, we used tBid in similar experiments with SUVs and LUVs (which allow protein diffusion and oligomerization before SLB formation). In this case, tBid bound stably to the bilayer and colocalized with Bax (Fig.8.11.C, E). Our results suggest that Bax interacts with cBid/tBid, gets activated in solution and then binds to the membrane. Alternatively, cBid/tBid could bind first to the bilayer and act as a receptor for Bax binding and activation at the membrane. cBid leaves Bax in the membrane and translocates to the solution, but tBid stays bound to the membrane and partially associated to Bax. The fact that Bax particles also exist in the membrane without being bound to tBid indicates that this interaction during Bax activation is transient.

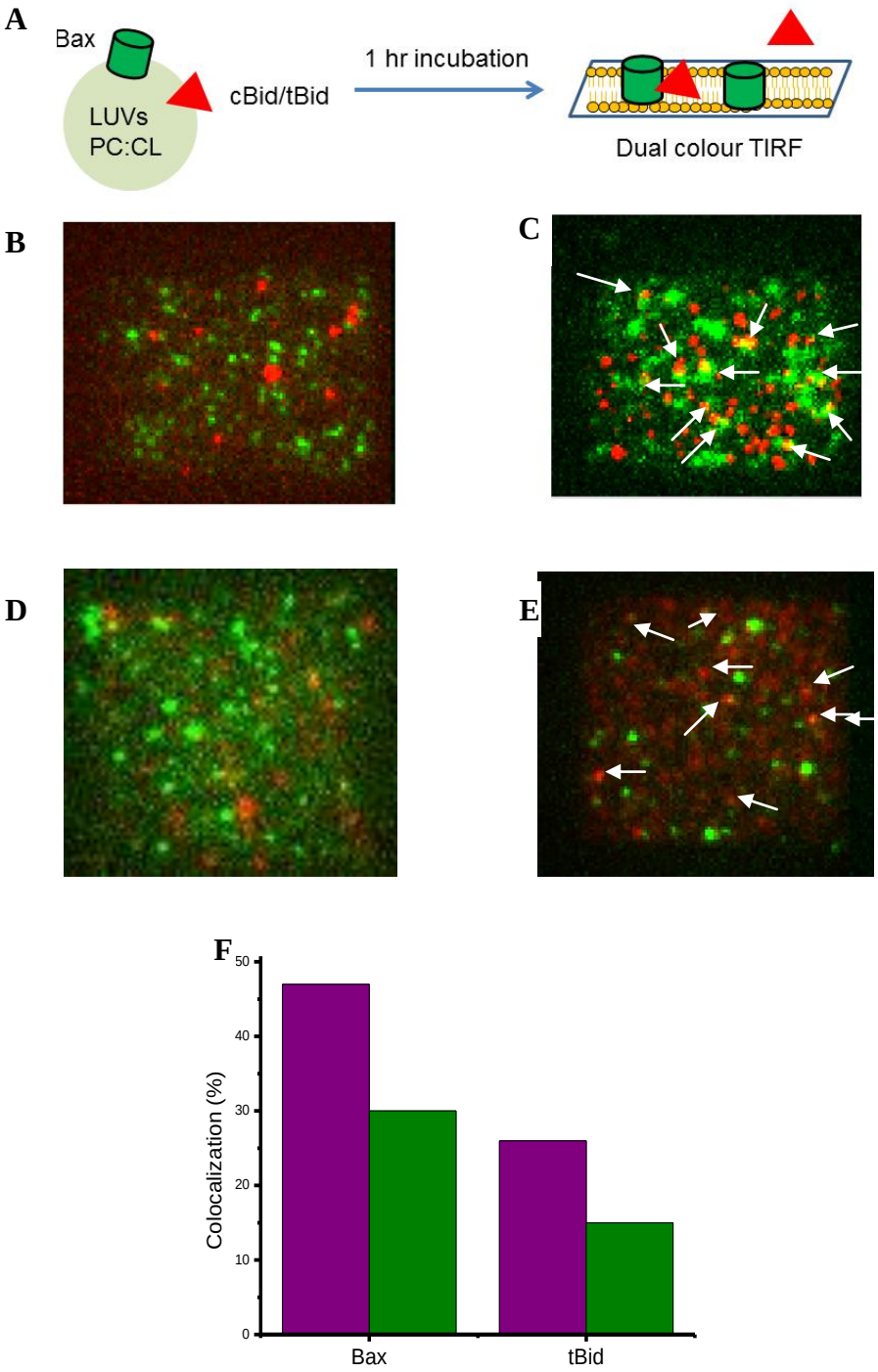

Figure.8.11. Two color TIRF imaging. A) Schematic representation of LUVs incubated with Bax-Al488 and cBid-Al633/tBid-Al647 prior to SLB formation. B) Merged TIRF image of a SLB prepared from LUVs incubated with Bax and cBid for 1 h. C) Merged TIRF image of a SLB prepared from LUVs incubated with Bax and tBid for 1 h. D) Merged TIRF image of a SLB prepared from SUVs, and Bax and cBid added directly to the bilayer. E) Merged TIRF image of a SLB prepared from SUVs, and Bax and tBid added directly to the bilayer and imaged immediately. F) Percentage of Bax particles colocalized with tBid and tBid particles colocalized with Bax when both the proteins are incubated with LUVs for 1 h (purple) and added directly to the SLBs (green).

8.6.2 cBid binds stably to the membrane in presence of Bcl-xL

Similar kind of experiments were done to visualize the interaction between Bcl-xL and cBid/tBid. In this case, SUVs and LUVs were prepared from the lipid mixtures containing EggPC:CL (8:2) as well as Mitomix. SLBs were prepared from SUVs and the corresponding proteins (Bcl-xL + cBid) were added directly to the bilayers. Images were acquired immediately. Additionally, we also incubated LUVs (both lipid compositions) with proteins (Bcl-xL + cBid/tBid) for 1 and 1.5 h in order to allow them to reach equilibrium and prepared bilayers from those proteoliposomes (Fig.8.12.A). To investigate the interactions between cBid and Bcl-xL in our system, we analyzed the colocalization of both labeled proteins in the images/movies acquired with dual color TIRF microscopy. As shown in Fig.8.12.B, C, D, F, we did not observe any interactions between Bcl-xL and cBid when added directly to the bilayer or incubated with LUVs. Under these conditions cBid was sparsely bound to membranes probably due to the ability of this protein to constantly associate and dissociate from the membrane (Wang et al., 1998). In order to work under conditions of stable binding to the membrane, we used tBid in similar experiments with LUVs (which allow protein diffusion and oligomerization before SLB formation). In this case, tBid bound stably to the bilayer and colocalized with Bcl-xL (Fig.8.12. E, G). Interestingly, Bcl-xL bound to Mitomix membranes more prominently than to PC:CL bilayers. With Mitomix, cBid alone did not significantly bind to the membrane, but in presence of Bcl-xL we could observe very weak binding.

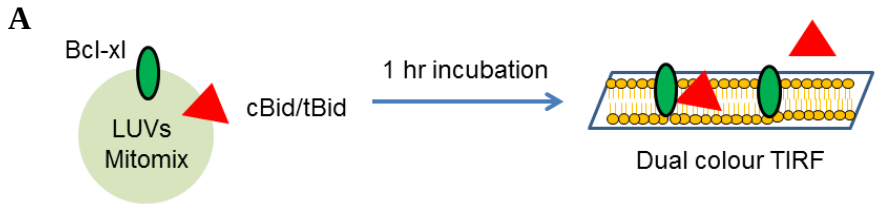

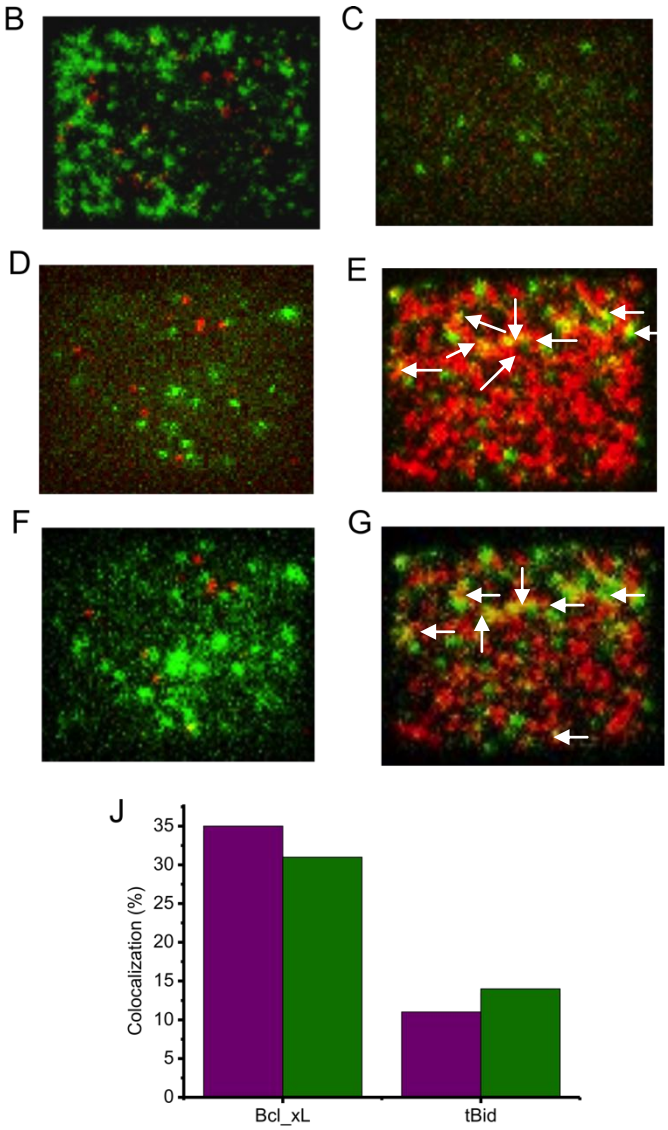

Figure.8.12. Two color TIRF imaging of Bcl-xL and cBid/tBid. A) Schematic representation of LUVs incubated with Bcl-xL-Al488 and cBid-Al633/tBid-Al647 prior to the formation of SLB. B) Merged TIRF image of a SLB prepared from SUVs containing PC:CL (8:2), and Bcl-xL and cBid added directly to the bilayer . C) Merged TIRF image of a SLB prepared from SUVs containing Mitomix, and Bcl-xL and cBid added directly to the bilayer. D) Merged TIRF image of a SLB prepared from LUVs (PC: CL (8:2)) incubated with Bcl-xL and cBid for 1h. E) Merged TIRF image of a SLB prepared from LUVs [PC: CL (8:2)] incubated with Bcl-xL and tBid for 1h. F) Merged TIRF image of a SLB prepared from LUVs (Mitomix) incubated with Bcl-xL and cBid for 1h. G) Merged TIRF image of a SLB prepared from LUVs (Mitomix) incubated with Bcl-xL and tBid for 1h. J) Percentage of Bcl-xL particles colocalized with tBid and tBid particles colocalized with Bcl-xL when both the proteins are incubated with LUVs for 1 h (purple) and added directly to the SLBs (green).

8.7. Discussion

The Bcl-2 family of proteins has a vital role in the regulation of the mitochondrial apoptosis pathway (Taylor et al., 2008; Tsujimoto and Shimizu, 2007; Yip and Reed, 2008). Bax, a proapoptotic protein, mediates the permeabilization of the outer mitochondrial membrane upon activation by tBid (Bleicken et al., 2010a; Westphal et al., 2011). *In vitro*, it has been shown that Bax oligomerizes to form a pore similar to other pore forming proteins. It is believed that a similar mechanism is responsible for the release of cytochrome c and other apoptotic factors during apoptosis (Bleicken et al., 2010a; Dejean et al., 2005; Ott et al., 2002; Shimizu et al., 1999). In this work, we have employed single molecule microscopy to provide a better understanding on the dynamics of oligomerization and stoichiometry of Bax in the membrane. We have also investigated the interaction between Bcl-2 proteins using a two-color approach.

Cardiolipin (CL) containing membranes were used in this study because it is a mitochondria-specific phospholipid that may play an important role in Bax action (Gonzalvez et al., 2008; Hoch, 1992; Lutter et al., 2000; Schafer et al., 2009). Consistent with other studies, we also observed that Bax does not bind to membranes lacking CL (Epand et al., 2002; Kuwana et al., 2002; Schug and Gottlieb, 2009). CL is known to exert curvature stress and to form inverted micelles (Siegel, 1984; Smaal et al., 1987). This effect on membrane organization has been suggested to be important for Bax pore formation.

In our studies Bax did not diffuse in supported bilayers. Probably, membrane inserted Bax interacts with the highly hydrophilic glass support inhibiting the diffusion. However, the fact that Bax is mostly monomeric after binding to SLBs supports that Bax oligomerizes only after inserting into the membrane (Annis et al., 2005; Cartron et al., 2008; Lovell et al., 2008). Furthermore, Bax oligomerization was highly enhanced when the protein was incubated with liposomes (SUVs, LUVs, and GUVs) prior to SLB formation. We also found that the occurrence of oligomeric species does not differ significantly between different types of liposomes. This demonstrates that Bax needs a free-standing bilayer to diffuse and form higher order oligomers. In addition, our results show that membrane curvature does not significantly affect Bax oligomerization, at least in the scale of curvatures used in this study. These observations are in contrast to a previous report proposing that liposomes smaller than 200 nm in diameter barely support Bax binding and do not support Bax oligomerization (Lucken-Ardjomande et al., 2008).

However, the lipid composition used in that study was different from ours and contained PE, PI and cholesterol besides PC and CL. It has been proposed that PE does not have an impact on Bax insertion, but that it inhibits Bax oligomerization to a certain extent as well as the permeabilization of liposomes. The presence of PE could also be responsible for the differences in oligomerization we observed (Terrones et al., 2004). Despite all of this, it could still be that the extremely high curvature found at mitochondrial fission sites actually has an effect on Bax oligomerization, as proposed by Martinou and coworkers in their study reporting the activatory effect of Drp1 on Bax (Karbowski et al., 2002; Montessuit et al., 2010; Rolland and Conradt, 2010). Further experiments will be needed to test this hypothesis.

Interestingly, we found that Bax oligomerizes via dimer condensations in all types of liposomes tested. Only in SUVs we observed a fraction of trimers, which could be due to the fact that SUVs are highly curved and may promote non-specific forms of Bax. For Bak, a homologue of Bax, it has been proposed to form oligomers via dimer condensations. This is based on the observation that symmetric Bak dimers formed initially by BH3-groove contacts, and then higher order oligomers formed via a second interaction surface formed by helix α-6 (Ma et al., 2013).

We also found that there is no significant difference in the occurrence of oligomers at different time points. This indicates that Bax oligomerization is extremely quick and after 1 min it has reached equilibrium and does not further evolve over time, unlike in the case of Equinatoxin II (See Chapter 7). Moreover, the largest identified oligomers consist of 4 and 6 subunits, which suggest that Bax pores are formed via tetramers and hexamers. However, we cannot exclude that Bax dimers or monomers are also permeabilizing the membrane, as suggested by a recent study (Xu et al., 2013).

It is important to note that Bax cannot form a pure proteinaceous pore of the size required to release cytochrome c at these oligomeric states. Therefore our results support that Bax forms a toroidal pore (Terrones et al., 2004). However, in our analysis there is a small amount of oligomers higher than hexamers that could not be included in the fitting for technical reasons. In any case, the number does not exceed 8 subunits, which supports the role of small Bax oligomers in pore formation. Some biochemical studies have shown Bax oligomers of sizes up to 10-12 subunits (Bleicken et al., 2010a; Epand et al., 2002, 2003; Zhang et al., 2010). Indeed, in cells undergoing apoptosis, Bax gets activated and translocates from the cytosol to the outer mitochondrial membranes, where it aggregates into large clusters at later stages of apoptosis. The size of these clusters has been proposed

to be substantially larger than our oligomers, consisting of around 100 Bax molecules (Zhou and Chang, 2008). This could be due to the presence of additional factors and/or reactions on the mitochondrial membrane that promote the formation of these large clusters. In this context, our results in pure lipid membranes suggest that Bax tends to associate mostly into smaller oligomers when only lipids and cBid are present.

In this study, we have used a dual color single molecule approach to examine the membrane binding and interactions of Bid (cBid/tBid) to Bax and Bcl-xL. We attempted to directly visualize how Bax and Bid (cBid/tBid) interact. Because of the constant shuttling from solution to membrane, we could not detect any colocalization of Bax and cBid. But with tBid, which rapidly binds to membrane and remains stably associated, we show that 47% of Bax particles interact with tBid. Bid has been shown to induce a conformational change in Bax while activation, and no longer stay associated with Bax after oligomerization (Desagher et al., 1999; Eskes et al., 2000; Kim et al., 2009; Lovell et al., 2008; Roucou et al., 2002; Wei et al., 2000). Our results demonstrate that tBid activates Bax via a direct interaction (Juin et al., 2005; Ott et al., 2007). Moreover, the fact that we detect activated Bax molecules associated to the membrane and not bound to Bid supports a transient contact between these two proteins, in agreement with the "hit and run" model (Wei et al., 2000).

Interestingly, cBid doesn't bind alone to Mitomix bilayers but it does in presence of Bcl-xL. In contrast, tBid binding does not require Bcl-xL. Similar to Bax, the interaction between Bcl-xL and tBid was more pronounced than between Bcl-xL and cBid. As it has been reported previously, Bcl-xL and tBid interact in solution but their interaction is enhanced in the presence of membranes (Garcia-Saez et al., 2009a). Our results support these observations. However, the most challenging task in these experiments is to have both proteins efficiently labelled. This is the most important factor to reduce the probability of interaction between a labeled and an unlabeled protein that do not appear in our images as a complex. In our experiments, all the proteins used had a labeling efficiency ranging from 70-80%. As there are 20-30 % of unlabeled proteins, we might lose some of the interactions. In the future, this has to be taken in account while quantifying the interaction between proteins as it is extremely difficult to obtain 100% labeling.

To summarize, here we carried out a stoichiometric analysis of Bax based on the intensity of individual fluorophores. We demonstrate that Bax forms oligomers of up to six units and that it oligomerizes via dimer condensation. Moreover, the oligomerization

does not depend on membrane curvature at least in the range studied here. Bax assembly is very fast, as it forms oligomers in less than a minute. Importantly, our results have shown that activation of Bax happens prior to the insertion into bilayer and that interaction with tBid is not necessary for oligomerization.

Chapter 9

Appendix

9.1. List of Abbreviations

Bax	Bcl-2 associated protein x
Bax-Al488	Bax protein labeled with Alexa fluor 488
Bcl-xL	B cell lymphoma extra-large protein
Bcl-xL-Al488	Bcl-xL labeled with Alexa fluor 488
Bid	BH3- interacting domain death agonist
BH	Bcl-2 homology domain
cBid	Cleaved Bid, Bid cleaved with caspase 8
cBid-Al633	Cleaved Bid labeled with Alexa fluor 633
CDC	Cholesterol dependent cytolysins
CL	Cardiolipin
Chol	Cholesterol
Did	1,1'-dioctadecyl-3,3,3',3'-tetramethylindodicarbocyanine, 4 chlorobenzenesulfonate salt
DLS	Dynamic light scattering
DOPC	1, 2-dioleoyl-sn-glycero-3-phosphocholine
EggPC	Egg phosphotidylcholine
EqtII	Equinatoxin II
EqtII-Al555	Equinatoxin II labeled with Alexa fluor 555
FraC	Fragaceatoxin C
GUV	Giant unilamellar vesicle
IMM	Mitochondrial inner membrane
LUV	Large unilamellar vesicle
MOM	Mitochondrial outer membrane
MSD	Mean square displacement
ODE	Ordinary differential equations
PA	Phosphatidic acid
PE	Phosphatidylethanolamine
PFP	Pore forming protein
PFT	Pore forming toxin
PI	Phosphatidylinositol

PS	Phosphatidylserine
SLB	Supported lipid bilayer
SM	Sphigomyelin
SPT	Single particle tracking
Stn I	Sticholysin I
Stn II	Sticholysin II
SUV	Small unilamellar vesicle
tBid	truncated Bid
TIRF	Total internal reflection microscopy

9.2. List of Figures

Chapter 8

9.3. List of Tables

Chapter 10

Bibliography

10. References:

Abrami, L., Fivaz, M., Decroly, E., Seidah, N.G., Jean, F., Thomas, G., Leppla, S.H., Buckley, J.T., and van der Goot, F.G. (1998). The pore-forming toxin proaerolysin is activated by furin. J Biol Chem *273*, 32656-32661.

Alegre-Cebollada, J., Onaderra, M., Gavilanes, J.G., and del Pozo, A.M. (2007). Sea anemone actinoporins: The transition from a folded soluble state to a functionally active membrane-bound oligomeric pore. Curr Protein Pept Sc *8*, 558-572.

Allured, V.S., Collier, R.J., Carroll, S.F., and McKay, D.B. (1986). Structure of exotoxin A of Pseudomonas aeruginosa at 3.0-Angstrom resolution. Proc Natl Acad Sci U S A *83*, 1320-1324.

Alouf, J.E. (2001). Pore-forming bacterial protein toxins: an overview. Curr Top Microbiol Immunol *257*, 1-14.

Alvarez, C., Mancheno, J.M., Martinez, D., Tejuca, M., Pazos, F., and Lanio, M.E. (2009). Sticholysins, two pore-forming toxins produced by the Caribbean Sea anemone Stichodactyla helianthus: their interaction with membranes. Toxicon *54*, 1135-1147.

Anderluh, G., Dalla Serra, M., Viero, G., Guella, G., Macek, P., and Menestrina, G. (2003). Pore formation by equinatoxin II, a eukaryotic protein toxin, occurs by induction of nonlamellar lipid structures. J Biol Chem *278*, 45216-45223.

Anderluh, G., and Lakey, J.H. (2008). Disparate proteins use similar architectures to damage membranes. Trends Biochem Sci *33*, 482-490.

Anderluh, G., and Macek, P. (2002a). Cytolytic peptide and protein toxins from sea anemones (Anthozoa : Actiniaria). Toxicon *40*, 111-124.

Anderluh, G., and Macek, P. (2002b). Cytolytic peptide and protein toxins from sea anemones (Anthozoa: Actiniaria). Toxicon *40*, 111-124.

Anderson, C.M., Georgiou, G.N., Morrison, I.E.G., Stevenson, G.V.W., and Cherry, R.J. (1992). Tracking of Cell-Surface Receptors by Fluorescence Digital Imaging Microscopy Using a Charge-Coupled Device Camera - Low-Density-Lipoprotein and Influenza-Virus Receptor Mobility at 4-Degrees-C. Journal of Cell Science *101*, 415-425.

Andreeva-Kovalevskaya Zh, I., Solonin, A.S., Sineva, E.V., and Ternovsky, V.I. (2008). Pore-forming proteins and adaptation of living organisms to environmental conditions. Biochemistry (Mosc) *73*, 1473-1492.

Andrews, N.L., Lidke, K.A., Pfeiffer, J.R., Burns, A.R., Wilson, B.S., Oliver, J.M., and Lidke, D.S. (2008). Actin restricts FcepsilonRI diffusion and facilitates antigen-induced receptor immobilization. Nat Cell Biol *10*, 955-963.

Annis, M.G., Soucie, E.L., Dlugosz, P.J., Cruz-Aguado, J.A., Penn, L.Z., Leber, B., and Andrews, D.W. (2005). Bax forms multispanning monomers that oligomerize to permeabilize membranes during apoptosis. EMBO J *24*, 2096-2103.

Antignani, A., and Youle, R.J. (2006). How do Bax and Bak lead to permeabilization of the outer mitochondrial membrane? Current Opinion in Cell Biology *18*, 685-689.

Athanasiadis, A., Anderluh, G., Macek, P., and Turk, D. (2001). Crystal structure of the soluble form of equinatoxin II, a pore-forming toxin from the sea anemone Actinia equina. Structure *9*, 341-346.

Axelrod, D., Burghardt, T.P., and Thompson, N.L (1984). Total internal reflection fluorescence. Annu Rev Biophys Bioeng *13*, 247-268.

Axelrod, D., Koppel, D.E., Schlessinger, J., Elson, E., and Webb, W.W. (1976). Mobility measurement by analysis of fluorescence photobleaching recovery kinetics. Biophys J *16*, 1055-1069.

Axelrod, D., Thompson, N.L., and Burghardt, T.P. (1983). Total internal reflection fluorescent microscopy. J Microsc *129*, 19-28.

Bachir, A.I., Durisic, N., Hebert, B., Grutter, P., and Wiseman, P.W. (2006). Characterization of blinking dynamics in quantum dot ensembles using image correlation spectroscopy. Journal of Applied Physics *99*.

Bakrac, B., and Anderluh, G. (2010). Molecular mechanism of sphingomyelin-specific membrane binding and pore formation by actinoporins. Adv Exp Med Biol *677*, 106-115.

Bakrac, B., Gutierrez-Aguirre, I., Podlesek, Z., Sonnen, A.F., Gilbert, R.J., Macek, P., Lakey, J.H., and Anderluh, G. (2008). Molecular determinants of sphingomyelin specificity of a eukaryotic pore-forming toxin. J Biol Chem *283*, 18665-18677.

Barak, L.S., and Webb, W.W. (1982). Diffusion of low density lipoprotein-receptor complex on human fibroblasts. J Cell Biol *95*, 846-852.

Barlic, A., Gutierrez-Aguirre, I., Caaveiro, J.M., Cruz, A., Ruiz-Arguello, M.B., Perez-Gil, J., and Gonzalez-Manas, J.M. (2004). Lipid phase coexistence favors membrane insertion of equinatoxin-II, a pore-forming toxin from Actinia equina. J Biol Chem *279*, 34209-34216.

Barry, R., Moore, S., Alonso, A., Ausio, J., and Buckley, J.T. (2001). The channel-forming protein proaerolysin remains a dimer at low concentrations in solution. J Biol Chem *276*, 551-554.

Basanez, G., Sharpe, J.C., Galanis, J., Brandt, T.B., Hardwick, J.M., and Zimmerberg, J. (2002). Bax-type apoptotic proteins porate pure lipid bilayers through a mechanism sensitive to intrinsic monolayer curvature. Journal of Biological Chemistry *277*, 49360-49365.

Bayley, H. (2009). Membrane-protein structure: Piercing insights. Nature *459*, 651-652.

Belmonte, G., Pederzolli, C., Macek, P., and Menestrina, G. (1993a). Pore formation by the sea anemone cytolysin equinatoxin II in red blood cells and model lipid membranes. J Membr Biol *131*, 11-22.

Belmonte, G., Pederzolli, C., Maček, P., and Menestrina, G. (1993b). Pore formation by the sea anemone cytolysin equinatoxin II in red blood cells and model lipid membranes. Journal of Membrane Biology *131*, 11-22.

Bender, T., and Martinou, J.C. (2013). Where Killers Meet-Permeabilization of the Outer Mitochondrial Membrane during Apoptosis. Cold Spring Harbor Perspectives in Biology *5*.

Bernheimer, A.W., and Avigad, L.S. (1976). Properties of a toxin from the sea anemone Stoichacis helianthus, including specific binding to sphingomyelin. Proc Natl Acad Sci U S A *73*, 467-471.

Bleicken, S., Classen, M., Padmavathi, P.V., Ishikawa, T., Zeth, K., Steinhoff, H.J., and Bordignon, E. (2010a). Molecular details of Bax activation, oligomerization, and membrane insertion. J Biol Chem *285*, 6636-6647.

Bleicken, S., Classen, M., Padmavathi, P.V.L., Ishikawa, T., Zeth, K., Steinhoff, H.J., and Bordignon, E. (2010b). Molecular Details of Bax Activation, Oligomerization, and Membrane Insertion. Journal of Biological Chemistry *285*, 6636-6647.

Bleicken, S., Landeta, O., Landajuela, A., Basanez, G., and Garcia-Saez, A.J. (2013a). Proapoptotic Bax and Bak form stable protein-permeable pores of tunable size. J Biol Chem.

Bleicken, S., Wagner, C., and Garcia-Saez, A.J. (2013b). Mechanistic differences in the membrane activity of Bax and Bcl-xL correlate with their opposing roles in apoptosis. Biophys J *104*, 421-431.

Bobroff, N. (1986). Position measurement with a resolution and noise-limited instrument Review of Scientific Instruments *57*, 6.

Brameshuber, M., and Schutz, G.J. (2012). Detection and Quantification of Biomolecular Association in Living Cells Using Single-Molecule Microscopy. Methods in Enzymology, Vol 505: Imaging and Spectroscopic Analysis of Living Cells *505*, 159-186.

Bravo, A., Gill, S.S., and Soberon, M. (2007a). Mode of action of Bacillus thuringiensis Cry and Cyt toxins and their potential for insect control. Toxicon *49*, 423-435.

Bravo, A., Gill, S.S., and Soberon, M. (2007b). Mode of action of Bacillus thuringiensis Cry and Cyt toxins and their potential for insect control. Toxicon *49*, 423-435.

Bruce Alberts, A.J., Julian Lewis, Martin Raff, Keith Roberts, and Peter Walter. (2002). Molecular Biology of the Cell, 4th edition edn (Newyork Garland science).

Buckley, J.T. (1990). Purification of cloned proaerolysin released by a low protease mutant of Aeromonas salmonicida. Biochem Cell Biol *68*, 221-224.

Bullock, J.O., and Kolen, E.R. (1995). Ion selectivity of colicin E1: III. Anion permeability. J Membr Biol *144*, 131-145.

Bunc, M., Drevensek, G., Budihna, M., and Suput, D. (1999). Effects of equinatoxin II from Actinia equina (L.) on isolated rat heart: the role of direct cardiotoxic effects in equinatoxin II lethality. Toxicon *37*, 109-123.

Burks, R.L., and Lodge, D.M. (2002). Cued in: Advances and opportunities in freshwater chemical ecology. J Chem Ecol *28*, 1901-1917.

Burmeister, J.S., Truskey, G.A., Yarbrough, J.L., and Reichert, W.M. (1994). Imaging of cell/substrate contacts on polymers by total internal reflection fluorescence microscopy. Biotechnol Prog *10*, 26-31.

Calebiro, D., Rieken, F., Wagner, J., Sungkaworn, T., Zabel, U., Borzi, A., Cocucci, E., Zurn, A., and Lohse, M.J. (2013). Single-molecule analysis of fluorescently labeled G-protein-coupled receptors reveals complexes with distinct dynamics and organization. Proc Natl Acad Sci U S A *110*, 743-748.

Carter, B.C., Shubeita, G.T., and Gross, S.P. (2005). Tracking single particles: a user-friendly quantitative evaluation. Physical Biology *2*, 60-72.

Cartron, P.F., Bellot, G., Oliver, L., Grandier-Vazeille, X., Manon, S., and Vallette, F.M. (2008). Bax inserts into the mitochondrial outer membrane by different mechanisms. Febs Lett *582*, 3045-3051.

Cascales, E., Buchanan, S.K., Duche, D., Kleanthous, C., Lloubes, R., Postle, K., Riley, M., Slatin, S., and Cavard, D. (2007). Colicin biology. Microbiol Mol Biol Rev *71*, 158-229.

Cheezum, M.K., Walker, W.F., and Guilford, W.H. (2001). Quantitative comparison of algorithms for tracking single fluorescent particles. biophysical journal *81*, 2378-2388.

Chiantia, S., Kahya, N., and Schwille, P. (2005). Dehydration damage of domain-exhibiting supported bilayers: an AFM study on the protective effects of disaccharides and other stabilizing substances. Langmuir *21*, 6317-6323.

Chinnaiyan, A.M., Tepper, C.G., Seldin, M.F., ORourke, K., Kischkel, F.C., Hellbardt, S., Krammer, P.H., Peter, M.E., and Dixit, V.M. (1996). FADD/MORT1 is a common mediator of CD95 (Fas/APO-1) and tumor necrosis factor receptor-induced apoptosis. Journal of Biological Chemistry *271*, 4961-4965.

Chipuk, J.E., McStay, G.P., Bharti, A., Kuwana, T., Clarke, C.J., Siskind, L.J., Obeid, L.M., and Green, D.R. (2012). Sphingolipid metabolism cooperates with BAK and BAX to promote the mitochondrial pathway of apoptosis. Cell *148*, 988-1000.

Chipuk, J.E., Moldoveanu, T., Llambi, F., Parsons, M.J., and Green, D.R. (2010). The BCL-2 Family Reunion. Molecular Cell *37*, 299-310.

Choe, S., Bennett, M.J., Fujii, G., Curmi, P.M., Kantardjieff, K.A., Collier, R.J., and Eisenberg, D. (1992). The crystal structure of diphtheria toxin. Nature *357*, 216-222.

Cocucci, E., Aguet, F., Boulant, S., and Kirchhausen, T. (2012). The first five seconds in the life of a clathrin-coated pit. Cell *150*, 495-507.

Cortajarena, A.L., Goni, F.M., and Ostolaza, H. (2003). A receptor-binding region in Escherichia coli alpha-haemolysin. J Biol Chem *278*, 19159-19163.

Cowell, S., Aschauer, W., Gruber, H.J., Nelson, K.L., and Buckley, J.T. (1997). The erythrocyte receptor for the channel-forming toxin aerolysin is a novel glycosylphosphatidylinositol-anchored protein. Mol Microbiol *25*, 343-350.

Czabotar, P.E., Colman, P.M., and Huang, D.C.S. (2009). Bax activation by Bim? Cell Death and Differentiation *16*, 1187-1191.

Czabotar, P.E., Westphal, D., Dewson, G., Ma, S., Hockings, C., Fairlie, W.D., Lee, E.F., Yao, S., Robin, A.Y., Smith, B.J., *et al.* (2013). Bax crystal structures reveal how BH3 domains activate Bax and nucleate its oligomerization to induce apoptosis. Cell *152*, 519-531.

D'Silva, P.R., and Lala, A.K. (2000). Organization of diphtheria toxin in membranes: a hydrophobic photolabeling study. J Biol Chem *275*, 27500.

Dalla Serra, M., and Menestrina, G. (2003). Liposomes in the study of pore-forming toxins. Methods Enzymol *372*, 99-124.

Daumas, F., Destainville, N., Millot, C., Lopez, A., Dean, D., and Salome, L. (2003). Confined diffusion without fences of a g-protein-coupled receptor as revealed by single particle tracking. Biophys J *84*, 356-366.

de Sousa, M.V., and Morhy, L. (1989). Enterolobin, a hemolytic protein from Enterolobium contortisiliquum seeds (Leguminosae--Mimosoideae). Purification and characterization. An Acad Bras Cienc *61*, 405-412.

Dejean, L.M., Martinez-Caballero, S., Guo, L., Hughes, C., Teijido, O., Ducret, T., Ichas, F., Korsmeyer, S.J., Antonsson, B., Jonas, E.A., *et al.* (2005). Oligomeric Bax is a component of the putative cytochrome c release channel MAC, mitochondrial apoptosis-induced channel. Mol Biol Cell *16*, 2424-2432.

Desagher, S., Osen-Sand, A., Nichols, A., Eskes, R., Montessuit, S., Lauper, S., Maundrell, K., Antonsson, B., and Martinou, J.C. (1999). Bid-induced conformational change of Bax is responsible for mitochondrial cytochrome c release during apoptosis. J Cell Biol *144*, 891-901.

Deverall, M.A., Gindl, E., Sinner, E.K., Besir, H., Ruehe, J., Saxton, M.J., and Naumann, C.A. (2005). Membrane lateral mobility obstructed by polymer-tethered lipids studied at the single molecule level. Biophys J *88*, 1875-1886.

Dewson, G., Kratina, T., Czabotar, P., Day, C.L., Adams, J.M., and Kluck, R.M. (2009). Bak Activation for Apoptosis Involves Oligomerization of Dimers via Their alpha 6 Helices. Molecular Cell *36*, 696-703.

Dewson, G., Kratina, T., Sim, H.W., Puthalakath, H., Adams, J.M., Colman, P.M., and Kluck, R.M. (2008). To trigger apoptosis, Bak exposes its BH3 domain and homodimerizes via BH3:groove interactions. Mol Cell *30*, 369-380.

Dewson, G., Ma, S., Frederick, P., Hockings, C., Tan, I., Kratina, T., and Kluck, R.M. (2012). Bax dimerizes via a symmetric BH3:groove interface during apoptosis. Cell Death Differ *19*, 661-670.

Diep, D.B., Nelson, K.L., Lawrence, T.S., Sellman, B.R., Tweten, R.K., and Buckley, J.T. (1999). Expression and properties of an aerolysin--Clostridium septicum alpha toxin hybrid protein. Mol Microbiol *31*, 785-794.

Dietrich, C., Bagatolli, L.A., Volovyk, Z.N., Thompson, N.L., Levi, M., Jacobson, K., and Gratton, E. (2001). Lipid rafts reconstituted in model membranes. Biophys J *80*, 1417-1428.

Dietrich, C., Yang, B., Fujiwara, T., Kusumi, A., and Jacobson, K. (2002). Relationship of lipid rafts to transient confinement zones detected by single particle tracking. Biophys J *82*, 274-284.

Digman, M.A., and Gratton, E. (2009). Imaging Barriers to Diffusion by Pair Correlation Functions. biophysical journal *97*, 665-673.

Dimitrov, M.I.A.a.D.S. (1986). Liposome Electro formation. Faraday Discuss Chem SOC *81*, 9.

Douglass, A.D., and Vale, R.D. (2005). Single-molecule microscopy reveals plasma membrane microdomains created by protein-protein networks that exclude or trap signaling molecules in T cells. Cell *121*, 937-950.

Epand, R.F., Martinou, J.C., Montessuit, S., and Epand, R.M. (2002). Membrane perturbations induced by the apoptotic Bax protein. Biochem J *367*, 849-855.

Epand, R.F., Martinou, J.C., Montessuit, S., and Epand, R.M. (2003). Transbilayer lipid diffusion promoted by Bax: implications for apoptosis. Biochemistry *42*, 14576-14582.

Eskes, R., Desagher, S., Antonsson, B., and Martinou, J.C. (2000). Bid induces the oligomerization and insertion of Bax into the outer mitochondrial membrane. Mol Cell Biol *20*, 929-935.

Falcon-Perez, J.M., Nazarian, R., Sabatti, C., and Dell'Angelica, E.C. (2005). Distribution and dynamics of Lamp1-containing endocytic organelles in fibroblasts deficient in BLOC-3. Journal of Cell Science *118*, 5243-5255.

Fernandez-Suarez, M., and Ting, A.Y. (2008). Fluorescent probes for super-resolution imaging in living cells. Nature Reviews Molecular Cell Biology *9*, 929-943.

Fesik, S.W. (2000). Insights into programmed cell death through structural biology. Cell *103*, 273-282.

Fivaz, M., Velluz, M.C., and van der Goot, F.G. (1999). Dimer dissociation of the pore-forming toxin aerolysin precedes receptor binding. J Biol Chem *274*, 37705-37708.

Fivaz, M., Vilbois, F., Thurnheer, S., Pasquali, C., Abrami, L., Bickel, P.E., Parton, R.G., and van der Goot, F.G. (2002). Differential sorting and fate of endocytosed GPI-anchored proteins. EMBO J *21*, 3989-4000.

Gallenne, T., Gautier, F., Oliver, L., Hervouet, E., Noel, B., Hickman, J.A., Geneste, O., Cartron, P.F., Vallette, F.M., Manon, S., *et al.* (2009). Bax activation by the BH3-only protein Puma promotes cell dependence on antiapoptotic Bcl-2 family members. J Cell Biol *185*, 279-290.

Garcia-Linares, S., Castrillo, I., Bruix, M., Menendez, M., Alegre-Cebollada, J., Martinez-del-Pozo, A., and Gavilanes, J.G. (2013). Three-dimensional structure of the actinoporin sticholysin I. Influence of long-distance effects on protein function. Arch Biochem Biophys *532*, 39-45.

Garcia-Ortega, L., Alegre-Cebollada, J., Garcia-Linares, S., Bruix, M., Martinez-del-Pozo, A., and Gavilanes, J.G. (2011). The behavior of sea anemone actinoporins at the water‚Äìmembrane interface. Biochimica et Biophysica Acta (BBA) - Biomembranes *1808*, 2275-2288.

Garcia-Saez, A.J., Buschhorn, S.B., Keller, H., Anderluh, G., Simons, K., and Schwille, P. (2011a). Oligomerization and pore formation by equinatoxin II inhibit endocytosis and lead to plasma membrane reorganization. J Biol Chem *286*, 37768-37777.

Garcia-Saez, A.J., Buschhorn, S.B., Keller, H., Anderluh, G., Simons, K., and Schwille, P. (2011b). Oligomerization and pore formation by Equinatoxin II inhibit endocytosis and lead to plasma membrane reorganization. J Biol Chem.

Garcia-Saez, A.J., Coraiola, M., Dalla Serra, M., Mingarro, I., Menestrina, G., and Salgado, J. (2005). Peptides derived from apoptotic Bax and Bid reproduce the poration activity of the parent full-length proteins. Biophys J *88*, 3976-3990.

Garcia-Saez, A.J., Coraiola, M., Serra, M.D., Mingarro, I., Muller, P., and Salgado, J. (2006). Peptides corresponding to helices 5 and 6 of Bax can independently form large lipid pores. Febs J *273*, 971-981.

Garcia-Saez, A.J., Mingarro, I., Perez-Paya, E., and Salgado, J. (2004). Membrane-insertion fragments of Bcl-xL, Bax, and Bid. Biochemistry *43*, 10930-10943.

Garcia-Saez, A.J., Ries, J., Orzaez, M., Perez-Paya, E., and Schwille, P. (2009a). Membrane promotes tBID interaction with BCL(XL). Nat Struct Mol Biol *16*, 1178-1185.

Garcia-Saez, A.J., Ries, J., Orzaez, M., Perez-Paya, E., and Schwille, P. (2009b). Membrane promotes tBID interaction with BCLXL. Nat Struct Mol Biol *16*, 1178-U1179.

Garcia, P.S., Chieppa, G., Desideri, A., Cannata, S., Romano, E., Luly, P., and Rufini, S. (2012). Sticholysin II: A pore-forming toxin as a probe to recognize sphingomyelin in artificial and cellular membranes. Toxicon *60*, 724-733.

Gavathiotis, E., Reyna, D.E., Davis, M.L., Bird, G.H., and Walensky, L.D. (2010). BH3-triggered structural reorganization drives the activation of proapoptotic BAX. Mol Cell *40*, 481-492.

Geerts, H., De Brabander, M., Nuydens, R., Geuens, S., Moeremans, M., De Mey, J., and Hollenbeck, P. (1987). Nanovid tracking: a new automatic method for the study of mobility in living cells based on colloidal gold and video microscopy. Biophys J *52*, 775-782.

Gelles, J., Schnapp, B.J., and Sheetz, M.P. (1988). Tracking kinesin-driven movements with nanometre-scale precision. Nature *331*, 450-453.

Ghibelli, L., and Diederich, M. (2010). Multistep and multitask Bax activation. Mitochondrion *10*, 604-613.

Ghosh, R.N., and Webb, W.W. (1994). Automated Detection and Tracking of Individual and Clustered Cell-Surface Low-Density-Lipoprotein Receptor Molecules. biophysical journal *66*, 1301-1318.

Giam, M., Huang, D.C.S., and Bouillet, P. (2008). BH3-only proteins and their roles in programmed cell death. Oncogene *27*, S128-S136.

Giddings, K.S., Johnson, A.E., and Tweten, R.K. (2003). Redefining cholesterol's role in the mechanism of the cholesterol-dependent cytolysins. Proc Natl Acad Sci U S A *100*, 11315-11320.

Gonzalez, M.R., Bischofberger, M., Pernot, L., van der Goot, F.G., and Freche, B. (2008). Bacterial pore-forming toxins: the (w)hole story? Cell Mol Life Sci *65*, 493-507.

Gonzalvez, F., Schug, Z.T., Houtkooper, R.H., MacKenzie, E.D., Brooks, D.G., Wanders, R.J., Petit, P.X., Vaz, F.M., and Gottlieb, E. (2008). Cardiolipin provides an essential activating platform for caspase-8 on mitochondria. J Cell Biol *183*, 681-696.

Goping, I.S., Gross, A., Lavoie, J.N., Nguyen, M., Jemmerson, R., Roth, K., Korsmeyer, S.J., and Shore, G.C. (1998). Regulated targeting of BAX to mitochondria. J Cell Biol *143*, 207-215.

Gouaux.E. (1997). Channel-forming toxinstales of transformation. Nature Struct Biol *7*, 11.

Grochulski, P., Masson, L., Borisova, S., Pusztai-Carey, M., Schwartz, J.L., Brousseau, R., and Cygler, M. (1995a). Bacillus thuringiensis CryIA(a) insecticidal toxin: crystal structure and channel formation. J Mol Biol *254*, 447-464.

Grochulski, P., Masson, L., Borisova, S., Pusztaicarey, M., Schwartz, J.L., Brousseau, R., and Cygler, M. (1995b). Bacillus-Thuringiensis Cryla(a) Insecticidal Toxin - Crystal-Structure and Channel Formation. Journal of Molecular Biology *254*, 447-464.

Gross, D.J., and W. W. Webb (1988). Cell surface clustering and mobility of the liganded LDL receptor measured by digital video fluorescence microscopy (CRC Press, Boca Raton, FL).

Gutierrez-Aguirre, I., Barlic, A., Podlesek, Z., Macek, P., Anderluh, G., and Gonzalez-Manas, J.M. (2004). Membrane insertion of the N-terminal alpha-helix of equinatoxin II, a sea anemone cytolytic toxin. Biochem J *384*, 421-428.

Hadders, M.A., Beringer, D.X., and Gros, P. (2007). Structure of C8alpha-MACPF reveals mechanism of membrane attack in complement immune defense. Science *317*, 1552-1554.

Hanahan, D., and Weinberg, R.A. (2000). The hallmarks of cancer. Cell *100*, 57-70.

Hastie, P., Ulbrich, M.H., Wang, H.-L., Arant, R.J., Lau, A.G., Zhang, Z., Isacoff, E.Y., and Chen, L. (2013). AMPA receptor/TARP stoichiometry visualized by single-molecule subunit counting. Proceedings of the National Academy of Sciences *110*, 5163-5168.

Heuck, A.P., Hotze, E.M., Tweten, R.K., and Johnson, A.E. (2000). Mechanism of membrane insertion of a multimeric beta-barrel protein: perfringolysin O creates a pore using ordered and coupled conformational changes. Mol Cell *6*, 1233-1242.

Heuck, A.P., Savva, C.G., Holzenburg, A., and Johnson, A.E. (2007). Conformational changes that effect oligomerization and initiate pore formation are triggered throughout perfringolysin O upon binding to cholesterol. J Biol Chem *282*, 22629-22637.

Heuck, A.P., Tweten, R.K., and Johnson, A.E. (2003). Assembly and topography of the prepore complex in cholesterol-dependent cytolysins. J Biol Chem *278*, 31218-31225.

Hinds, M.G., Zhang, W., Anderluh, G., Hansen, P.E., and Norton, R.S. (2002). Solution structure of the eukaryotic pore-forming cytolysin equinatoxin II: implications for pore formation. J Mol Biol *315*, 1219-1229.

Hoch, F.L. (1992). Cardiolipins and biomembrane function. Biochim Biophys Acta *1113*, 71-133.

Holtzer, L., Meckel, T., and Schmidt, T. (2007). Nanometric three-dimensional tracking of individual quantum dots in cells. Appl Phys Lett *90*.

Hong, Q., Gutierrez-Aguirre, I., Barlic, A., Malovrh, P., Kristan, K., Podlesek, Z., Macek, P., Turk, D., Gonzalez-Manas, J.M., Lakey, J.H., *et al.* (2002). Two-step membrane binding by Equinatoxin II, a pore-forming toxin from the sea anemone, involves an exposed aromatic cluster and a flexible helix. J Biol Chem *277*, 41916-41924.

Hotze, E.M., Heuck, A.P., Czajkowsky, D.M., Shao, Z., Johnson, A.E., and Tweten, R.K. (2002). Monomer-monomer interactions drive the prepore to pore conversion of a beta-barrel-forming cholesterol-dependent cytolysin. J Biol Chem *277*, 11597-11605.

Howard, S.P., and Buckley, J.T. (1985). Activation of the hole-forming toxin aerolysin by extracellular processing. J Bacteriol *163*, 336-340.

Huang, H.W., Chen, F.Y., and Lee, M.T. (2004). Molecular mechanism of Peptide-induced pores in membranes. Phys Rev Lett *92*, 198304.

Iacovache, I., Bischofberger, M., and van der Goot, F.G. (2010). Structure and assembly of pore-forming proteins. Curr Opin Struct Biol *20*, 241-246.

Iacovache, I., van der Goot, F.G., and Pernot, L. (2008). Pore formation: an ancient yet complex form of attack. Biochim Biophys Acta *1778*, 1611-1623.

J.E. Alouf, J.H.F. (2005). The Comprehensive Sourcebook of Bacterial Protein Toxins (Academic Press, London).

Jacquier, V., Prummer, M., Segura, J.M., Pick, H., and Vogel, H. (2006). Visualizing odorant receptor trafficking in living cells down to the single-molecule level. Proc Natl Acad Sci U S A *103*, 14325-14330.

Jaiswal, J.K., and Simon, S.M. (2004). Potentials and pitfalls of fluorescent quantum dots for biological imaging. Trends in Cell Biology *14*, 497-504.

Jaqaman, K., Loerke, D., Mettlen, M., Kuwata, H., Grinstein, S., Schmid, S.L., and Danuser, G. (2008). Robust single-particle tracking in live-cell time-lapse sequences. Nat Methods *5*, 695-702.

Jayasinghe, L., and Bayley, H. (2005). The leukocidin pore: evidence for an octamer with four LukF subunits and four LukS subunits alternating around a central axis. Protein Sci *14*, 2550-2561.

Juin, P., Cartron, P.F., and Vallette, F.M. (2005). Activation of Bax by BH3 domains during apoptosis: the unfolding of a deadly plot. Cell Cycle *4*, 637-642.

Karbowski, M., Lee, Y.J., Gaume, B., Jeong, S.Y., Frank, S., Nechushtan, A., Santel, A., Fuller, M., Smith, C.L., and Youle, R.J. (2002). Spatial and temporal association of Bax with mitochondrial fission sites, Drp1, and Mfn2 during apoptosis. J Cell Biol *159*, 931-938.

Katayama, Y., Burkacky, O., Meyer, M., Brauchle, C., Gratton, E., and Lamb, D.C. (2009). Real-Time Nanomicroscopy via Three-Dimensional Single-Particle Tracking. Chemphyschem *10*, 2458-2464.

Kawate, T., and Gouaux, E. (2003). Arresting and releasing Staphylococcal alpha-hemolysin at intermediate stages of pore formation by engineered disulfide bonds. Protein Sci *12*, 997-1006.

Kelekar, A., and Thompson, C.B. (1998). Bcl-2-family proteins: the role of the BH3 domain in apoptosis. Trends Cell Biol *8*, 324-330.

Kem, W.R., and Dunn, B.M. (1988). Separation and characterization of four different amino acid sequence variants of a sea anemone (Stichodactyla helianthus) protein cytolysin. Toxicon *26*, 997-1008.

Kennedy, C.L., Krejany, E.O., Young, L.F., O'Connor, J.R., Awad, M.M., Boyd, R.L., Emmins, J.J., Lyras, D., and Rood, J.I. (2005). The alpha-toxin of Clostridium septicum is essential for virulence. Mol Microbiol *57*, 1357-1366.

Kennedy, M.W., and Beauchamp, J. (2000). Sticky-finger interaction sites on cytosolic lipid-binding proteins? Cell Mol Life Sci *57*, 1379-1387.

Kent, M.S., Yim, H., Murton, J.K., Satija, S., Majewski, J., and Kuzmenko, I. (2008). Oligomerization of membrane-bound diphtheria toxin (CRM197) facilitates a transition to the open form and deep insertion. Biophys J *94*, 2115-2127.

Kerr, J.F., Wyllie, A.H., and Currie, A.R. (1972). Apoptosis: a basic biological phenomenon with wide-ranging implications in tissue kinetics. Br J Cancer *26*, 239-257.

Kim, H., Tu, H.C., Ren, D.R., Takeuchi, O., Jeffers, J.R., Zambetti, G.P., Hsieh, J.J.D., and Cheng, E.H.Y. (2009). Stepwise Activation of BAX and BAK by tBID, BIM, and PUMA Initiates Mitochondrial Apoptosis. Molecular Cell *36*, 487-499.

Kristan, K., Podlesek, Z., Hojnik, V., Gutierrez-Aguirre, I., Guncar, G., Turk, D., Gonzalez-Manas, J.M., Lakey, J.H., Macek, P., and Anderluh, G. (2004). Pore formation by equinatoxin, a eukaryotic pore-forming toxin, requires a flexible N-terminal region and a stable beta-sandwich. J Biol Chem *279*, 46509-46517.

Kristan, K., Viero, G., Macek, P., Dalla Serra, M., and Anderluh, G. (2007). The equinatoxin N-terminus is transferred across planar lipid membranes and helps to stabilize the transmembrane pore. FEBS J *274*, 539-550.

Kristan, K.C., Viero, G., Dalla Serra, M., Macek, P., and Anderluh, G. (2009). Molecular mechanism of pore formation by actinoporins. Toxicon *54*, 1125-1134.

Kusumi, A., Koyama-Honda, I., and Suzuki, K. (2004). Molecular dynamics and interactions for creation of stimulation-induced stabilized rafts from small unstable steady-state rafts. Traffic *5*, 213-230.

Kusumi, A., Sako, Y., and Yamamoto, M. (1993a). Confined Lateral Diffusion of Membrane-Receptors as Studied by Single-Particle Tracking (Nanovid Microscopy) - Effects of Calcium-Induced Differentiation in Cultured Epithelial-Cells. Biophysical Journal *65*, 2021-2040.

Kusumi, A., Sako, Y., and Yamamoto, M. (1993b). Confined lateral diffusion of membrane receptors as studied by single particle tracking (nanovid microscopy). Effects of calcium-induced differentiation in cultured epithelial cells. Biophys J *65*, 2021-2040.

Kusumi, A., Suzuki, K.G., Kasai, R.S., Ritchie, K., and Fujiwara, T.K. (2011). Hierarchical mesoscale domain organization of the plasma membrane. Trends Biochem Sci *36*, 604-615.

Kuwana, T., Mackey, M.R., Perkins, G., Ellisman, M.H., Latterich, M., Schneiter, R., Green, D.R., and Newmeyer, D.D. (2002). Bid, Bax, and lipids cooperate to form supramolecular openings in the outer mitochondrial membrane. Cell *111*, 331-342.

Kvansakul, M., Yang, H., Fairlie, W.D., Czabotar, P.E., Fischer, S.F., Perugini, M.A., Huang, D.C.S., and Colman, P.M. (2008). Vaccinia virus anti-apoptotic F1L is a novel Bcl-2-like domain-swapped dimer that binds a highly selective subset of BH3-containing death ligands. Cell Death and Differentiation *15*, 1564-1571.

Ladokhin, A.S., Selsted, M.E., and White, S.H. (1997). Sizing membrane pores in lipid vesicles by leakage of co-encapsulated markers: pore formation by melittin. Biophys J *72*, 1762-1766.

Lafranconi, W.M., Ferlan, I., Russell, F.E., and Huxtable, R.J. (1984). The action of equinatoxin, a peptide from the venom of the sea anemone, Actinia equina, on the isolated lung. Toxicon *22*, 347-352.

Lakey, J.H., and Slatin, S.L. (2001). Pore-forming colicins and their relatives. Curr Top Microbiol *257*, 131-161.

Landeta, O., Landajuela, A., Gil, D., Taneva, S., DiPrimo, C., Sot, B., Valle, M., Frolov, V.A., and Basanez, G. (2011). Reconstitution of Proapoptotic BAK Function in Liposomes Reveals a Dual Role for Mitochondrial Lipids in the BAK-driven Membrane Permeabilization Process. Journal of Biological Chemistry *286*, 8213-8230.

Lee, G.M., Ishihara, A., and Jacobson, K.A. (1991a). Direct Observation of Brownian-Motion of Lipids in a Membrane. P Natl Acad Sci USA *88*, 6274-6278.

Lee, G.M., Ishihara, A., and Jacobson, K.A. (1991b). Direct observation of brownian motion of lipids in a membrane. Proc Natl Acad Sci U S A *88*, 6274-6278.

Li, J.D., Carroll, J., and Ellar, D.J. (1991). Crystal structure of insecticidal delta-endotoxin from Bacillus thuringiensis at 2.5 A resolution. Nature *353*, 815-821.

Lindsten, T., Ross, A.J., King, A., Zong, W.X., Rathmell, J.C., Shiels, H.A., Ulrich, E., Waymire, K.G., Mahar, P., Frauwirth, K., *et al.* (2000). The combined functions of proapoptotic Bcl-2 family members Bak and Bax are essential for normal development of multiple tissues. Molecular Cell *6*, 1389-1399.

Lingwood, D., and Simons, K. (2011). Lipid rafts as a membrane-organizing principle. Science *327*, 46-50.

Lommerse, P.H., Vastenhoud, K., Pirinen, N.J., Magee, A.I., Spaink, H.P., and Schmidt, T. (2006). Single-molecule diffusion reveals similar mobility for the Lck, H-ras, and K-ras membrane anchors. Biophys J *91*, 1090-1097.

Lommerse, P.H.M., Blab, G.A., Cognet, L., Harms, G.S., Snaar-Jagalska, E.B., Spaink, H.P., and Schmidt, T. (2002). Single-molecule imaging of lipid-anchored proteins reveals domains in the cytoplasmic leaflet of the cell membrane. biophysical journal *82*, 48a-48a.

Lomonosova, E., and Chinnadurai, G. (2008). BH3-only proteins in apoptosis and beyond: an overview. Oncogene *27 Suppl 1*, S2-19.

Lotan, A., Fishman, L., and Zlotkin, E. (1996). Toxin compartmentation and delivery in the Cnidaria: the nematocyst's tubule as a multiheaded poisonous arrow. J Exp Zool *275*, 444-451.

Lovell, J.F., Billen, L.P., Bindner, S., Shamas-Din, A., Fradin, C., Leber, B., and Andrews, D.W. (2008). Membrane binding by tBid initiates an ordered series of events culminating in membrane permeabilization by Bax. Cell *135*, 1074-1084.

Lucken-Ardjomande, S., Montessuit, S., and Martinou, J.C. (2008). Contributions to Bax insertion and oligomerization of lipids of the mitochondrial outer membrane. Cell Death Differ *15*, 929-937.

Lukoyanova, N., and Saibil, H.R. (2008). Friend or foe: the same fold for attack and defense. Trends Immunol *29*, 51-53.

Lutter, M., Fang, M., Luo, X., Nishijima, M., Xie, X., and Wang, X. (2000). Cardiolipin provides specificity for targeting of tBid to mitochondria. Nat Cell Biol *2*, 754-761.

Lutter, M., Perkins, G.A., and Wang, X. (2001). The pro-apoptotic Bcl-2 family member tBid localizes to mitochondrial contact sites. BMC Cell Biol *2*, 22.

M.Fivaz, L.A., F.G.van der Goot (2000). Pathogens,toxins,and lipid rafts Vol 212 (Austria, Springer).

Ma, S., Hockings, C., Anwari, K., Kratina, T., Fennell, S., Lazarou, M., Ryan, M.T., Kluck, R.M., and Dewson, G. (2013). Assembly of the Bak apoptotic pore: a critical role for the Bak protein alpha6 helix in the multimerization of homodimers during apoptosis. J Biol Chem *288*, 26027-26038.

Macek, P. (1992). Polypeptide cytolytic toxins from sea anemones (Actiniaria). FEMS Microbiol Immunol *5*, 121-129.

Macek, P., Belmonte, G., Pederzolli, C., and Menestrina, G. (1994). Mechanism of action of equinatoxin II, a cytolysin from the sea anemone Actinia equina L. belonging to the family of actinoporins. Toxicology *87*, 205-227.

MacKenzie, C.R., Hirama, T., and Buckley, J.T. (1999). Analysis of receptor binding by the channel-forming toxin aerolysin using surface plasmon resonance. J Biol Chem *274*, 22604-22609.

Malovrh, P., Barlic, A., Podlesek, Z., MaCek, P., Menestrina, G., and Anderluh, G. (2000). Structure-function studies of tryptophan mutants of equinatoxin II, a sea anemone pore-forming protein. Biochem J *346 Pt 1*, 223-232.

Malovrh, P., Viero, G., Serra, M.D., Podlesek, Z., Lakey, J.H., Macek, P., Menestrina, G., and Anderluh, G. (2003a). A Novel Mechanism of Pore Formation. Journal of Biological Chemistry *278*, 22678-22685.

Malovrh, P., Viero, G., Serra, M.D., Podlesek, Z., Lakey, J.H., Macek, P., Menestrina, G., and Anderluh, G. (2003b). A novel mechanism of pore formation: membrane penetration by the N-terminal amphipathic region of equinatoxin. J Biol Chem *278*, 22678-22685.

Mancheño, J.M., Martín-Benito, J., Gavilanes, J.G., and Vázquez, L. (2006). A complementary microscopy analysis of Sticholysin II crystals on lipid films: Atomic force and transmission electron characterizations. Biophysical Chemistry *119*, 219-223.

Mancheno, J.M., Martin-Benito, J., Martinez-Ripoll, M., Gavilanes, J.G., and Hermoso, J.A. (2003). Crystal and electron microscopy structures of sticholysin II actinoporin reveal insights into the mechanism of membrane pore formation. Structure *11*, 1319-1328.

Martín-Benito, J., Gavilanes, F., de los Ríos, V., Mancheño, J.M., Fernández, J.J., and Gavilanes, J.G. (2000). Two-Dimensional Crystallization on Lipid Monolayers and Three-Dimensional Structure of Sticholysin II, a Cytolysin from the Sea Anemone Stichodactyla helianthus. Biophysical Journal *78*, 3186-3194.

Martinez-Caballero, S., Dejean, L.M., Kinnally, M.S., Oh, K.J., Mannella, C.A., and Kinnally, K.W. (2009). Assembly of the mitochondrial apoptosis-induced channel, MAC. J Biol Chem *284*, 12235-12245.

Matsuzaki, K., Sugishita, K., Ishibe, N., Ueha, M., Nakata, S., Miyajima, K., and Epand, R.M. (1998). Relationship of membrane curvature to the formation of pores by magainin 2. Biochemistry *37*, 11856-11863.

Matsuzaki, K., Yoneyama, S., and Miyajima, K. (1997). Pore formation and translocation of melittin. Biophys J *73*, 831-838.

McIlwain, D.R., Berger, T., and Mak, T.W. (2013). Caspase functions in cell death and disease. Cold Spring Harb Perspect Biol *5*, a008656.

Mechaly, A.E., Bellomio, A., Gil-Carton, D., Morante, K., Valle, M., Gonzalez-Manas, J.M., and Guerin, D.M.A. (2011a). Structural Insights into the Oligomerization and Architecture of Eukaryotic Membrane Pore-Forming Toxins. Structure *19*, 181-191.

Mechaly, A.E., Bellomio, A., Gil-Cartún, D., Morante, K., Valle, M., González-Mañas, J.M., and Guérin, D.M.A. (2011b). Structural Insights into the Oligomerization and Architecture of Eukaryotic Membrane Pore-Forming Toxins. Structure *19*, 181-191.

Mechaly, A.E., Bellomio, A., Morante, K., Gonzalez-Manas, J.M., and Guerin, D.M. (2009). Crystallization and preliminary crystallographic analysis of fragaceatoxin C, a pore-forming toxin from the sea anemone Actinia fragacea. Acta Crystallogr Sect F Struct Biol Cryst Commun *65*, 357-360.

Meckel, T., Semrau, S., Schaaf, M.J.M., and Schmidt, T. (2011a). Robust assessment of protein complex formation in vivo via single-molecule intensity distributions of autofluorescent proteins. Journal of Biomedical Optics *16*, 076016-076016.

Meckel, T., Semrau, S., Schaaf, M.J.M., and Schmidt, T. (2011b). Robust assessment of protein complex formation in vivo via single-molecule intensity distributions of autofluorescent proteins. Journal of Biomedical Optics *16*.

Medema, J.P., Scaffidi, C., Kischkel, F.C., Shevchenko, A., Mann, M., Krammer, P.H., and Peter, M.E. (1997). FLICE is activated by association with the CD95 death-inducing signaling complex (DISC). Embo Journal *16*, 2794-2804.

Menestrina, G., Dalla Serra, M., Comai, M., Coraiola, M., Viero, G., Werner, S., Colin, D.A., Monteil, H., and Prevost, G. (2003). Ion channels and bacterial infection: the case of beta-barrel pore-forming protein toxins of Staphylococcus aureus. FEBS Lett *552*, 54-60.

Menestrina, G., Moser, C., Pellet, S., and Welch, R. (1994). Pore-formation by Escherichia coli hemolysin (HlyA) and other members of the RTX toxins family. Toxicology *87*, 249-267.

Michalet, X., Pinaud, F.F., Bentolila, L.A., Tsay, J.M., Doose, S., Li, J.J., Sundaresan, G., Wu, A.M., Gambhir, S.S., and Weiss, S. (2005). Quantum dots for live cells, in vivo imaging, and diagnostics. Science *307*, 538-544.

Miles, G., Jayasinghe, L., and Bayley, H. (2006). Assembly of the Bi-component leukocidin pore examined by truncation mutagenesis. J Biol Chem *281*, 2205-2214.

Moertelmaier, M., Brameshuber, M., Linimeier, M., Schutz, G.J., and Stockinger, H. (2005). Thinning out clusters while conserving stoichiometry of labeling. Appl Phys Lett *87*.

Moniatte, M., van der Goot, F.G., Buckley, J.T., Pattus, F., and van Dorsselaer, A. (1996). Characterisation of the heptameric pore-forming complex of the Aeromonas toxin aerolysin using MALDI-TOF mass spectrometry. FEBS Lett *384*, 269-272.

Montessuit, S., Somasekharan, S.P., Terrones, O., Lucken-Ardjomande, S., Herzig, S., Schwarzenbacher, R., Manstein, D.J., Bossy-Wetzel, E., Basanez, G., Meda, P., *et al.* (2010). Membrane remodeling induced by the dynamin-related protein Drp1 stimulates Bax oligomerization. Cell *142*, 889-901.

Morone, N., Fujiwara, T., Murase, K., Kasai, R.S., Ike, H., Yuasa, S., Usukura, J., and Kusumi, A. (2006). Three-dimensional reconstruction of the membrane skeleton at the plasma membrane interface by electron tomography. Journal of Cell Biology *174*, 851-862.

Mueller, M., Grauschopf, U., Maier, T., Glockshuber, R., and Ban, N. (2009). The structure of a cytolytic alpha-helical toxin pore reveals its assembly mechanism. Nature *459*, 726-730.

Murase, K., Fujiwara, T., Umemura, Y., Suzuki, K., Iino, R., Yamashita, H., Saito, M., Murakoshi, H., Ritchie, K., and Kusumi, A. (2004). Ultrafine membrane compartments for molecular diffusion as revealed by single molecule techniques. Biophysical Journal *86*, 4075-4093.

Nakagawa, T., Shimizu, S., Watanabe, T., Yamaguchi, O., Otsu, K., Yamagata, H., Inohara, H., Kubo, T., and Tsujimoto, Y. (2005). Cyclophilin D-dependent mitochondrial permeability transition regulates some necrotic but not apoptotic cell death. Nature *434*, 652-658.

Nakamura, M., Sekino, N., Iwamoto, M., and Ohno-Iwashita, Y. (1995). Interaction of theta-toxin (perfringolysin O), a cholesterol-binding cytolysin, with liposomal membranes: change in the aromatic side chains upon binding and insertion. Biochemistry *34*, 6513-6520.

Nechushtan, A., Smith, C.L., Lamensdorf, I., Yoon, S.H., and Youle, R.J. (2001). Bax and Bak coalesce into novel mitochondria-associated clusters during apoptosis. J Cell Biol *153*, 1265-1276.

Norton, R.S. (1991). Structure and Structure-Function-Relationships of Sea-Anemone Proteins That Interact with the Sodium-Channel. Toxicon *29*, 1051-1084.

Norton, R.S. (2009). Structures of sea anemone toxins. Toxicon *54*, 1075-1088.

O'Neill, J.W., Manion, M.K., Maguire, B., and Hockenbery, D.M. (2006). BCL-XL dimerization by three-dimensional domain swapping. J Mol Biol *356*, 367-381.

Olson, R., Nariya, H., Yokota, K., Kamio, Y., and Gouaux, E. (1999). Crystal structure of staphylococcal LukF delineates conformational changes accompanying formation of a transmembrane channel. Nat Struct Biol *6*, 134-140.

Ott, M., Norberg, E., Walter, K.M., Schreiner, P., Kemper, C., Rapaport, D., Zhivotovsky, B., and Orrenius, S. (2007). The mitochondrial TOM complex is required for tBid/Bax-induced cytochrome c release. Journal of Biological Chemistry *282*, 27633-27639.

Ott, M., Robertson, J.D., Gogvadze, V., Zhivotovsky, B., and Orrenius, S. (2002). Cytochrome c release from mitochondria proceeds by a two-step process. Proc Natl Acad Sci U S A *99*, 1259-1263.

Palmer, M., Harris, R., Freytag, C., Kehoe, M., Tranum-Jensen, J., and Bhakdi, S. (1998). Assembly mechanism of the oligomeric streptolysin O pore: the early membrane lesion is lined by a free edge of the lipid membrane and is extended gradually during oligomerization. EMBO J *17*, 1598-1605.

Parker, M.W., Buckley, J.T., Postma, J.P., Tucker, A.D., Leonard, K., Pattus, F., and Tsernoglou, D. (1994). Structure of the Aeromonas toxin proaerolysin in its water-soluble and membrane-channel states. Nature *367*, 292-295.

Parker, M.W., and Feil, S.C. (2005). Pore-forming protein toxins: from structure to function. Prog Biophys Mol Biol *88*, 91-142.

Parker, M.W., Pattus, F., Tucker, A.D., and Tsernoglou, D. (1989). Structure of the membrane-pore-forming fragment of colicin A. Nature *337*, 93-96.

Parker, M.W., Postma, J.P., Pattus, F., Tucker, A.D., and Tsernoglou, D. (1992). Refined structure of the pore-forming domain of colicin A at 2.4 A resolution. J Mol Biol *224*, 639-657.

Peng, J., Ding, J., Tan, C., Baggenstoss, B., Zhang, Z., Lapolla, S.M., and Lin, J. (2009). Oligomerization of membrane-bound Bcl-2 is involved in its pore formation induced by tBid. Apoptosis *14*, 1145-1153.

Peter, M.E., Kischkel, F.C., Hellbardt, S., Chinnaiyan, A.M., Krammer, P.H., and Dixit, V.M. (1996). CD95 (APO-1/Fas)-associating signalling proteins. Cell Death Differ *3*, 161-170.

Pinaud, F., Michalet, X., Iyer, G., Margeat, E., Moore, H.P., and Weiss, S. (2009). Dynamic partitioning of a glycosyl-phosphatidylinositol-anchored protein in glycosphingolipid-rich microdomains imaged by single-quantum dot tracking. Traffic *10*, 691-712.

Polekhina, G., Giddings, K.S., Tweten, R.K., and Parker, M.W. (2005). Insights into the action of the superfamily of cholesterol-dependent cytolysins from studies of intermedilysin. Proc Natl Acad Sci U S A *102*, 600-605.

Qian, H., Sheetz, M.P., and Elson, E.L. (1991). Single particle tracking. Analysis of diffusion and flow in two-dimensional systems. Biophys J *60*, 910-921.

Qian, S., Wang, W., Yang, L., and Huang, H.W. (2008a). Structure of the alamethicin pore reconstructed by x-ray diffraction analysis. Biophys J *94*, 3512-3522.

Qian, S., Wang, W., Yang, L., and Huang, H.W. (2008b). Structure of transmembrane pore induced by Bax-derived peptide: evidence for lipidic pores. Proc Natl Acad Sci U S A *105*, 17379-17383.

Qiu, X.Q., Jakes, K.S., Kienker, P.K., Finkelstein, A., and Slatin, S.L. (1996). Major transmembrane movement associated with colicin Ia channel gating. J Gen Physiol *107*, 313-328.

Ragan, T., Huang, H.D., So, P., and Gratton, E. (2006). 3D particle tracking on a two-photon microscope. Journal of Fluorescence *16*, 325-336.

Reichert, W.M. (1989). Evanscent detection of absorbed films: Assessment of optical considerations for absorbance and fluorescence spectroscopy at the crystal/solution and polymer/ solution interfaces. Crit Rev Biocompat

5

173-205.

Reichert, W.M.a.T., G.A. (1990). Total internal reflection fluorescence (TIRF) microscopy. I. Modeling cell contact region fluorescence. J Cell Sci *96*, 219-230.

Reiner, A., Arant, R.J., and Isacoff, E.Y. (2012). Assembly Stoichiometry of the GluK2/GluK5 Kainate Receptor Complex. Cell Reports *1*, 234-240.

Reinfeld , N. (1958). Mathematical Programming (Prentice - Hall , Englewood Cliffs, New Jersey .).

Renault, T.T., and Manon, S. (2011). Bax: Addressed to kill. Biochimie *93*, 1379-1391.

Renner, M., Domanov, Y., Sandrin, F., Izeddin, I., Bassereau, P., and Triller, A. (2011). Lateral Diffusion on Tubular Membranes: Quantification of Measurements Bias. Plos One *6*.

Ritchie, K., Shan, X.Y., Kondo, J., Iwasawa, K., Fujiwara, T., and Kusumi, A. (2005). Detection of non-Brownian diffusion in the cell membrane in single molecule tracking. Biophys J *88*, 2266-2277.

Rizzuto, R., Brini, M., Pizzo, P., Murgia, M., and Pozzan, T. (1995). Chimeric Green Fluorescent Protein as a Tool for Visualizing Subcellular Organelles in Living Cells. Current Biology *5*, 635-642.

Rolland, S.G., and Conradt, B. (2010). New role of the BCL2 family of proteins in the regulation of mitochondrial dynamics. Curr Opin Cell Biol *22*, 852-858.

Rosado, C.J., Buckle, A.M., Law, R.H., Butcher, R.E., Kan, W.T., Bird, C.H., Ung, K., Browne, K.A., Baran, K., Bashtannyk-Puhalovich, T.A., *et al.* (2007). A common fold mediates vertebrate defense and bacterial attack. Science *317*, 1548-1551.

Rossjohn, J., Polekhina, G., Feil, S.C., Morton, C.J., Tweten, R.K., and Parker, M.W. (2007). Structures of perfringolysin O suggest a pathway for activation of cholesterol-dependent cytolysins. J Mol Biol *367*, 1227-1236.

Roucou, X., Montessuit, S., Antonsson, B., and Martinou, J.C. (2002). Bax oligomerization in mitochondrial membranes requires tBid (caspase-8-cleaved Bid) and a mitochondrial protein. Biochem J *368*, 915-921.

Rutledge, S.E., Chin, J.W., and Schepartz, A. (2002). A view to a kill: ligands for Bcl-2 family proteins. Current Opinion in Chemical Biology *6*, 479-485.

S.L. Iverson, M.E., V. Gogvadze, M. Ott, S. Orrenius (2004). Cardiolipin is not required for Bax-mediated cytochrome c release from yeast mitochondria. J Biol Chem, *279*, 7.

Saito, M., Korsmeyer, S.J., and Schlesinger, P.H. (2000). BAX-dependent transport of cytochrome c reconstituted in pure liposomes. Nat Cell Biol *2*, 553-555.

Sako, Y., and Uyemura, T. (2002). Total internal reflection fluorescence microscopy for single-molecule imaging in living cells. Cell Struct Funct *27*, 357-365.

Saxton, M.J. (1993). Lateral Diffusion in an Archipelago - Single-Particle Diffusion. biophysical journal *64*, 1766-1780.

Saxton, M.J., and Jacobson, K. (1997). Single-particle tracking: applications to membrane dynamics. Annu Rev Biophys Biomol Struct *26*, 373-399.

Scaffidi, C., Fulda, S., Srinivasan, A., Friesen, C., Li, F., Tomaselli, K.J., Debatin, K.M., Krammer, P.H., and Peter, M.E. (1998). Two CD95 (APO-1/Fas) signaling pathways. EMBO J *17*, 1675-1687.

Scaffidi, C., Schmitz, I., Zha, J., Korsmeyer, S.J., Krammer, P.H., and Peter, M.E. (1999). Differential modulation of apoptosis sensitivity in CD95 type I and type II cells. J Biol Chem *274*, 22532-22538.

Schafer, B., Quispe, J., Choudhary, V., Chipuk, J.E., Ajero, T.G., Du, H., Schneiter, R., and Kuwana, T. (2009). Mitochondrial outer membrane proteins assist Bid in Bax-mediated lipidic pore formation. Mol Biol Cell *20*, 2276-2285.

Schendel, S.L., Montal, M., and Reed, J.C. (1998). Bcl-2 family proteins as ion-channels. Cell Death and Differentiation *5*, 372-380.

Schlame, M., and Greenberg, M.L. (1997). Cardiolipin synthase from yeast. Biochim Biophys Acta *1348*, 201-206.

Schlame, M., and Hostetler, K.Y. (1997). Cardiolipin synthase from mammalian mitochondria. Biochim Biophys Acta *1348*, 207-213.

Schlesinger, P.H., Gross, A., Yin, X.M., Yamamoto, K., Saito, M., Waksman, G., and Korsmeyer, S.J. (1997). Comparison of the ion channel characteristics of proapoptotic BAX and antiapoptotic BCL-2. Proc Natl Acad Sci U S A *94*, 11357-11362.

Schmidt, T., Schutz, G.J., Baumgartner, W., Gruber, H.J., and Schindler, H. (1995). Characterization of Photophysics and Mobility of Single Molecules in a Fluid Lipid-Membrane. Journal of Physical Chemistry *99*, 17662-17668.

Schmidt, T., Schutz, G.J., Baumgartner, W., Gruber, H.J., and Schindler, H. (1996a). Imaging of single molecule diffusion. Proceedings of the National Academy of Sciences of the United States of America *93*, 2926-2929.

Schmidt, T., Schutz, G.J., Gruber, H.J., and Schindler, H. (1996b). Local stoichiometries determined by counting individual molecules. Anal Chem *68*, 4397-4401.

Schnapp BJ, G.J., Sheetz MP. (1988). Nanometer-scale measurements using video light microscopy. Cell Motil Cytoskeleton *10*, 47-53.

Schon, P., Garcia-Saez, A.J., Malovrh, P., Bacia, K., Anderluh, G., and Schwille, P. (2008). Equinatoxin II permeabilizing activity depends on the presence of sphingomyelin and lipid phase coexistence. Biophys J *95*, 691-698.

Schug, Z.T., and Gottlieb, E. (2009). Cardiolipin acts as a mitochondrial signalling platform to launch apoptosis. Bba-Biomembranes *1788*, 2022-2031.

Schutz, G.J., Schindler, H., and Schmidt, T. (1997). Single-molecule microscopy on model membranes reveals anomalous diffusion. Biophys J *73*, 1073-1080.

Sengupta, D., Leontiadou, H., Mark, A.E., and Marrink, S.J. (2008). Toroidal pores formed by antimicrobial peptides show significant disorder. Bba-Biomembranes *1778*, 2308-2317.

Serge, A., Bertaux, N., Rigneault, H., and Marguet, D. (2008). Dynamic multiple-target tracing to probe spatiotemporal cartography of cell membranes. Nat Methods *5*, 687-694.

Shaner, N.C., Steinbach, P.A., and Tsien, R.Y. (2005). A guide to choosing fluorescent proteins. Nat Methods *2*, 905-909.

Sheets, E.D., Lee, G.M., Simson, R., and Jacobson, K. (1997). Transient confinement of a glycosylphosphatidylinositol-anchored protein in the plasma membrane. Biochemistry *36*, 12449-12458.

Sheetz, M.P., and Kuo, S.C. (1993). Tracking Nanometer Movements of Single Motor Molecules. Methods in Cell Biology, Vol 39 *39*, 129-136.

Shepard, L.A., Shatursky, O., Johnson, A.E., and Tweten, R.K. (2000). The mechanism of pore assembly for a cholesterol-dependent cytolysin: formation of a large prepore complex precedes the insertion of the transmembrane beta-hairpins. Biochemistry *39*, 10284-10293.

Sher, D., Fishman, Y., Zhang, M., Lebendiker, M., Gaathon, A., Mancheno, J.M., and Zlotkin, E. (2005a). Hydralysins, a new category of beta-pore-forming toxins in cnidaria. J Biol Chem *280*, 22847-22855.

Sher, D., Knebel, A., Bsor, T., Nesher, N., Tal, T., Morgenstern, D., Cohen, E., Fishman, Y., and Zlotkin, E. (2005b). Toxic polypeptides of the hydra - a bioinformatic approach to cnidarian allomones. Toxicon *45*, 865-879.

Shimizu, S., Narita, M., and Tsujimoto, Y. (1999). Bcl-2 family proteins regulate the release of apoptogenic cytochrome c by the mitochondrial channel VDAC. Nature *399*, 483-487.

Shogomori, H., and Kobayashi, T. (2008). Lysenin: a sphingomyelin specific pore-forming toxin. Biochim Biophys Acta *1780*, 612-618.

Sieben, A., Kaminski, T., Kubitscheck, U., and Haberlein, H. (2011). Terbutaline causes immobilization of single beta(2)-adrenergic receptor-ligand complexes in the plasma membrane of living A549 cells as revealed by single-molecule microscopy. Journal of Biomedical Optics *16*.

Siegel, D.P. (1984). Inverted micellar structures in bilayer membranes. Formation rates and half-lives. Biophys J *45*, 399-420.

Simson, R., Yang, B., Moore, S.E., Doherty, P., Walsh, F.S., and Jacobson, K.A. (1998). Structural mosaicism on the submicron scale in the plasma membrane. Biophys J *74*, 297-308.

Slatin, S.L., Qiu, X.Q., Jakes, K.S., and Finkelstein, A. (1994). Identification of a translocated protein segment in a voltage-dependent channel. Nature *371*, 158-161.

Smaal, E.B., Schreuder, C., van Baal, J.B., Tijburg, P.N., Mandersloot, J.G., de Kruijff, B., and de Gier, J. (1987). Calcium-induced changes in permeability of dioleoylphosphatidylcholine model membranes containing bovine heart cardiolipin. Biochim Biophys Acta *897*, 191-196.

Sobko, A.A., Kotova, E.A., Antonenko, Y.N., Zakharov, S.D., and Cramer, W.A. (2006). Lipid dependence of the channel properties of a colicin E1-lipid toroidal pore. J Biol Chem *281*, 14408-14416.

Song, L., Hobaugh, M.R., Shustak, C., Cheley, S., Bayley, H., and Gouaux, J.E. (1996). Structure of staphylococcal alpha-hemolysin, a heptameric transmembrane pore. Science *274*, 1859-1866.

Straus SE, S.M., Lenardo MJ, Puck JM, Strober W. (1999). An inherited disorder of lymphocyte apoptosis: the autoimmune lymphoproliferative syndrome. Ann Intern Med *130*, 10.

Suzuki, K.G., Fujiwara, T.K., Edidin, M., and Kusumi, A. (2007a). Dynamic recruitment of phospholipase C gamma at transiently immobilized GPI-anchored receptor clusters induces IP3-Ca2+ signaling: single-molecule tracking study 2. J Cell Biol *177*, 731-742.

Suzuki, K.G., Fujiwara, T.K., Sanematsu, F., Iino, R., Edidin, M., and Kusumi, A. (2007b). GPI-anchored receptor clusters transiently recruit Lyn and G alpha for temporary cluster immobilization and Lyn activation: single-molecule tracking study 1. J Cell Biol *177*, 717-730.

Suzuki, M., Youle, R.J., and Tjandra, N. (2000). Structure of Bax: coregulation of dimer formation and intracellular localization. Cell *103*, 645-654.

Taylor, R.C., Cullen, S.P., and Martin, S.J. (2008). Apoptosis: controlled demolition at the cellular level. Nat Rev Mol Cell Bio *9*, 231-241.

Tejuca, M., Serra, M.D., Ferreras, M., Lanio, M.E., and Menestrina, G. (1996). Mechanism of membrane permeabilization by sticholysin I, a cytolysin isolated from the venom of the sea anemone Stichodactyla helianthus. Biochemistry *35*, 14947-14957.

Teng, C.M., Lee, L.G., Lee, C.Y., and Ferlan, I. (1988). Platelet aggregation induced by equinatoxin. Thromb Res *52*, 401-411.

Terrones, O., Antonsson, B., Yamaguchi, H., Wang, H.G., Liu, J., Lee, R.M., Herrmann, A., and Basanez, G. (2004). Lipidic pore formation by the concerted action of proapoptotic BAX and tBID. J Biol Chem *279*, 30081-30091.

Thompson, C.B. (1995). Apoptosis in the pathogenesis and treatment of disease. Science *267*, 1456-1462.

Thompson, J.R., Cronin, B., Bayley, H., and Wallace, M.I. (2011). Rapid assembly of a multimeric membrane protein pore. Biophys J *101*, 2679-2683.

Thompson, R.E., Larson, D.R., and Webb, W.W. (2002). Precise nanometer localization analysis for individual fluorescent probes. biophysical journal *82*, 2775-2783.

Tilley, S.J., Orlova, E.V., Gilbert, R.J., Andrew, P.W., and Saibil, H.R. (2005). Structural basis of pore formation by the bacterial toxin pneumolysin. Cell *121*, 247-256.

Trache, A., and Meininger, G.A. (2008). Total internal reflection fluorescence (TIRF) microscopy. Curr Protoc Microbiol *Chapter 2*, Unit 2A 2 1-2A 2 22.

Tsujimoto, Y., and Shimizu, S. (2007). Role of the mitochondrial membrane permeability transition in cell death. Apoptosis *12*, 835-840.

Tweten, R.K. (2005). Cholesterol-dependent cytolysins, a family of versatile pore-forming toxins. Infect Immun *73*, 6199-6209.

Tweten, R.K., Parker, M.W., and Johnson, A.E. (2001). The cholesterol-dependent cytolysins. Curr Top Microbiol Immunol *257*, 15-33.

Unsay, J.D., and Garcia-Saez, A.J. (2013). Scanning fluorescence correlation spectroscopy in model membrane systems. Methods Mol Biol *1033*, 185-205.

Valcarcel, C.A., Dalla Serra, M., Potrich, C., Bernhart, I., Tejuca, M., Martinez, D., Pazos, F., Lanio, M.E., and Menestrina, G. (2001). Effects of Lipid Composition on Membrane Permeabilization by Sticholysin I and II, Two Cytolysins of the Sea Anemone Stichodactyla helianthus. Biophysical Journal *80*, 2761-2774.

van der Goot, F.G., Lakey, J., Pattus, F., Kay, C.M., Sorokine, O., Van Dorsselaer, A., and Buckley, J.T. (1992). Spectroscopic study of the activation and oligomerization of the

channel-forming toxin aerolysin: identification of the site of proteolytic activation. Biochemistry *31*, 8566-8570.

Vander Heiden, M.G., Chandel, N.S., Williamson, E.K., Schumacker, P.T., and Thompson, C.B. (1997). Bcl-xL regulates the membrane potential and volume homeostasis of mitochondria. Cell *91*, 627-637.

Walker, B., Krishnasastry, M., Zorn, L., and Bayley, H. (1992). Assembly of the oligomeric membrane pore formed by Staphylococcal alpha-hemolysin examined by truncation mutagenesis. J Biol Chem *267*, 21782-21786.

Wallace, A.J., Stillman, T.J., Atkins, A., Jamieson, S.J., Bullough, P.A., Green, J., and Artymiuk, P.J. (2000). E. coli hemolysin E (HlyE, ClyA, SheA): X-ray crystal structure of the toxin and observation of membrane pores by electron microscopy. Cell *100*, 265-276.

Wang, K., Gross, A., Waksman, G., and Korsmeyer, S.J. (1998). Mutagenesis of the BH3 domain of BAX identifies residues critical for dimerization and killing. Mol Cell Biol *18*, 6083-6089.

Wedekind, J.E., Trame, C.B., Dorywalska, M., Koehl, P., Raschke, T.M., McKee, M., FitzGerald, D., Collier, R.J., and McKay, D.B. (2001). Refined crystallographic structure of Pseudomonas aeruginosa exotoxin A and its implications for the molecular mechanism of toxicity. J Mol Biol *314*, 823-837.

Wei, M.C., Lindsten, T., Mootha, V.K., Weiler, S., Gross, A., Ashiya, M., Thompson, C.B., and Korsmeyer, S.J. (2000). tBID, a membrane-targeted death ligand, oligomerizes BAK to release cytochrome c. Genes Dev *14*, 2060-2071.

Wei, M.C., Zong, W.X., Cheng, E.H.Y., Lindsten, T., Panoutsakopoulou, V., Ross, A.J., Roth, K.A., MacCregor, G.R., Thompson, C.B., and Korsmeyer, S.J. (2001). Proapoptotic BAX and BAK: A requisite gateway to mitochondrial dysfunction and death. Science *292*, 727-730.

Weiss, S. (1999). Fluorescence spectroscopy of single biomolecules. Science *283*, 1676-1683.

Westphal, D., Dewson, G., Czabotar, P.E., and Kluck, R.M. (2011). Molecular biology of Bax and Bak activation and action. Biochim Biophys Acta *1813*, 521-531.

Wieser, S., and Schutz, G.J. (2008). Tracking single molecules in the live cell plasma membrane-Do's and Don't's. Methods *46*, 131-140.

Willis, S.N., and Adams, J.M. (2005). Life in the balance: how BH3-only proteins induce apoptosis. Current Opinion in Cell Biology *17*, 617-625.

Wilmsen, H.U., Leonard, K.R., Tichelaar, W., Buckley, J.T., and Pattus, F. (1992). The aerolysin membrane channel is formed by heptamerization of the monomer. EMBO J *11*, 2457-2463.

Xia, T., Li, N., and Fang, X. (2013). Single-molecule fluorescence imaging in living cells. Annu Rev Phys Chem *64*, 459-480.

Xu, X.P., Zhai, D., Kim, E., Swift, M., Reed, J.C., Volkmann, N., and Hanein, D. (2013). Three-dimensional structure of Bax-mediated pores in membrane bilayers. Cell Death Dis *4*, e683.

Yip, K.W., and Reed, J.C. (2008). Bcl-2 family proteins and cancer. Oncogene *27*, 6398-6406.

Youle, R.J., and Strasser, A. (2008). The BCL-2 protein family: opposing activities that mediate cell death. Nat Rev Mol Cell Bio *9*, 47-59.

Young, J.A., and Collier, R.J. (2007). Anthrax toxin: receptor binding, internalization, pore formation, and translocation. Annu Rev Biochem *76*, 243-265.

Zakharov, S.D., and Cramer, W.A. (2002). Colicin crystal structures: pathways and mechanisms for colicin insertion into membranes. Bba-Biomembranes *1565*, 333-346.

Zhang, B., Zerubia, J., and Olivo-Marin, J.C. (2007). Gaussian approximations of fluorescence microscope point-spread function models. Applied Optics *46*, 1819-1829.

Zhang, Z., Zhu, W., Lapolla, S.M., Miao, Y., Shao, Y., Falcone, M., Boreham, D., McFarlane, N., Ding, J., Johnson, A.E., *et al.* (2010). Bax forms an oligomer via separate, yet interdependent, surfaces. J Biol Chem *285*, 17614-17627.

Zhou, L., and Chang, D.C. (2008). Dynamics and structure of the Bax-Bak complex responsible for releasing mitochondrial proteins during apoptosis. J Cell Sci *121*, 2186-2196.

Zou, H., Henzel, W.J., Liu, X., Lutschg, A., and Wang, X. (1997). Apaf-1, a human protein homologous to C. elegans CED-4, participates in cytochrome c-dependent activation of caspase-3. Cell *90*, 405-413.